

---

Electronic Thesis and Dissertation Repository

---

2-17-2016 12:00 AM

## The Design and Synthesis of Ghrelin Analogues as Non-Invasive GHS-R1a Imaging Probes

Carlie L. Charlton  
*The University of Western Ontario*

Supervisor  
Dr. Leonard Luyt  
*The University of Western Ontario*

Graduate Program in Chemistry  
A thesis submitted in partial fulfillment of the requirements for the degree in Doctor of  
Philosophy  
© Carlie L. Charlton 2016

Follow this and additional works at: <https://ir.lib.uwo.ca/etd>

 Part of the [Medicinal-Pharmaceutical Chemistry Commons](#), [Organic Chemistry Commons](#), and the [Radiochemistry Commons](#)

---

### Recommended Citation

Charlton, Carlie L., "The Design and Synthesis of Ghrelin Analogues as Non-Invasive GHS-R1a Imaging Probes" (2016). *Electronic Thesis and Dissertation Repository*. 3732.  
<https://ir.lib.uwo.ca/etd/3732>

This Dissertation/Thesis is brought to you for free and open access by Scholarship@Western. It has been accepted for inclusion in Electronic Thesis and Dissertation Repository by an authorized administrator of Scholarship@Western. For more information, please contact [wlsadmin@uwo.ca](mailto:wlsadmin@uwo.ca).

## Abstract

The field of molecular imaging is constantly growing and evolving in order to provide the best possible healthcare for patients in various stages of disease and therapy. Molecular imaging aims to locate specific markers of disease by selectively targeting the markers of interest with high selectivity and visualizing the accumulation using external detection.

The growth hormone secretagogue receptor-1a (GHS-R1a) has been shown to be involved in various important biological functions such as energy homeostasis and cardiac contractility. GHS-R1a has shown involvement in proliferation, migration and cell invasion of specific cancer subtypes. Therefore, targeting GHS-R1a is an important marker of different disease states and would be advantageous to selectively target for diagnostic and therapeutic purposes.

This thesis will document the development of peptide-based molecular imaging agents capable of targeting GHS-R1a with high affinity designed off the structure of ghrelin, the endogenous ligand for GHS-R1a.

Chapter 2 discusses the synthesis and evaluation of gallium-69/71 and gallium-68 labelled ghrelin(1-19) analogues. The first generation of ghrelin analogues was designed to detect GHS-R1a by positron emission tomography (PET). Chelation of gallium had a positive effect on binding affinity to GHS-R1a resulting in an  $IC_{50}$  comparable to natural ghrelin(1-28). Preclinical evaluation of HT1080/GHSR-1a xenografts showed higher SUVR values than the HT1080 xenograft with no GHS-R1a.

Chapter 3 discusses the second generation of ghrelin analogues that were further truncated to eight amino acids. A structural activity study investigated residues 1, 3, 4, and 8 to determine whether amino acid substitutions produce the best binding affinity GHS-R1a. The optimized ghrelin analogue has 12-fold higher binding affinity to GHS-R1a than natural ghrelin. New radiochemical syntheses were reported for a 6- $^{18}F$ -fluoro-2-pentafluorophenyl naphthoate prosthetic group. The lead peptide analogue was radiolabelled in a 3% radiochemical yield and resulted in the first fluorine-18 labelled ghrelin(1-8) analogue with greater affinity to GHS-R1a.

The final chapter describes the effects of targeting GHS-R1a with a dimerized ghrelin(1-8) peptide. Dimerizing other peptide targeting entities has increased binding affinity to the target however, this is not the case found with ghrelin. The *in vitro* kinetics were evaluated using fluorescence microscopy in GHS-R1a expressing cells.

All three chapters discuss the systematic modification of an endogenous peptide ligand into a high affinity, PET imaging agent through classical methods of peptide modification and radiochemistry.

## Keywords

Ghrelin, GHS-R1a, Peptide, Molecular Imaging, PET, Optical Imaging, Solid-Phase Peptide Synthesis

## Co-Authorship Statement

Chapter 1, sections 1.1 through 1.8 (with the exception of 1.6 and 1.7) were adapted from the published review C. L. Charron, J. L. Hickey, T. K. Nsiama, D. R. Cruickshank, W. L. Turnbull and L. G. Luyt, *Nat Prod Rep*, 2016.

Chapter 2 is a manuscript in preparation. All the peptides within this chapter were synthesized, purified, characterized and radiolabelled by Carlie Charlton. The *in vitro* competitive binding assays were carried out by Dr. Jinqiang Hou and Rebecca McGirr using instruments provided by Dr. Savita Dhanvantari. The HT1080 and HT1080/GHS-R1a cell lines were cultured by Dr. Lihai Yu. The  $\mu$ PET imaging was also performed by Carlie Charlton with the help of Dr. Jonatan Snir (imaging software) and Jennifer Hadway (animal technician).

Chapter 3 is a manuscript in preparation. All the peptides within this chapter were synthesized, purified, characterized and radiolabelled by Carlie Charlton. The *in vitro* competitive binding assays were carried out by Dr. Jinqiang Hou using instruments provided by Dr. Savita Dhanvantari. Fluorine-18 was donated by Dr. Michael Kovacs at the Nordan Cyclotron & PET Radiochemistry Facility in St. Josephs Hospital in London, Ontario.

All the peptides within this chapter 4 were synthesized, purified, characterized and radiolabelled by Carlie Charlton. The *in vitro* competitive binding assays were carried out by Dr. Jinqiang Hou using instruments provided by Dr. Savita Dhanvantari. HT1080 and HT1080/GHS-R1a cell culturing and confocal fluorescence imaging was carried out by Hilary Groom.



## Acknowledgments

So many amazing people have made this an enjoyable experience for me from start to end.

I have to thank my awesome supervisor, Len, for trusting me with the ghrelin project that held so much potential and letting me take the project in all the directions I envisioned. Without his constant support, expertise and friendship, I could have never developed this project into the thesis it is today. I cannot thank him enough for giving me the opportunity to share my chemistry at various venues all over the world and for introducing me to so many bright minds that helped me overcome the many hurdles I've encountered. It's going to be difficult finding another lab and supervisor that makes me feel so at home.

I also thank all my Luyt Lab colleagues, especially Jen Hickey, Emily Simpson, Lihai Yu and JQ Hou, for showing me the dedication required to be a successful PhD candidate and having the expertise to show me a new perspective on my chemistry when it seemed like there was no way to climb the wall.

I would never have had the opportunity to take my education this far without the help of my loving and supporting parents. They always saw the potential in myself and urged me to shoot higher, follow my dreams and never settle for the easy road. Without their constant support, I could not have made it through the many years of school, and I have no doubt I would have starved to death.

Lastly, I have to thank my loving husband, Mathew. He has spent endless hours listening to my complaints, celebrating my success and reminding me there is a light at the end of the tunnel. No one has been more supportive and patient with me as I insisted on staying in school for what seemed like a lifetime.

## Table of Contents

Abstract.....	i
Co-Authorship Statement.....	iii
Acknowledgments.....	iv
Table of Contents.....	v
List of Tables.....	ix
List of Figures.....	x
List of Schemes.....	xii
List of Abbreviations.....	xiii
Chapter 1.....	1
1 Introduction.....	1
1.1 Peptides and Molecular Imaging.....	1
1.2 Suitable Signaling Sources for PET and OI.....	1
1.3 Methods for Adding Radionuclides to Peptides.....	3
1.4 Modifying Radiolabelled Peptides for Improved <i>In Vivo</i> Stability and Target Affinity.....	8
1.5 Modifying Natural Peptides for Improved Pharmacokinetics.....	11
1.6 Increasing Receptor Affinity using Multimerization.....	12
1.7 Growth Hormone Secretagogue Receptor-1a and Ghrelin.....	14
1.8 Summary.....	17
1.9 References.....	17
Chapter 2.....	22
2 Development of a Novel [ <sup>68</sup> Ga]-Ghrelin Analogue for PET Imaging of GHS-R1a....	22
2.1 Introduction.....	22
2.2 Results and Discussion.....	24

2.2.1	Design and Synthesis .....	24
2.2.2	<i>In Vitro</i> Analysis .....	26
2.2.3	Radiochemistry .....	27
2.2.4	<i>In Vitro</i> Evaluation of <sup>68</sup> Ga-Ghrelin (1-19) .....	29
2.2.5	<i>In Vivo</i> Evaluation of <sup>68</sup> Ga-Ghrelin (1-19) .....	30
2.2.6	Conclusions .....	32
2.3	Experimental .....	33
2.3.1	Materials and Methods .....	33
2.3.2	Synthesis of <b>2.3d</b> .....	33
2.3.3	Synthesis of [ <sup>69/71</sup> Ga]- <b>2.3d</b> .....	35
2.3.4	Radiochemistry .....	35
2.3.5	Competitive Binding Assays (IC <sub>50</sub> ) .....	35
2.3.6	<i>In Vitro</i> Evaluation of [ <sup>68</sup> Ga]- <b>2.3d</b> .....	36
2.3.7	<i>In Vivo</i> Evaluation .....	36
2.4	Acknowledgements .....	37
2.5	References .....	37
Chapter 3 .....		41
3	Structural-Activity Study of Ghrelin(1-8) Resulting in Potent Fluorine-bearing Ligands for GHS-R1a .....	41
3.1	Introduction .....	41
3.2	Results and Discussion .....	43
3.2.1	Design of Ghrelin Analogues for Positron Emission Tomography (PET) .....	43
3.2.2	Synthesis of Prosthetic Groups and Standards .....	49
3.2.3	Radiochemistry .....	51
3.2.4	Conclusions .....	54
3.3	Experimental .....	55

3.3.1	Materials and Methods.....	55
3.3.2	General Fmoc Synthesis of Ghrelin(1-8) Peptides.....	56
3.3.3	Competitive Binding Assay (IC <sub>50</sub> ).....	57
3.3.4	Synthesis of 6-amino-2-ethylnaphthoate ( <b>3.9</b> ).....	58
3.3.5	Synthesis of 6-dimethylamino-2-ethylnaphthoate ( <b>3.10</b> ).....	58
3.3.6	Synthesis of 6-trimethylamino-2-ethylnaphthoate triflate ( <b>3.11</b> ).....	59
3.3.7	Synthesis of [ <sup>19</sup> F]-PFPN.....	60
3.3.8	Radiolabelling Procedure of [ <sup>18</sup> F]-PFPN.....	60
3.3.9	Quality Control of [ <sup>19</sup> F]-PFPN.....	62
3.4	Acknowledgments.....	62
3.5	References.....	62
Chapter 4.....		65
4	Synthesis of Monomeric and Dimeric Dye Labelled Ghrelin(1-8) Analogues for Evaluation in GHS-R1a Expressing Cells by Fluorescence Microscopy.....	65
4.1	Introduction.....	65
4.2	Results and Discussion.....	67
4.2.1	Synthesis and Characterization of a NIR Ghrelin(1-10) Monomer and Dimer.....	67
4.2.2	Binding Affinity of <b>4.4</b> and <b>4.10</b> to GHS-R1a.....	72
4.2.3	<i>In Vitro</i> Fluorescence Imaging in HT1080 and HT1080/GHS-R1a.....	73
4.3	Conclusions.....	74
4.4	Experimental.....	75
4.4.1	Materials and Methods.....	75
4.4.2	Automated Peptide Synthesis of <b>4.4</b> .....	75
4.4.3	Automated Peptide Synthesis of <b>4.10</b> .....	77
4.4.4	Competitive Binding Assay (IC <sub>50</sub> ).....	78
4.4.5	Fluorescence Microscopy of <b>4.4</b> and <b>4.10</b> with GHS-R1a.....	79

4.5	References.....	79
Chapter 5	.....	82
5	Conclusions.....	82
5.1	Outlook and Conclusions.....	82
5.2	References.....	86
6	Appendix.....	88
6.1	Chapter 2 HPLC Traces.....	88
6.2	Chapter 3 HPLC Traces.....	89
6.3	Chapter 3 ESI <sup>+</sup> Mass Spectrums.....	97
6.4	Chapter 3 IC <sub>50</sub> Curves.....	105
6.5	Chapter 3 <sup>1</sup> H NMR.....	113
6.6	Chapter 4 UHPLC Traces.....	118
6.7	Chapter 4 ESI <sup>+</sup> Mass Spectrums.....	119
Curriculum Vitae	.....	120

## List of Tables

Table 1.1 Common PET radionuclides and half-lives.....	2
Table 1.2 Published Modified Ghrelin Analogues.....	15
Table 2.1 IC <sub>50</sub> Values for Synthesized Ghrelin Analogues 2.1, 2.3d and [ <sup>69/71</sup> Ga]-2.3d.....	27
Table 2.2 Radiolabelling conditions for [ <sup>68</sup> Ga]-2.3d.....	28
Table 3.1 : Substitution of residue 8 with various natural and unnatural amino acids and the resulting IC <sub>50</sub> (nM) for GHS-R1a.....	45
Table 3.2 Substitution of Dpr side chain with various fluorine-bearing aromatic prosthetic groups and the resulting IC <sub>50</sub> (nM) for GHS-R1a.....	47
Table 3.3 Substitution of residue 1 and 4 with various unnatural amino acids and the resulting IC <sub>50</sub> (nM) for GHS-R1a.....	48
Table 3.4 Analytical data of ghrelin analogues 3.3-3.3j, 3.4a-3.4b, 3.5a-3.5c, 3.6a-3.6b and 3.7.....	57
Table 4.1 Analytical data for 4.4 and 4.10.....	69

## List of Figures

- Figure 1.1 Depiction of an annihilation event within a PET Scanner. A  $\beta^+$  emitting radioisotope ejects a positron from its nucleus that meets an electron. Upon contact, the positron and electron undergo an annihilation event resulting in two 511 keV gamma rays being emitted approximately  $180^\circ$  apart. The emitted gamma rays are detected by a ring of scintillation detectors and further processed into a PET image..... 3
- Figure 1.2 Various methods for introducing a radioisotope into a peptide sequence: pendant labelling, prosthetic group labelling, direct labelling and integrated labelling..... 6
- Figure 1.3 Common cyclic and acyclic chelators capable of chelating various radiometals: (A) 1,4,7,10-tetraazacyclododecane-1,4,7,10-tetraacetic acid (DOTA), (B) 1,4,7-triazacyclononane-1,4,7,-trisacetic acid (NOTA), (C) diethylenetriamine-*N,N,N',N',N''*-pentaacetic acid (DTPA), (D) 6-hydrozinonicotinic acid (HYNIC)..... 8
- Figure 1.4 Stereochemistry of natural L-amino acids as well as unnatural D-amino acids,  $\alpha$ -amino acids,  $\beta$ -amino acids, and  $\gamma$ -amino acids. R represents the applicable amino acid side chains. .... 9
- Figure 1.5 Various backbone modifications to alter *in vivo* stability of natural peptides. R represents various amino acid side chains. .... 11
- Figure 1.6 Pictorial representation of receptor targeting with homomultimers and heteromultimers. .... 12
- Figure 1.7 The structure of natural human ghrelin. .... 14
- Figure 2.1 . Amino acid sequence of natural human ghrelin (2.1) and des-acyl ghrelin (2.2) with the corresponding  $IC_{50}$  for GHS-R1a, as determined by a competitive binding assay with HEK293 cells stably transfected with GHS-R1a. .... 22
- Figure 2.2 Half-maximal inhibitory concentration curves of ghrelin analogues against [ $^{125}I$ ]-human ghrelin in HEK293/GHS-R1a cells. 2.1 (A), 2.3d (B), [ $^{69/71}Ga$ ]-2.3d (C)..... 26

Figure 2.3 RP-HPLC of [ <sup>69/71</sup> Ga]-2.3d and [ <sup>68</sup> Ga]-2.3d .....	29
Figure 2.4 Uptake of [ <sup>68</sup> Ga]-2.3d in HEK293/GHS-R1a cell with and without blocking of GHS-R1a with 2.1.....	29
Figure 2.5 A 60 minute dynamic uPET scan showing uptake of [ <sup>68</sup> Ga]-2.3d from 30-40 minutes in HT1080 and HT1080/GHS-R1a xenografts. (A) HT1080 – coronal. (B) HT1080/GHS-R1a – coronal, (C) HT1080 – 3D projection and (D) HT1080/GHS-R1a – 3D projection. ....	31
Figure 2.6 Graphical representation of SUVs for [ <sup>68</sup> Ga]-2.3d in HT1080/GHS-R1a and HT1080 xenografts over 60 minutes. ....	32
Figure 3.1 Preproghrelin undergoes proteolytic cleavage resulting in desacyl ghrelin (3.1) which undergoes acylation by ghrelin O-acyl transferase resulting in ghrelin(1-28) (3.2). ....	42
Figure 3.2 IC <sub>50</sub> curves of lead analogues 3.3f (A), 3.5b (B) and 3.6a (C) after modifications were made to positions 8, 1 and 4, respectively. ....	45
Figure 3.3 Amino acid structure (A) and IC <sub>50</sub> curve (B) of the the ghrelin (1-8) analogue bearing lead modifications to all positions 1, 3, 4 and 8.....	49
Figure 3.4 The modified schematic of Tracer Lab FX <sub>FN</sub> for the synthesis of 6-[ <sup>18</sup> F]-fluoro-2-naphthoic acid (3.15). ....	52
Figure 3.5 Overlaid C18 reverse-phase HPLC chromatograms of [ <sup>19</sup> F]-3.7 (AU) and [ <sup>18</sup> F]-3.7 (mV).....	54
Figure 4.1 Competitive binding curves in HEK293/GHS-R1a cells and IC <sub>50</sub> (nM) values for 4.4 (A) and 4.10 (B).....	72
Figure 4.2 Confocal microscopy results of 4.4 and 4.10 with HT1080 (GHS-R1a negative) and HT1080/GHS-R1a (GHS-R1a positive) (magnification x 60).....	73



## List of Schemes

Scheme 2.1 Synthesis of 2.3d.	25
Scheme 2.2 Gallium-68 chelation of 2.3d	27
Scheme 3.1 Synthesis of 6-trimethylamino-2-ethyl-naphthoate triflate (3.11)	50
Scheme 3.2 Synthesis of the non-radioactive standard 6-fluoro-2-pentafluorophenyl naphthoate (PFPN, 3.13)	51
Scheme 3.3 The radiosynthetic pathway for the synthesis of [ <sup>18</sup> F]-PFPN by automated and manual synthesis.	52
Scheme 3.4 Coupling of [ <sup>18</sup> F]-PFPN to the lead ghrelin(1-8) analogue resulting in [ <sup>18</sup> F]-3.7.	54

## List of Abbreviations

- 3D: three dimensional  
4-FBA: 4-fluorobenzoic acid  
4-FNA: 4-fluoronaphthoic acid  
 $\mu$ PET: micro positron emission tomography  
[<sup>18</sup>F]-FDG: 4-[<sup>18</sup>F]-fluorobenzoic acid  
[<sup>18</sup>F]-PFPN: 6-[<sup>18</sup>F]-fluoro-2-pentafluorophenyl naphthoate  
[<sup>19</sup>F]-PFPN: 6-[<sup>19</sup>F]-fluoro-2-pentafluorophenyl naphthoate  
Aib: aminoisobutyric acid  
ACN: acetonitrile  
AEEA: aminoethanolethylamine  
Alloc: allyloxycarbonyl  
BSA: Bovine Serum Albumin  
BOC: t-butoxycarbonyl  
BPH: benign hyperplasia  
Bq/cc: Becquerel per milliliter  
CI: chemical ionization  
cpm: counts per minute  
CXCR4: chemokine receptor type 4  
Cy5: cyanine 5  
d: days  
d.c.: decay corrected  
DAPI: 4',6-diamino-2-phenylindole  
DCM: dichloromethane  
DIPEA: *N,N*-diisopropylethylamine  
DMAP: 4-dimethylaminopyridine  
DMEM: dulbecco's modified eagles medium  
DMF: dimethylformamide  
DMSO: dimethylsulfoxide  
DOTA: 1,4,5,10-tetraazacyclododecane-1,4,7,10-tetraacetic acid  
Dpr: diaminopropionic acid  
DTPA: diethylene triamine pentaacetic acid

EDC: N-(3-dimethylaminopropyl)-N'-ethylcarbodiimide  
EDTA: ethylenediaminetetraacetic acid  
ESI<sup>+</sup>: electrospray ionization  
equiv: equivalents  
eV: electronvolt  
FBS: fetal bovine serum  
FMOC: fluorenylmethyloxycarbonyl  
g: gram  
GBq/ $\mu$ mol: gigabecquerel per micromole  
GH: growth hormone  
GHS-R1a: growth hormone secretagogue receptor-1a  
GHS-R1b: growth hormone secretagogue receptor-1b  
GOAT: ghrelin-*O*-acyl transferase  
GPCR: g-protein coupled receptor  
h: hours  
HCTU: (2-(6-Chloro-1H-benzotriazole-1-yl)-1,1,3,3-tetramethylammonium hexafluorophosphate)  
HEK293: human embryonic kidney 293 cells  
HEPES: 4-(2-hydroxyethyl)piperazine-1-ethanesulfonic acid  
HPLC: high-performance liquid chromatography  
HRMS: high resolution mass spectrometry  
HYNIC: hydrazinonicotinic acid  
IC50: half maximal inhibitory concentration  
Inp: isonipecotic acid  
LC: liquid chromatography  
m: minutes  
M: molar  
MeOTf: methyl trifluoromethanesulfonate  
mg: milligram  
mL: milliliter  
mm: millimeter  
mM: millimolar

mmol: millimole  
m/z: mass over charge ratio  
MBq: megabecquerel  
MSH: melanocyte-stimulating hormone  
MHz: megahertz  
Mtt: methyl trityl  
mV: megavolts  
n: number  
Nal-1: 1-naphthylalanine  
Nal-2: 2-naphthylalanine  
NHS: N-hydroxysuccinimide  
NIR: near infrared  
nM: nanomolar  
NMR: nuclear magnetic resonance  
NODAGA: 2,2'-(7-(1-carboxy-4-((2,5-dioxopyrrolidin-1-yl)oxy)-4-oxobutyl)-1,4,7-triazonane-1,4-diyl)diacetic acid  
NOTA: 1,4,7-triazacyclononane-triacetic acid  
OI: optical imaging  
PBS: phosphate buffered saline  
PCa: prostate cancer  
PET: positron emission tomography  
pM: picomolar  
PIN: prostatic interneoplasia  
RP: reverse phase  
rpm: rotations per minute  
Sar: sarcosine  
SPECT: single-photon emission computed tomography  
SUV: standard uptake value  
SUVr: relative standard uptake value  
TBME: *tert*-butylmethylether  
TFA: trifluoroacetic acid  
TIS: triisopropylsilane

TMAH: tetramethylammonium hydroxide

UHPLC: ultra high-performance liquid chromatography

V: voltage

V14: valve 14

VOI: volume of interest

## Chapter 1

### 1 Introduction

#### 1.1 Peptides and Molecular Imaging

The complexity of all living systems is a daunting task to understand. Yet, when broken down into fundamental building blocks, the complexity of these systems appears to be an eloquent work of art. One fundamental building block of all complex living systems is peptides. Found in all living systems, peptides are diverse naturally occurring compounds responsible for many biological functions. They are capable of acting as neurotransmitters, growth factors or antimicrobials, as well as facilitating cell-to-cell communication and ion-channel regulation, to name only a few. Peptides fit a specialized niche between the two molecular weight extremes of small molecules and proteins. They are able to combine the benefits of small molecules, such as low cost, membrane permeability and metabolic stability, with target specificity and high potency seen in proteins and antibodies. More importantly, peptides and their endogenous receptors have been implicated in disease states such as oncology, metabolic disorders and cardiovascular disease.<sup>1</sup>

Natural peptides, composed entirely of natural components, are known to have a relatively short *in vivo* half-life and are readily metabolized by endo- and exo- peptidases. Fortunately, peptides can be easily manipulated to increase *in vivo* stability, membrane permeability and target selectivity using well-known methods. These methods have been applied to many natural peptides to target their endogenous receptors for diagnosis and therapeutic applications. In order to detect these natural peptides externally, they must be modified to contain a signalling source capable of being detected with the various molecular imaging modalities. Molecular imaging modalities commonly used in both preclinical and clinical settings are positron emission tomography (PET), single-photon emission computed tomography (SPECT), magnetic resonance imaging (MRI), ultrasound (US) and optical imaging (OI). Each modality has their own strengths and weaknesses with respect to imaging sensitivity and spatial resolution.<sup>2</sup> In comparison to

the other modalities, PET has attractive attributes due to its high image sensitivity and requires radionuclides as a signalling source that have suitable attributes for diagnostic molecular imaging. Optical imaging is another imaging modality with high image sensitivity that doesn't require a radioactive signalling source. The commonly used methods to incorporate PET and OI signalling sources into natural peptides, as well as the many approaches to modifying these peptides for improved *in vivo* pharmacokinetics will be outlined.

## 1.2 Suitable Signaling Sources for PET and OI

Peptide-based targeting entities are a versatile class of radiopharmaceuticals able to selectively target receptors within the human body, allowing for a disease to be detected, staged, or treated. External monitoring of radiolabelled targeting entities can be achieved via a sensitive molecular imaging modality currently used in nuclear medicine: PET.<sup>1</sup> PET has slowly gained popularity since its discovery in the 1960's and has since become clinically acceptable. This modality requires a radionuclide to emit photons in the form of radiation, which can then be externally detected and processed into an image. PET requires radionuclides that decay via positron emission (Table 1.1). Once a positron is ejected from the nucleus, it travels a short distance before colliding with an electron. An annihilation event produces two 511 keV gamma rays emitted at a coincidence angle of 180° and are simultaneously detected by two scintillation detectors (Figure 1.1).

**Table 1.1 Common PET radionuclides and half-lives.**

Isotope	Half-life
Carbon-11	20.4 m
Copper-64	12.7 h
Fluorine-18	109.7 m
Gallium-68	68 m
Nitrogen-13	9.96 m
Oxygen-15	2.07 m
Yttrium-86	14.7 m
Zirconium-89	3.27 d

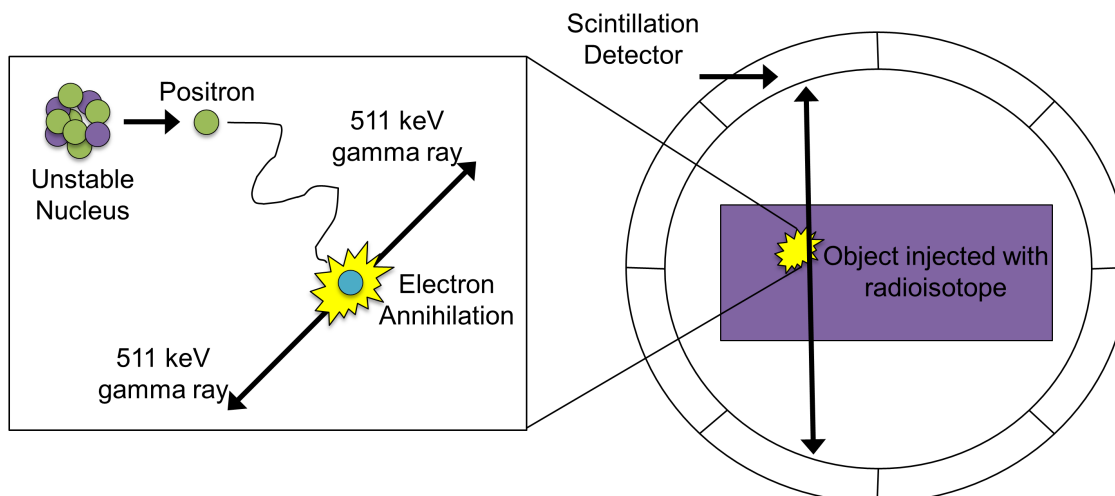


**Figure 1.1** Depiction of an annihilation event within a PET Scanner. A  $\beta^+$  emitting radioisotope ejects a positron from its nucleus that meets an electron. Upon contact, the positron and electron undergo an annihilation event resulting in two 511 keV gamma rays being emitted approximately  $180^\circ$  apart. The emitted gamma rays are detected by a ring of scintillation detectors and further processed into a PET image.

There are a number of radioisotopes that have applications in PET imaging. The most prevalent PET radioisotope, as well as the most important isotope in the radiopharmaceutical industry due to 2-deoxy-2'-fluoro-D-glucose (FDG), is fluorine-18 ( $^{18}\text{F}$ ). F-18 is a cyclotron-produced radioisotope made from an oxygen-18 ( $^{18}\text{O}$ ) enriched target. The half-life of 110 minutes allows the isotope to be made off-site and shipped to facilities for use. Most commonly the radioisotope is shipped as synthesized [ $^{18}\text{F}$ ]-FDG. [ $^{18}\text{F}$ ]-FDG is used to monitor glucose metabolism and has gained popularity in the field of oncology due to the high metabolic activity observed in most types of malignant tumours. [ $^{18}\text{F}$ ]-FDG can also be used to monitor treatment regimens. Unfortunately, [ $^{18}\text{F}$ ]-FDG uptake is not specific to tumours, but is also taken up by areas of natural high glucose metabolism such as the brain and kidney. Therefore, there is interest in developing a peptide-based targeting agent that bears fluorine-18 and can achieve higher specificity for its target. Due to the small atomic radius of fluorine, it can be integrated into many biomolecules without greatly affecting the binding region. Fluorine-18 has been integrated into most natural peptides such as somatostatin,  $\alpha$ -melanocyte stimulating hormone (MSH), neurotensin, RGD, and bombesin.<sup>3, 4</sup> In addition to fluorine, carbon,



which is known for its ability to form a vast number of compounds, also has a radioactive isotope, carbon-11 ( $^{11}\text{C}$ ). Carbon-11 has a short half-life of 20.4 minutes and can be incorporated into many molecules resulting in a negligible isotope effect. Due to its half-life, it is most suited for short-lived radiopharmaceuticals in facilities that have access to an in-house cyclotron. Gallium-68 ( $^{68}\text{Ga}$ ) is an additional radiometal with a 68-minute half-life that is gaining popularity as a PET isotope. The parent isotope, germanium-68 ( $^{68}\text{Ge}$ ), has a 271-day half-life, allowing it to be packaged into a  $^{68}\text{Ge}/^{68}\text{Ga}$  generator that functions similarly to the  $^{99}\text{Mo}/^{99\text{m}}\text{Tc}$  generators. Since germanium-68 has a long half-life, these generators can last over a year before being replaced. The most common use for gallium-68 is DOTA-TOC, a peptide-based imaging agent used to target somatostatin receptors in neuroendocrine tumours.<sup>5,6</sup>

The choice of radionuclide is dependent on the half-life, availability, method of incorporation, and method of radioactive decay. The half-life must be long enough to withstand synthesis, administration and distribution of the probe while maintaining enough radioactivity to be detectable by the imaging modality. The availability and proximity of a cyclotron limits the choice of radionuclides to generator-produced isotopes that can be produced on-site. There are different methods for incorporating a radioisotope that will be mentioned later on. The positron emission energy is an important aspect of PET imaging. Isotopes with lower positron emission energy, usually measured in electron volts (eV), produce images with higher resolution than those with higher positron emission energy.

On the other hand, optical imaging is a low cost, high sensitivity and facile method of molecular imaging. In order to successfully synthesize an optical imaging agent, a targeting entity must contain a fluorophore signaling source for external detection.<sup>7</sup> Fluorophores used in the early development of optical imaging emitted photons of 300 to 600 nm after excitation by an external source. Unfortunately, due to the many structures within a cell, the scattering and absorption of the shorter photons in the visible region limited the use of these fluorophores for *in vivo* applications. Longer wavelengths in the near-infrared (NIR) region of 600 to 900 nm are less likely to be absorbed and scattered by the structures within cells. This allows photons emitted in the NIR region to penetrate

tissue several centimeters deep.<sup>8</sup> These longer wavelengths are capable of penetrating tissues and expand the use of fluorescence to *in vivo* applications that were not previously applicable.<sup>9</sup>

With respect to oncology, optical imaging and the other molecular imaging modalities have made large advancements with respect to tumour detection, staging and treatment using targeted imaging modalities, such as peptides. When it comes to removal of cancerous tissues by surgery, translation of the information gained from a PET, SPECT or MRI image can be difficult to apply to the operation field.<sup>10</sup> This makes complete resection of a tumour difficult and leads to a chance of disease reoccurrence.<sup>11</sup> NIR-OI has been used to effectively address this issue. NIR-OI has the adequate image resolution and tissue visualization required for real-time fluorescence imaging that can be used to distinguish between cancerous and healthy tissue not apparent to the naked eye.<sup>10</sup> Using this technique, surgeons can effectively visualize and remove the cancerous tissue leaving all healthy tissues intact and limiting the chance of disease reoccurrence. One example of this was evaluated in colonic dysplasia using an octapeptide, QPIHPNNM, bearing a NIR Cyanine-5.5 (Cy-5.5) dye.<sup>12</sup> Using real time fluorescence imaging, NIR images were collected endoscopically in mice with colonic dysplasia. There was significant contrast between areas of dysplasia and normal colonic mucosa not visualized in the white light image.<sup>12</sup>

### 1.3 Methods for Adding Radionuclides to Peptides

In an ideal situation, a radionuclide would be added into a natural peptide sequence without changing the biological behaviour of the peptide, such as binding to a protein receptor. This is generally not the case and different methods of incorporation have varying levels of effect on binding affinity. Addition of a radionuclide can be achieved in four general ways: pendant labelling, integrated labelling, prosthetic group incorporation, or direct labelling (Figure 1.2). Most commonly, radiometals are attached to peptides

through pendant labelling. This method requires a bifunctional metal chelator to be

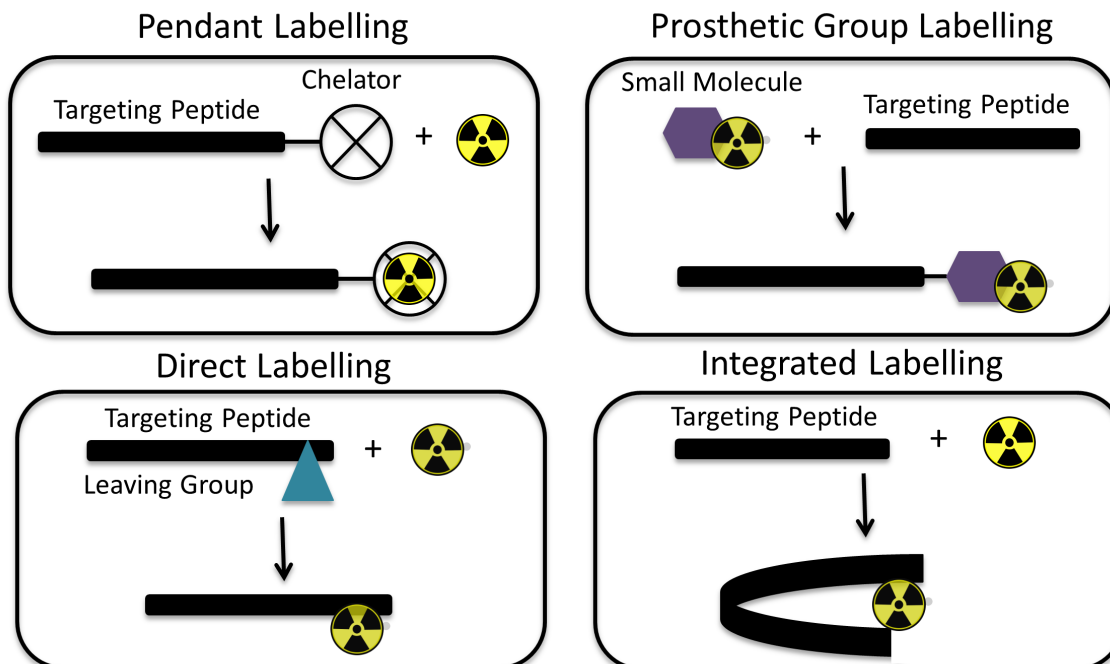


**Figure 1.2** Various methods for introducing a radioisotope into a peptide sequence: pendant labelling, prosthetic group labelling, direct labelling and integrated labelling.

appended to the peptide sequence; bifunctional in that the chelator can be attached to the peptide and also can coordinate a metal. Cyclic chelators, such as 1,4,7,10-tetraazacyclododecane-1,4,7,10-tetraacetic acid (DOTA) and 1,4,7-triazacyclononane-1,4,7-trisacetic acid (NOTA), are used for radiometals including  $^{67}\text{Ga}$ ,  $^{68}\text{Ga}$ , and  $^{64}\text{Cu}$ . Acyclic multidentate chelators such as diethylene triamine pentaacetic acid (DTPA) and 6-hydrazinonicotinic acid (HYNIC) analogues, can also be used (Figure 1.3).<sup>13-15</sup> It is challenging to incorporate these chelators into a peptide without having a detrimental effect upon the ability of the peptide to target a protein receptor. Due to the size of the chelation moiety, it must be located away from the binding region within the sequence to avoid steric interactions or other undesirable non-covalent interactions with the receptor. To achieve this distance, the chelators are often placed at the *N*- or *C*-terminus of the peptide, on an amino acid side chain such as lysine, or following an aliphatic spacer. This additional linkage increases the molecular weight of the peptide and is therefore not an ideal way to radiolabel small targeting peptides. Integrated labelling, on the other hand,

aims to hide a radiometal within the targeting peptide resulting in the metal being a key structural component of the peptide. One approach to this is to have the metal induce secondary structure formation, such as cyclization of the peptide, around the isotope. Examples of this method are used for cyclization of natural peptides such as gonadotropin-releasing hormone and somatostatin during technetium chelation.<sup>16-18</sup> This mode of concealing the isotope within the peptide would ideally have little effect on the binding affinity of the targeting entity. The third method for radiolabelling a peptide is the prosthetic group labelling approach, which is ideal for radionuclides with lower atomic mass, such as <sup>18</sup>F and <sup>11</sup>C. A small molecule is developed as a precursor for radiolabelling that can be easily incorporated into an amino acid side chain in one or two synthetic steps. This method often includes purification and deprotection steps to achieve a final pure radiolabelled peptide. In order to retain radiochemical yield, time efficient and high yielding reactions must be used for every synthetic step, especially when working with short-lived radionuclides. The most common synthetic approaches for incorporating fluorine-18 into a prosthetic group are nucleophilic acyl substitution and nucleophilic aromatic substitution.<sup>19,20</sup> The development of bioorthogonal chemistry has led to high yielding, high specificity reactions capable of incorporating a radiolabelled prosthetic group into a natural peptide sequence. These reactions include Staudinger ligation, azide-alkyne Huisgen cycloaddition, and inverse demand Diels-Alder cycloadditions.<sup>21, 22</sup> Prosthetic group labelling has led to increases in reaction rates and yields; however, the numerous synthetic and purification steps required are detrimental to overall radiochemical yields. In order to further improve radiochemical yields, a direct labelling approach has become increasingly popular. This method places a radionuclide on a modified amino acid side chain using a simple one-step reaction. However, the main challenge with this method is to obtain site specific radiolabelling without disrupting the functionality of the side chains, which may contain amines, carboxylic acids or amides that are found in most peptide sequences. The direct labelling method has had varying success with respect to radiochemical yields, with a variety of approaches being described, including: di-*tert*-butylsilyl functionalized bombesin analogues, one-step nucleophilic aromatic substitution with a trimethylammonium leaving group, chelation of

[<sup>18</sup>F] aluminium fluoride, and nucleophilic aromatic substitution on an aromatic ring with a nitro leaving group containing withdrawing groups in ortho and para positions.<sup>23-25</sup>

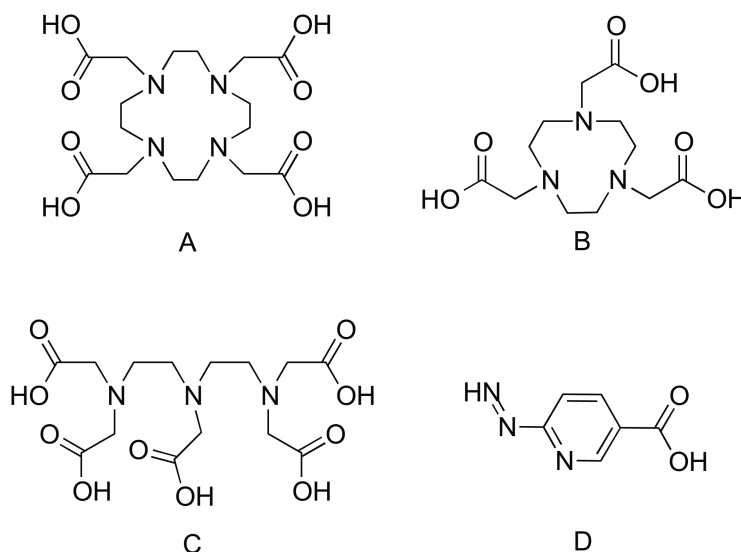


**Figure 1.3** Common cyclic and acyclic chelators capable of chelating various radiometals: (A) 1,4,7,10-tetraazacyclododecane-1,4,7,10-tetraacetic acid (DOTA), (B) 1,4,7-triazacyclononane-1,4,7,-trisacetic acid (NOTA), (C) diethylenetriamine-*N,N,N',N',N''*-pentaacetic acid (DTPA), (D) 6-hydrozinonicotinic acid (HYNIC).

## 1.4 Modifying Radiolabelled Peptides for Improved *In Vivo* Stability and Target Affinity

Peptides as targeting vectors offer many advantages with respect to other molecules, but of course come with their own set of limitations. Natural peptides are known to have poor oral bioavailability as well as low metabolic stability *in vivo*. Poor oral bioavailability is less of a concern for imaging agents as opposed to therapeutic drugs, since radiopharmaceuticals are typically administered intravenously, while poor metabolic stability can be overcome using structural modifications designed to inhibit enzymatic degradation. Peptides are often degraded by exopeptidases, enzymes that specifically hydrolyze the *C*- and *N*-termini of a linear peptide. In order to resist exopeptidase degradation, the functionality of the termini can be altered. The simplest approach is to have the *C*-terminus synthesized as an amide and the *N*-terminus acetylated. Degradation by exopeptidases can also be countered by head-to-tail cyclization, which removes the

termini completely. Endopeptidases that are capable of hydrolyzing peptide bonds within a peptide sequence are also of concern. Endopeptidases are only able to recognize natural L-amino acids; therefore replacing positions of hydrolysis with D-amino acid or unnatural amino acid residues causes the peptides to become unrecognizable to the peptidase. Contrary to the standard alpha-( $\alpha$ ) amino acids, unnatural beta-( $\beta$ ) and gamma-( $\gamma$ ) amino acid substitutions have the ability to arrange amino acid side chains into specific three-dimensional conformations, tending to form helical and pleated sheet-like structural motifs (Figure 1.4).<sup>26</sup> These small structural modifications result in greater *in vivo* stability, while the peptide sequence remains virtually unchanged, allowing it to maintain target affinity.

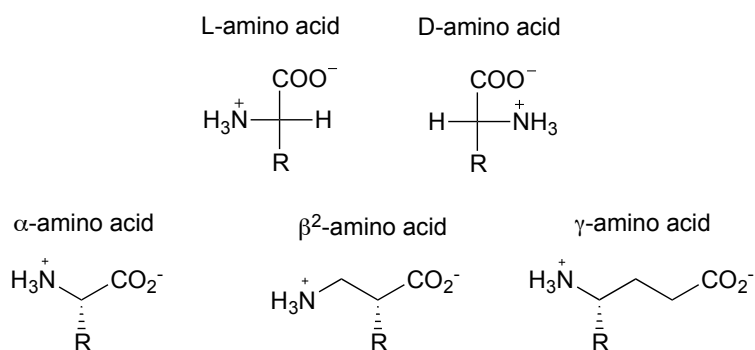


**Figure 1.4** Stereochemistry of natural L-amino acids as well as unnatural D-amino acids,  $\alpha$ -amino acids,  $\beta$ -amino acids, and  $\gamma$ -amino acids. R represents the applicable amino acid side chains.

A more complex method to increasing *in vivo* stability is to employ the pseudo-peptide approach. Pseudo-peptides resemble the natural peptide structure, but contain chemical modifications to the backbone that render them unrecognizable to peptidases. Some examples include peptoids, aza-peptides, and amide-bond surrogates as shown in Figure 1.5. Peptoids, also known as *N*-substituted glycine's, have not only been found to increase peptide stability but also increase cell permeability by 20-fold compared to the analogous peptide sequence. Attachment of the peptide side chains to the backbone nitrogen eliminates the polar N-H bond causing an increase in lipophilicity, and in turn, an increase in cell permeability.<sup>26</sup> Aza-peptides, which replace one or more alpha-carbons with a nitrogen atom, have been shown to result in a loss of stereogenicity and reduced flexibility by replacing the rotatable  $\alpha$ C-C(O) bond with a more rigid  $\alpha$ N-C(O) bond.

This reduction in flexibility has shown turn-inducing capabilities when the aza-residue is placed in the  $i+1$  or  $i+2$  position favouring beta-turn conformations.<sup>27, 28</sup> Amide bond surrogates are designed to mimic the geometric structure of a peptide bond as well as maintaining the positioning of side chains. Well known amide bond surrogates include thioamides, esters, alkenes and fluoroalkenes but could be more detrimental to *in vivo* stability. Thioamides are the most closely related surrogate to the standard amide bond based on its number of atoms and the arrangement of valence electrons. Sulphur is a poor hydrogen bond acceptor compared to oxygen, but the nitrogen proton maintains hydrogen bond donation when part of a thioamide. Ester substitutions, although geometrically similar to amide bonds, are not able to undergo hydrogen bond donation and act as poor hydrogen bond acceptors, resulting in poor stability of secondary structure. More importantly, esters are vulnerable to hydrolysis *in vivo* and are therefore not an attractive surrogate. Alkene surrogates, on the other hand, completely lack a heteroatom capable of non-covalent interactions but remain a popular peptide bond substitution due to their ability to accurately mimic rigidity, bond angle, and bond length. It must be noted that alkenes are susceptible to isomerization, oxidation and chemical liability *in vivo*; however, they have been successfully incorporated into natural peptides such as the tripeptide RGD and C-X-C chemokine receptor 4 CXCR4.<sup>29, 30</sup> Heterocyclic moieties, such as 1,2,4-oxadiazole, 1,3,4-oxadiazole, 1,2,4-triazole and 1,2,3-triazole are also used as amide bond mimics.<sup>31, 32</sup> A variety of strategies can be used to increase *in vivo* stability of natural peptides ranging from simply exchanging L and D amino acids to more complex substitution of pseudo-peptides. Each approach is accompanied by its own advantages and disadvantages dependent on the natural peptide, target, and mode of action. Finding the optimal peptide analogue can require various permutations in peptide structure and the preparation and analysis of large libraries of peptide analogues is advantageous for discovering the most suitable candidate.

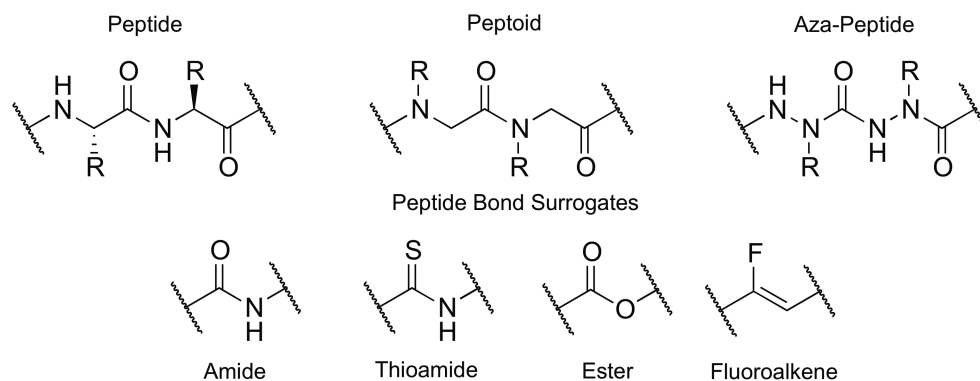


**Figure 1.5** Various backbone modifications to alter *in vivo* stability of natural peptides. R represents various amino acid side chains.

Much of the development of receptor targeting peptides has focused on receptor agonists. Agonists are known to possess high binding affinities for their receptors that trigger internalization of the ligand-receptor complex. It was rationalized that the internalization and accumulation of the radioligand in the cell over time would lead to better target-to-background ratios and overall a better radiopharmaceutical. It wasn't until the late 1990's that attention began to shift from agonists to potent antagonists. Antagonists are capable of binding orthosteric and/or allosteric sites on a receptor without eliciting a biological response and therefore, are not internalized, as agonists would be. Comparative studies show that antagonists have better chemical stability and longer duration of action than an agonist as well as binding can persist up to 8 days.<sup>33</sup> Many well-known receptor targets have been investigated for antagonist ligands and have resulted in improved stability and *in vivo* stability.

## 1.5 Modifying Natural Peptides for Improved Pharmacokinetics

The success of any pharmaceutical agent is dependent on its pharmacokinetics. Undesirable pharmacokinetics leads to faster degradation and clearance of the pharmaceutical. Elimination of radiolabelled peptides occurs rapidly and mainly by renal excretion. Rapid excretion of such molecules is advantageous for creating high quality images with low background activity but unfortunately radiolabelled peptides are often trapped in the kidneys due to tubular reabsorption.<sup>34</sup> The exact mechanism of this process



is not completely understood but studies suggest that megalin, a multiligand receptor, plays an important role. Retention in the kidneys not only causes high background noise, but also delivers high radiation doses. Renal uptake of various radiolabelled peptides has been reduced by co-administration of cationic amino acids, such as lysine and arginine, yet these methods come with undesired physical effects such as nausea and nephrotoxicity.<sup>35, 36</sup> Reducing renal uptake has also been achieved by co-administration of albumin, a megalin substrate.<sup>35</sup>

## 1.6 Increasing Receptor Affinity using Multimerization

In 1998, Mammen introduced the theoretical framework for multivalency by stating that biological species can have multiple simultaneous interactions with ligands or receptors at any one time.<sup>37</sup> Mammen also stated that polyvalency creates stronger interactions between biological entities.<sup>37</sup> Building off this theoretical framework, peptide multimers were hypothesized as a viable method to increase affinity of any monomeric targeting entity. Two types of multimers can exist; homomultimers or heteromultimers (Figure 1.6). Homomultimers contain two or more copies of identical targeting entities in one compound, for example, two copies of RGD tethered together.<sup>38</sup> In contrast, heteromultimers contain two or more different targeting entities in one compound, for example bombesin and RGD.<sup>39</sup>

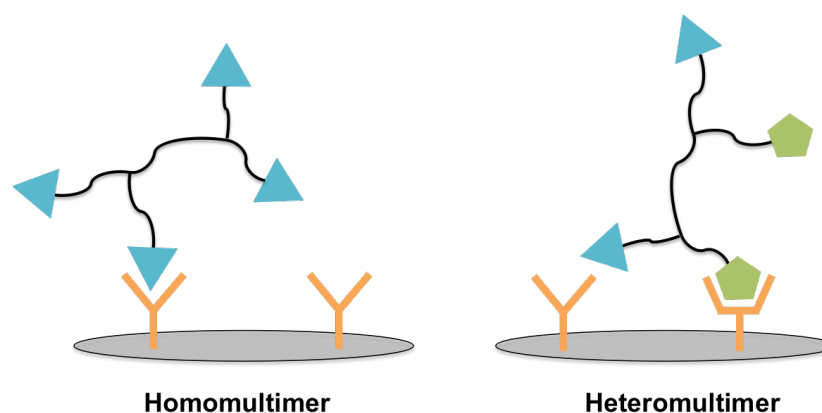


**Figure 1.6** Pictorial representation of receptor targeting with homomultimers and heteromultimers.

Peptide homodimers, or homomultimers have been well documented to obtain better binding affinity to biological targets than their monomeric counterparts. The increased binding affinity is caused by higher local concentration of the targeting entity around the receptor. More copies of the targeting entity in the immediate surroundings of the receptor creates a shielding effect that reduces the competition of other endogenous ligands for the receptor.<sup>40</sup> Therefore, after the receptor dissociates from the bound ligand, it is more likely to bind another copy of the targeting entity in the homodimer or homomultimer. Extensive studies have been done on multimerization using RGD, an integrin  $\alpha_v\beta_3$  targeting peptide, by synthesizing a homodimer, homotetramer and homooctamer of the peptide and integrated radionuclides for *in vitro* and *in vivo* detection. The binding affinity was directly dependent on the number of copies of RGD in each compound. The highest binding affinity was observed with the homooctamer, followed by the homotetramer, homodimer and finally the monomer.<sup>41</sup>

The basis for developing heteromultimers is based on the fact that the cell surfaces of diseased cells expression many different receptor subtypes. Integrating two targeting entities into one molecule creates a dual targeting approach. Studies have shown that heterodimers a bombesin/RGD result in better imaging results when compared to the monomeric counterparts.<sup>42</sup> This phenomenon is caused by an increase in overall receptor density. When targeting two receptor subtypes, the total available receptor binding sites increases to the sum of both receptors, where as monomeric targeting entities have less available binding sites in comparison.<sup>40</sup>

Multimerization is still a new concept in the area on molecular imaging but initial research supports the development of homomultimers and heteromultimers to improve binding affinity of monomeric peptide targeting entities. The design of these peptides can be difficult without a thorough understanding of the receptor expression. Various analogues of dimers may be necessary to optimize the molecular space between targeting entities and the overall three-dimensional conformation of the multimeric compound.<sup>43</sup>

## 1.7 Growth Hormone Secretagogue Receptor-1a and Ghrelin

Ghrelin is found within the growth hormone secretagogue family that was previously made up of small synthetic molecules known as growth hormone releasing peptides (GHRP).<sup>44</sup> Secretagogues stimulate the release of hormones, mainly growth hormone, from the pituitary by activating a G-protein coupled receptor, GHS-R1a. In 1999, Kojima was the first to discover the endogenous ligand for GHS-R1a that remained unknown for so long. It was discovered that ghrelin stimulates the release of growth hormone without affecting any other hormone release. The purified ligand resulted in a 28 amino acid peptide containing an n-octanoylated serine at residue 3. This ligand was named ghrelin from the Proto-Indo-European word “ghre” meaning grow.<sup>45</sup> The octanoylation observed in human ghrelin has not been observed previously in peptide modifications, thus this suggests that this modification happens in a post-translational manner. More interestingly, there is no structural homology between ghrelin and the synthetic GHSs previously discovered. Ghrelin also has no sequence homology to any known biologically active peptides.<sup>45</sup>

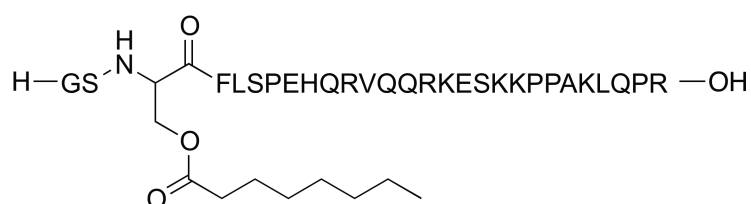


**Figure 1.7** The structure of natural human ghrelin.

Immediately after the discovery of ghrelin, the scientific community became very excited to understand the critical structural features involved in the ghrelin/GHS-R1a interaction. A mere four months after the discovery of the ghrelin sequence, the first modified ghrelin analogues were published. This study began investigating the role of the octanoylated serine side chain by introducing various other aliphatic and aromatic acids within that position, the biological importance of the ester linkage at the serine side chain by replacing this linkage with an amide bond and finally, the minimum human ghrelin

segment capable of activating GHS-R1a by synthesizing various truncated analogues (Table 1.2).<sup>46</sup>

Replacing the octanoylated side chain with hydrophobic acids of comparable size, such as unsaturated 2,4,6-octatrienoic acid or 11-undecanoic acid, resulted in compounds with comparable affinity to GHS-R1a. Although incorporation of amino and amido groups within the side chain resulted in detrimental binding affinity. Replacement of the ester linkage with an amide linkage had little effect on binding affinity resulted in a more stable linkage that is not susceptible to esterases or acyl migration. Finally, synthesis of various truncated ghrelin analogues from ghrelin(1-23) to ghrelin(1-4) were synthesized and determined that the first 5 N-terminal amino acids are required to not only bind to GHS-R1a but also to elicit effective activation of GHS-R1a.<sup>46</sup> A similar study was published in 2001 by Mutsumoto and supported the previous findings.<sup>47</sup>

**Table 1.2** Published Modified Ghrelin Analogues.

Ghrelin Analogue	Residue 3	Literature IC50 (nM)	Ref.
Ghrelin (1-28)	Ser(octanoyl)	0.25	42
Ghrelin(1-28)	Ser(2,4,6-octatrienoic acid)	0.98	42
Ghrelin(1-28)	Ser(11-undecanoic acid)	0.12	42
Ghrelin(1-28)	Ser((CH <sub>2</sub> ) <sub>6</sub> NH <sub>2</sub> )	>2000	42
Ghrelin(1-28)	Ser((CH <sub>2</sub> ) <sub>2</sub> CO-NH-(CH <sub>2</sub> ) <sub>2</sub> CH <sub>3</sub> )	1020	42
Ghrelin(1-28)	Dpr(octanoyl)	0.42	42
Ghrelin(1-23)	Ser(octanoyl)	0.16	42
Ghrelin(1-5)	Ser(octanoyl)	55	42
Ghrelin(1-4)	Ser(octanoyl)	889	42

The role of ghrelin is well known to control growth hormone release, metabolism, appetite and insulin secretion but interestingly, ghrelin has been shown more involvement in the various stages of cancer such as cell migration, proliferation and apoptosis.<sup>48</sup> From

as early as 2001, the presence of ghrelin production has been noted in many cancer subtypes such as adrenocortical, breast, colorectal, endocrine pancreatic, endometrial, gastric, lung, ovarian, pituitary, prostate, renal, and testicular cancers.<sup>49-57</sup>

Recently, a fluorescent-ghrelin(1-18) analogue was developed and was able to distinguish prostate cancer from benign hyperplasia in *ex vivo* prostate tissue (Figure 1.7).<sup>58</sup> Additionally, this optical agent was investigated for its ability to image the heart and may be useful for the imaging of cardiac myopathy, a complication of diabetes.<sup>59</sup>

Recently, a fluorescent-ghrelin(1-18) analogue was developed and was able to distinguish prostate cancer from benign hyperplasia in *ex vivo* prostate tissue (Figure 1.7).<sup>52</sup> Additionally, this optical agent was investigated for its ability to image the heart and may be useful for the imaging of cardiac myopathy, a complication of diabetes.<sup>53</sup>

Two approaches to the radiolabelling of ghrelin have been explored. The first approach is the classical method of adding a metal chelator pendant to the peptide analogues at the C-terminus via a lysine residue. In one instance, a DOTA conjugated ghrelin(1-19), which also contained a diaminopropanoic acid residue in position three, was radiolabelled with gallium-68 for use as a PET imaging agent and the gallium-69/71 variant was determined to have an  $IC_{50}$  of 9.1 nM for the GHSR.<sup>60</sup> In another instance, a monodentate isocyanide ligand conjugated ghrelin(1-6) was radiolabelled with technetium-99m and determined to have an  $IC_{50}$  of 45 nM for GHSR.<sup>61</sup> The second approach is an integrated design whereby the radioisotope is attached as part of a lipophilic side chain, replacing the octanoyl side chain of native ghrelin. Fluorine-containing side chains, both in the form of an aliphatic chain and as an aromatic entity, have been reported and the addition of a bulky fluoronaphthyl group appears the most promising to date for eventual use as a fluorine-18 labelled ghrelin analogue.<sup>62</sup> In addition, a side chain containing a rhenium cyclopentadienyl tricarbonyl group has also been discovered to have GHSR affinity and is a unique discovery in that it is a rare example where an organometallic species is a key recognition element for a peptide-receptor interaction.<sup>63</sup>

## 1.8 Summary

This thesis will document the development of human ghrelin from 28 amino acids, to 19 amino acids and subsequently to 8 amino acids while maintaining affinity to GHS-R1a. During these truncations, optical dyes and radioisotopes have been integrated into various positions of the peptide sequence without detriment effects on affinity and enabling these peptide to visualize GHS-R1a using optical imaging (OI) or PET. Chapter 2 will cover the first generation ghrelin(1-19) analogue bearing gallium-68 and the evaluation of this probe in preclinical studies. Chapter 3 will then cover the second generation of ghrelin(1-8) analogues including an extensive structural activity study followed by optimization of fluorine-18 for future use in preclinical PET studies. Chapter 4 will investigate the possible multimerization of a ghrelin(1-8) analogue into ghrelin(1-10) bearing a near-infrared dye, cyanine-5. Chapter 5 will draw together all aspects of this thesis and summarize the strengths and weaknesses of ghrelin as an imaging agent capable of targeting GHS-R1a.

## 1.9 References

1. M. Fani, H. R. Maecke and S. M. Okarvi, *Theranostics*, 2012, **2**, 481-501.
2. S. R. Meikle, P. Kench, M. Kassiou and R. B. Banati, *Physics in medicine and biology*, 2005, **50**, R45-61.
3. Z. Cheng, L. Zhang, E. Graves, Z. Xiong, M. Dandekar, X. Chen and S. S. Gambhir, *J. Nucl. Med.*, 2007, **48**, 987-994.
4. X. Zhang, Z. Xiong, Y. Wu, W. Cai, J. R. Tseng, S. S. Gambhir and X. Chen, *J. Nucl. Med.*, 2006, **47**, 113-121.
5. M. Gabriel, C. Decristoforo, D. Kendler, G. Dobrozemsky, D. Heute, C. Uprimny, P. Kovacs, E. Von Guggenberg, R. Bale and I. J. Virgolini, *J. Nucl. Med.*, 2007, **48**, 508-518.
6. I. Virgolini, V. Ambrosini, J. B. Bomanji, R. P. Baum, S. Fanti, M. Gabriel, N. D. Papathanasiou, G. Pepe, W. Oyen, C. De Cristoforo and A. Chiti, *Eur. J. Nucl. Med. Mol. Imaging*, 2010, **37**, 2004-2010.
7. H. Kobayashi, M. Ogawa, R. Alford, P. L. Choyke and Y. Urano, *Chemical reviews*, 2010, **110**, 2620-2640.

8. R. B. Schulz and W. Semmler, *Handbook of experimental pharmacology*, 2008, 3-22.
9. V. Ntziachristos, *Nature methods*, 2010, **7**, 603-614.
10. S. Keereweer, J. D. Kerrebijn, P. B. van Driel, B. Xie, E. L. Kaijzel, T. J. Snoeks, I. Que, M. Hutteman, J. R. van der Vorst, J. S. Mieog, A. L. Vahrmeijer, C. J. van de Velde, R. J. Baatenburg de Jong and C. W. Lowik, *Mol Imaging Biol*, 2011, **13**, 199-207.
11. L. E. Kelderhouse, V. Chelvam, C. Wayua, S. Mahalingam, S. Poh, S. A. Kularatne and P. S. Low, *Bioconjug Chem*, 2013, **24**, 1075-1080.
12. Z. Liu, S. J. Miller, B. P. Joshi and T. D. Wang, *Gut*, 2013, **62**, 395-403.
13. D. Psimadas, P. Georgoulas, V. Valotassiou and G. Loudos, *J. Pharm. Sci.*, 2012, **101**, 2271-2280.
14. L. K. Meszaros, A. Dose, S. C. Biagini and P. J. Blower, *Dalton Trans.*, 2011, **40**, 6260-6267.
15. R. Schibli and P. A. Schubiger, *Eur. J. Nucl. Med. Mol. Imaging*, 2002, **29**, 1529-1542.
16. J. R. Morgan, D. V. Nguyen, A. R. Frohman, S. R. Rybka and J. A. Zebala, *Bioconjugate Chem.*, 2012, **23**, 2020-2024.
17. Y. Barda, N. Cohen, V. Lev, N. Ben-Aroya, Y. Koch, E. Mishani, M. Fridkin and C. Gilon, *Nucl. Med. Biol.*, 2004, **31**, 921-933.
18. G. Fridkin, T. A. Bonasera, P. Litman and C. Gilon, *Nucl. Med. Biol.*, 2005, **32**, 39-50.
19. J. Becaud, L. Mu, M. Karamkam, P. A. Schubiger, S. M. Ametamey, K. Graham, T. Stellfeld, L. Lehmann, S. Borkowski, D. Berndorff, L. Dinkelborg, A. Srinivasan, R. Smits and B. Kokschi, *Bioconjugate Chem.*, 2009, **20**, 2254-2261.
20. P. Carberry, B. P. Lieberman, K. Ploessl, S. R. Choi, D. N. Haase and H. F. Kung, *Bioconjugate Chem.*, 2011, **22**, 642-653.
21. S. H. Hausner, J. Marik, M. K. Gagnon and J. L. Sutcliffe, *J Med Chem*, 2008, **51**, 5901-5904.
22. E. M. Sletten and C. R. Bertozzi, *Angew. Chem. Int. Edit.*, 2009, **48**, 6974-6998.
23. W. J. McBride, R. M. Sharkey, H. Karacay, C. A. D'Souza, E. A. Rossi, P. Laverman, C. H. Chang, O. C. Boerman and D. M. Goldenberg, *J. Nucl. Med.*, 2009, **50**, 991-998.

24. A. Hohne, L. Mu, M. Honer, P. A. Schubiger, S. M. Ametamey, K. Graham, T. Stellfeld, S. Borkowski, D. Berndorff, U. Klar, U. Voigtmann, J. E. Cyr, M. Friebe, L. Dinkelborg and A. Srinivasan, *Bioconjugate Chem.*, 2008, **19**, 1871-1879.
25. O. Jacobson, L. Zhu, Y. Ma, I. D. Weiss, X. Sun, G. Niu, D. O. Kiesewetter and X. Chen, *Bioconjugate Chem.*, 2011, **22**, 422-428.
26. P. Wipf, J. Xiao and C. R. Stephenson, *Chimia*, 2009, **63**, 764-775.
27. D. Boeglin and W. D. Lubell, *J. Comb. Chem.*, 2005, **7**, 864-878.
28. N. S. Freeman, Y. Tal-Gan, S. Klein, A. Levitzki and C. Gilon, *J. Org. Chem.*, 2011, **76**, 3078-3085.
29. T. Narumi, R. Hayashi, K. Tomita, K. Kobayashi, N. Tanahara, H. Ohno, T. Naito, E. Kodama, M. Matsuoka, S. Oishi and N. Fujii, *Org. Biomol. Chem.*, 2010, **8**, 616-621.
30. S. Oishi, K. Miyamoto, A. Niida, M. Yamamoto, K. Ajito, H. Tamamura, A. Otaka, Y. Kuroda, A. Asai and N. Fujii, *Tetrahedron*, 2006, **62**, 1416-1424.
31. S. Borg, G. Estenne-Bouhtou, K. Luthman, I. Csoeregh, W. Hesselink and U. Hacksell, *J. Org. Chem.*, 1995, **60**, 3112-3120.
32. V. D. Bock, D. Speijer, H. Hiemstra and J. H. van Maarseveen, *Org. Biomol. Chem.*, 2007, **5**, 971-975.
33. P. C. Wynn, C. A. Suarez-Quian, G. V. Childs and K. J. Catt, *Endocrinology*, 1986, **119**, 1852-1863.
34. A. Choudhary and R. T. Raines, *Chem Biochem*, 2011, **12**, 1801-1807.
35. E. Vegt, J. E. van Eerd, A. Eek, W. J. Oyen, J. F. Wetzels, M. de Jong, F. G. Russel, R. Masereeuw, M. Gotthardt and O. C. Boerman, *J. Nucl. Med.*, 2008, **49**, 1506-1511.
36. T. M. Behr, D. M. Goldenberg and W. Becker, *Eur. J. Nucl. Med.*, 1998, **25**, 201-212.
37. M. Mammen, S.-K. Choi and G. M. Whitesides, *Angewandte Chemie International Edition*, 1998, **37**, 2754-2794.
38. Z. Liu, G. Niu, J. Shi, S. Liu, F. Wang, S. Liu and X. Chen, *Eur J Nucl Med Mol Imaging*, 2009, **36**, 947-957.
39. P. Fournier, V. Dumulon-Perreault, S. Ait-Mohand, R. Langlois, F. Benard, R. Lecomte and B. Guerin, *EJNMMI research*, 2012, **2**, 8.



40. Y. Yan and X. Chen, *Amino Acids*, 2011, **41**, 1081-1092.
41. Z. B. Li, K. Chen and X. Chen, *Eur J Nucl Med Mol Imaging*, 2008, **35**, 1100-1108.
42. Z. B. Li, Z. Wu, K. Chen, E. K. Ryu and X. Chen, *J Nucl Med*, 2008, **49**, 453-461.
43. R. Pillai, E. R. Marinelli and R. E. Swenson, *Biopolymers*, 2006, **84**, 576-585.
44. C. Y. Bowers, F. A. Momany, G. A. Reynolds and A. Hong, *Endocrinology*, 1984, **114**, 1537-1545.
45. M. Kojima, H. Hosoda, Y. Date, M. Nakazato, H. Matsuo and K. Kangawa, *Nature*, 1999, **402**, 656-660.
46. M. A. Bednarek, S. D. Feighner, S.-S. Pong, K. K. McKee, D. L. Hreniuk, M. V. Silva, V. A. Warren, A. D. Howard, L. H. Y. Van der Ploeg and J. V. Heck, *J Med Chem*, 2000, **43**, 4370-4376.
47. M. Matsumoto, H. Hosoda, Y. Kitajima, N. Morozumi, Y. Minamitake, S. Tanaka, H. Matsuo, M. Kojima, Y. Hayashi and K. Kangawa, *Biochem. Biophys. Res. Commun.*, 2001, **287**, 142-146.
48. L. Chopin, C. Walpole, I. Seim, P. Cunningham, R. Murray, E. Whiteside, P. Josh and A. Herington, *Mol Cell Endocrinol*, 2011, **340**, 65-69.
49. B. Ueberberg, N. Unger, S. Y. Sheu, M. K. Walz, K. W. Schmid, W. Saeger, K. Mann and S. Petersenn, *Hormone and metabolic research = Hormon- und Stoffwechselforschung = Hormones et metabolisme*, 2008, **40**, 181-188.
50. P. L. Jeffery, R. E. Murray, A. H. Yeh, J. F. McNamara, R. P. Duncan, G. D. Francis, A. C. Herington and L. K. Chopin, *Endocrine-related cancer*, 2005, **12**, 839-850.
51. M. Papotti, P. Cassoni, M. Volante, R. Deghenghi, G. Muccioli and E. Ghigo, *J Clin Endocrinol Metab*, 2001, **86**, 5052-5059.
52. S. Ekeblad, B. Nilsson, M. H. Lejonklou, T. Johansson, P. Stalberg, O. Nilsson, H. Ahlman and B. Skogseid, *Endocrine-related cancer*, 2006, **13**, 963-970.
53. J. N. Fung, I. Seim, D. Wang, A. Obermair, L. K. Chopin and C. Chen, *Horm Cancer*, 2010, **1**, 245-255.
54. J. Y. An, M. G. Choi, J. H. Noh, T. S. Sohn, D. K. Jin and S. Kim, *The Journal of surgical research*, 2007, **143**, 344-349.

55. P. Cassoni, E. Allia, T. Marrocco, C. Ghe, E. Ghigo, G. Muccioli and M. Papotti, *J Endocrinol Invest*, 2006, **29**, 781-790.
56. F. Gaytan, C. Morales, M. L. Barreiro, P. Jeffery, L. K. Chopin, A. C. Herington, F. F. Casanueva, E. Aguilar, C. Dieguez and M. Tena-Sempere, *J Clin Endocrinol Metab*, 2005, **90**, 1798-1804.
57. P. L. Jeffery, A. C. Herington and L. K. Chopin, *The Journal of endocrinology*, 2002, **172**, R7-11.
58. C. Lu, M. S. McFarland, R.-L. Nesbitt, A. K. Williams, S. Chan, J. Gomez-Lemus, A. M. Autran-Gomez, A. Al-Zahrani, J. L. Chin, J. I. Izawa, L. G. Luyt and J. D. Lewis, *The Prostate*, 2012, **72**, 825-833.
59. R. McGirr, M. S. McFarland, J. McTavish, L. G. Luyt and S. Dhanvantari, *Regul. Peptides*, 2011, **172**, 69-76.
60. C. L. Charlton, B. McGirr, S. Dhanvantari, M. Kovacs and L. G. Luyt, *J. Labelled Comp. Radiopharm.*, 2013, **56**, S192.
61. P. Koźmiński and E. Gniazdowska, *Nucl. Med. Biol.*, 2015, **42**, 28-37.
62. M. S. McFarland, J. McTavish, S. Dhanvantari, M. Kovacs and L. G. Luyt, *J. Labelled Comp. Radiopharm.*, 2011, **54**, S430.
63. D. Rosita, M. A. DeWit and L. G. Luyt, *J Med Chem*, 2009, **52**, 2196-2203.

## Chapter 2

### 2 Development of a Novel [<sup>68</sup>Ga]-Ghrelin Analogue for PET Imaging of GHS-R1a

#### 2.1 Introduction

The endogenous ligand for the growth hormone secretagogue receptor (GHS-R) was discovered in 1999 by Kojima *et al.* and subsequently named ghrelin.<sup>1</sup> This 28 amino acid natural peptide hormone (Figure 2.1, **2.1**) was found to possess a unique post-translational modification that is not commonly seen in other peptide hormones. Through the action of ghrelin-O-acyltransferase, natural human ghrelin contains an *n*-octanoylated serine at residue 3 that has been found to be essential for its affinity and specificity to GHS-R. The highest concentration of ghrelin can be found in the stomach and this peptide is responsible for a diverse area of functions. Its primary role is to regulate growth hormone (GH) release but it has also shown to have stimulatory effects on appetite, gastric acid secretion, adiposity and gut motility.<sup>2</sup>

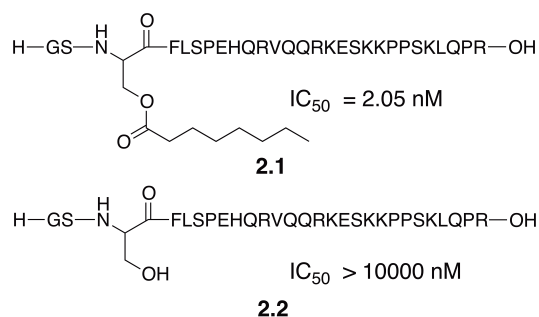


**Figure 2.1** . Amino acid sequence of natural human ghrelin (2.1) and des-acyl ghrelin (2.2) with the corresponding  $\text{IC}_{50}$  for GHS-R1a, as determined by a competitive binding assay with HEK293 cells stably transfected with GHS-R1a.

The GHS-R is present in two isoforms, types 1a and 1b. GHS-R1a is a 366 amino acid polypeptide and G-protein coupled receptor (GPCR) containing seven transmembrane domains. The third transmembrane domain has been recognized as the ligand-receptor binding pocket for human ghrelin. On the other hand, GHS-R1b is a 5-transmembrane receptor that has no binding affinity to human ghrelin and is not known to exhibit any

biological functions.<sup>3</sup> Therefore, GHS-R1a has been labelled the “ghrelin receptor”. The ghrelin receptor can be found at low concentrations in various tissues such as human brain, kidney, cardiovascular system and prostate.<sup>2,4</sup>

In addition to regulating the growth and differentiation of normal tissues, the GHS-R1a has been shown to play important roles in proliferation, apoptosis, cell invasion and migration associated with cancer progression.<sup>5-10</sup> More specifically, GHS-R1a has been found to be differentially expressed in prostate, breast, ovarian, testicular and intestinal carcinomas when compared to healthy tissue.<sup>11-14</sup> By exploiting the specificity of ghrelin to its endogenous receptor, it has been proposed that ghrelin can be used to locate these various carcinomas using molecular imaging.<sup>15</sup>

Within the literature, structure-activity studies of ghrelin have been thoroughly described.<sup>15-20</sup> These studies have revealed that the n-octanoylated serine side chain is crucial for receptor interaction. The half maximal inhibitory concentration ( $IC_{50}$ ) of natural ghrelin (**2.1**) for GHS-R1a has been reported as low as 0.25 nM and by simply removing the octanoylated modification, resulting in des-acyl ghrelin (Figure 2.1, **2.2**), the  $IC_{50}$  increases to  $>10 \mu\text{M}$ .<sup>17</sup> Truncation at the C-terminal end of ghrelin retained affinity to GHS-R1a, suggesting the N-terminal portion is more important for receptor interactions. Truncated analogues containing the octanoylated serine such as ghrelin (1-14) and ghrelin (1-5) resulted in respectable  $IC_{50}$ 's of 9.6 nM and 55 nM respectively.<sup>17</sup> Lu, et al. synthesized a ghrelin (1-19) analogue bearing a fluorescein dye at lysine<sup>19</sup> in order to optically image human *ex vivo* prostate tissue ranging from normal, benign hyperplasia, prostate interneoplasia and cancerous tissue. This modification to ghrelin resulted in an  $IC_{50}$  of 9.5 nM. Association of fluorescein-ghrelin (1-19) was found to be 4.7 times higher in cancerous prostate tissue than normal and benign hyperplasia.<sup>20</sup> This was the first example highlighting ghrelin's potential as an imaging probe for prostate cancer diagnosis and possibly for detection of metastatic disease. The ghrelin (1-19) skeleton was used again for optical imaging of cardiomyocytes by replacing the fluorescein dye in the 19<sup>th</sup> position with a cyanine-5 near-infrared dye. Replacement of the dye resulted in a slightly lower binding affinity of 25.8 nM but selective targeting of GHS-R1a is still observed. These findings support the use of ghrelin (1-19) as an

effective targeting entity in which modifications to position 19 result in minimal effect on the overall binding affinity.<sup>21</sup>

Development of ghrelin analogues into PET radiopeptides was first demonstrated with a therapeutic approach to address obesity, cachexia and anorexia. Ghrelin(1-28) and ghrelin(1-16) analogues bearing 1,4,7-triazacyclononane, 1-glutaric acid-4,7-acetic acid (NODAGA) for chelation of gallium-68 were studied *in vivo* and exhibited good receptor affinity.<sup>22</sup> Ghrelin was also developed as a SPECT radiopeptide by incorporation of technetium-99m into the ghrelin sequence using various chelating moieties. These analogues also demonstrated good receptor affinity as well as good biological properties for further development of ghrelin into diagnostic radiopharmaceuticals.<sup>23</sup>

These promising results sparked our interest in developing a ghrelin (1-19) analogue capable of bearing a radionuclide in order to detect prostate carcinomas using a more sensitive imaging technique. Herein, we describe the synthesis and evaluation of a new ghrelin (1-19) analogue capable of chelating gallium-68, a PET radionuclide, and describe preclinical *in vivo* results using this ghrelin-based PET imaging probe.

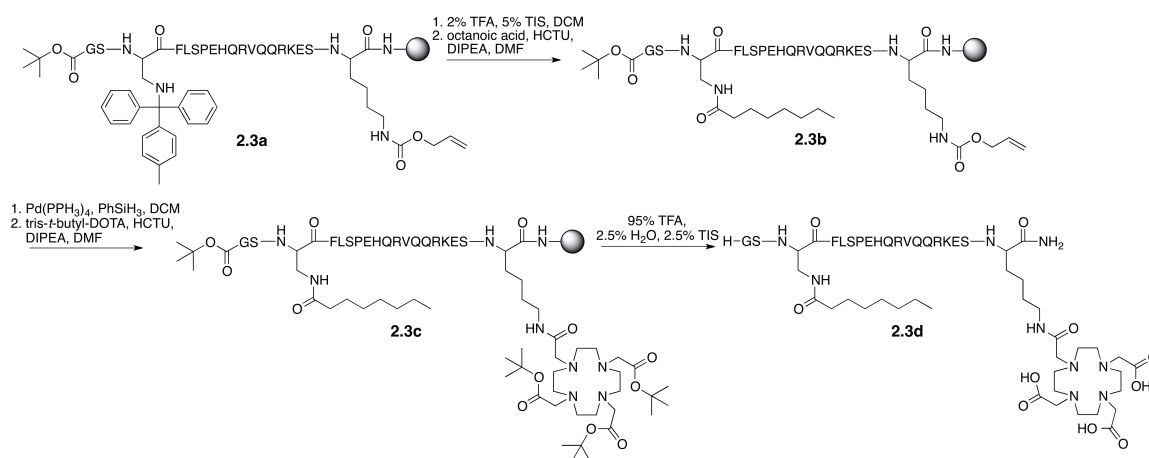
## 2.2 Results and Discussion

### 2.2.1 Design and Synthesis

Structure-activity studies performed on the ghrelin amino acid sequence suggest that only the first five N-terminal amino acids are necessary for ghrelin to maintain affinity to GHS-R1a. As more N-terminal amino acids are added, for example ghrelin (1-14), the binding affinity improves drastically. Recent literature has shown that ghrelin (1-19) is able to not only target GHS-R1a, but also tolerate modifications to position 19 without having a detrimental effect on binding affinity.<sup>20, 21</sup> In order to create a ghrelin-based PET imaging probe, the ghrelin (1-19) analogue was modified so as to possess a tris-*tert*-butyl 1,4,7,10-tetraazacyclododecane-1,4,7,10-tetraacetate (DOTA) chelator at position 19.

A non-radioactive Dpr<sup>3</sup>(octanoyl),Lys<sup>19</sup>(DOTA)-ghrelin(1-19) analogue (**2.3d**) was synthesized as a reference standard for *in vitro* assays and radiochemistry. **2.1** was truncated to contain the first 19 N-terminal amino acids and synthesized using standard

Fmoc solid-phase peptide synthesis techniques. In order to increase *in vivo* stability and incorporate a bifunctional chelating moiety, orthogonal protecting groups were used to modify residue 3 and 19 (Scheme 2.1). Within natural ghrelin, a unique octanoylated chain is appended to the serine side chain by an ester linkage at Ser-3. To reduce the occurrence of enzymatic hydrolysis of the ester *in vivo*, serine was replaced by diaminopropionic acid (Dpr). This substitution replaces the labile ester linkage with a more robust amide linkage to the octanoylated chain. Structural studies performed by Matsumoto *et. al.* revealed the active core of ghrelin is contained within *N*-terminal region of the peptide,<sup>41</sup> therefore the incorporation the bifunctional chelator tris-*tert*-butyl 1,4,7,10-tetraazacyclododecane-1,4,7,10-tetraacetate (DOTA) would cause the least effect if appended to the *C*-terminal lysine-19 side chain using a pendant design approach. Upon completion of these modifications, **2.3d** was purified by preparative HPLC. Analytical LC-MS was used to confirm the identity of the products isolated in >95% purity. **2.3d** was then coordinated to naturally occurring gallium-69/71 using gallium(III) nitrate. The non-radioactive reference standard, [<sup>69/71</sup>Ga]-**2.3d**, was used in further *in vitro* studies. The identity of the product was also confirmed by analytical LC-MS and isolated in >95% purity.



**Scheme 2.1** Synthesis of **2.3d**.

## 2.2.2 *In Vitro* Analysis

To ensure these modifications have had little detrimental effect on receptor binding, a competitive binding assay was performed on **2.3d**, and [ $^{69/71}\text{Ga}$ ]-**2.3d** against [ $^{125}\text{I}$ ]-ghrelin(1-28). The binding affinity was measured in human embryonic kidney-293 cells (HEK-293) that were transfected with the GHS-R1a receptor. Varying the concentrations of each ghrelin analogue in the presence of [ $^{125}\text{I}$ ] human ghrelin resulted in a sigmoidal binding curve in which the half maximal inhibitory concentration ( $\text{IC}_{50}$ ) values can be extrapolated (Figure 2.2). As summarized in table 2.1, **2.1** has the

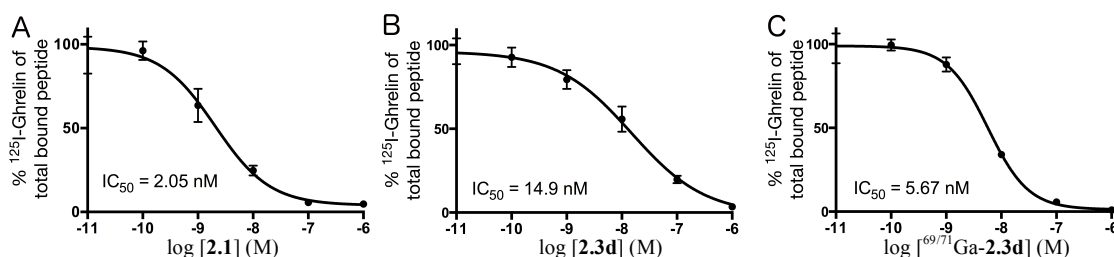


**Figure 2.2** Half-maximal inhibitory concentration curves of ghrelin analogues against [ $^{125}\text{I}$ ]-human ghrelin in HEK293/GHS-R1a cells. **2.1** (A), **2.3d** (B), [ $^{69/71}\text{Ga}$ ]-**2.3d** (C).

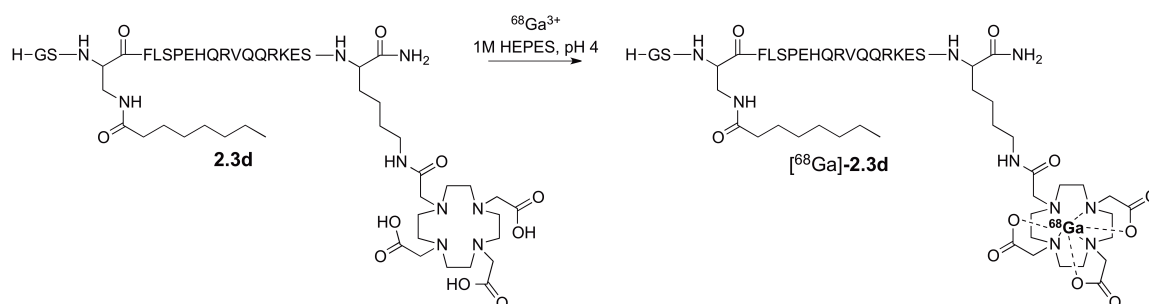
best binding affinity to GHS-R1a of 2.05 nM. When comparing the ghrelin(1-19) analogues, **2.3d** and [ $^{69/71}\text{Ga}$ ]-3d, it was observed that [ $^{69/71}\text{Ga}$ ] chelation improves the binding affinity from 14.9 nM to 5.1 nM. Matsumoto has explored the effect of charge on the C-terminal end of **2.1**. They found that elimination of the C-terminal carboxylic acid charge by amidation resulted in an eight-fold increase in potency to GHS-R1a.<sup>16</sup> This same trend is observed upon [ $^{69/71}\text{Ga}$ ] chelation to 3d. The carboxylic functionality charges present in the DOTA becomes neutral upon chelation and in turn, results in a stronger binding affinity to the GHS-R1a. The synthesized standard, [ $^{69/71}\text{Ga}$ ]-**2.3d**, possesses comparable binding affinity to GHS-R1a as the endogenous ligand 1 as well as the potential to be developed into a PET radiopeptide by complexation to radioactive gallium-68.

**Table 2.1** IC<sub>50</sub> Values for Synthesized Ghrelin Analogues **2.1**, **2.3d** and [<sup>69/71</sup>Ga]-**2.3d**

Ghrelin Analogue	IC <sub>50</sub> (nM)
<b>2.1</b>	2.05
<b>2.3d</b>	14.9
[ <sup>69/71</sup> Ga]- <b>2.3d</b>	5.67

### 2.2.3 Radiochemistry

Radiochemistry using gallium-68 (<sup>68</sup>Ga) has been investigated since the early 1970's,<sup>24</sup> but it wasn't until 2001 that breakthrough clinical work published on <sup>68</sup>Ga-DOTATOC for the imaging of neuroendocrine associated disease resulted in an interest in other clinical applications for gallium-68.<sup>25</sup> To date, Gallium-68 has been incorporated into many peptides, such as bombesin and somatostatin, to visualize various tumour models using PET.<sup>26</sup> Gallium-68 is a preferred isotope for clinical imaging because it has a short-lived half life of 68 minutes and decays 89% by positron emission. This isotope is also cost-efficient and convenient as it is produced from germanium-68/gallium-68 generators and does not require an on-site cyclotron. Gallium-68 is eluted as cationic Ga(III) and is often associated with high and reproducible peptide labelling yields.<sup>27</sup>

**Scheme 2.2** Gallium-68 chelation of **2.3d**

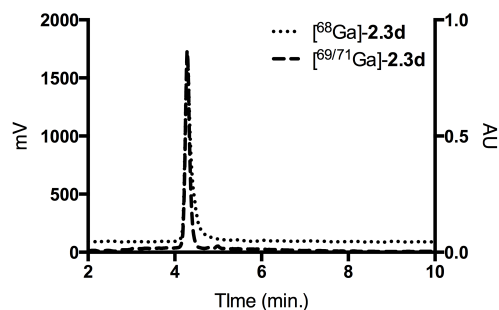
Radiolabelling of **2.3d** was optimized by varying conditions such as the mass of precursor and buffer concentration, in order to maximize radiochemical yield and specific activity. In all cases, the reaction mixture was heated at 90°C for 15 minutes before Sep Pak reverse-phase purification (Scheme 2.2). The various conditions are highlighted in



Table 2.2. Radiolabelling of 50  $\mu\text{g}$  of **2.3d** in 1 M HEPES buffer resulted in the best decay corrected yield of 96% (d.c) but did not result in a desirable specific activity. In order to increase the specific activity, the amount of **2.3d** was decreased to 25  $\mu\text{g}$ . These conditions maintained respectable yields of 45-91% (d.c) and increased the specific activity to more desirable levels, 17.6- 19.0 GBq/ $\mu\text{mol}$ . Further reduction of the amount of **2.3d** to 20  $\mu\text{g}$  resulted in similar yields of 54-83% (d.c) and resulted in the highest obtained specific activity of 10.2-22.8 GBq/ $\mu\text{mol}$ . A loss of radiochemical yield and specific activity was observed when precursor **2.3d** was further decreased to 10  $\mu\text{g}$ . Overall, the best labelling conditions for **2.3d** was determined to be 20  $\mu\text{g}$  of precursor in 1M HEPES buffer and these radiolabelling conditions remained standard for all subsequent studies. The identity of the radiolabelled [ $^{68}\text{Ga}$ ]-**2.3d** was confirmed by co-injection with [ $^{69/71}\text{Ga}$ ]-**2.3d** on RP-HPLC resulting in consistent retention times for the radiolabelled and product standard (Figure 2.3).

**Table 2.2** Radiolabelling conditions for [ $^{68}\text{Ga}$ ]-**2.3d**

Mass of <b>2.3d</b> ( $\mu\text{g}$ )	Buffer	Concentration ( $\mu\text{M}$ )	Decay Corrected Yield (%)	Specific Activity (GBq/ $\mu\text{mol}$ )
100	0.5 M HEPES	7.83	54	4.51
50	1 M HEPES	3.91	96	3.84-4.28
25	0.5 M HEPES	1.96	45-91	17.6-19.0
20	1M HEPES	1.56	54-83	10.2-22.8
10	1 M HEPES	0.78	17-23	5.39-7.72



**Figure 2.3** RP-HPLC of  $[^{69/71}\text{Ga}]\text{-2.3d}$  and  $[^{68}\text{Ga}]\text{-2.3d}$

#### 2.2.4 *In Vitro* Evaluation of $^{68}\text{Ga}$ -Ghrelin (1-19)

The uptake of  $[^{68}\text{Ga}]\text{-2.3d}$  was evaluated in GHS-R1a transfected HEK293 cells. After 60 minutes of incubation of  $[^{68}\text{Ga}]\text{-2.3d}$  with the GHS-R1a expressing cells, each of the cell pellets ( $n=6$ ) were placed on a gamma counter and quantified into counts per minute (cpm). To ensure  $[^{68}\text{Ga}]\text{-2.3d}$  is specifically targeting the same binding site on GHS-R1a, a blocking study was performed by administering non-radioactive **2.1** prior to  $[^{68}\text{Ga}]\text{-2.3d}$ . **2.1** is expected to bind the majority of available GHS-R1a before administration of  $[^{68}\text{Ga}]\text{-2.3d}$  and result in a decreased cpm as  $[^{68}\text{Ga}]\text{-2.3d}$  is no longer able to associate to these receptors. As seen in Figure 2.4, HEK293/GHS-R1a cells averaged 24744 counts/second in the presence of  $[^{68}\text{Ga}]\text{-2.3d}$ . When **2.1** is introduced along with the  $^{68}\text{Ga}$ -ghrelin, the activity taken up by the cells drops by 54%. This evidence supports that **2.1** and  $[^{68}\text{Ga}]\text{-2.3d}$  occupy the same binding region on the GHS-R1a.

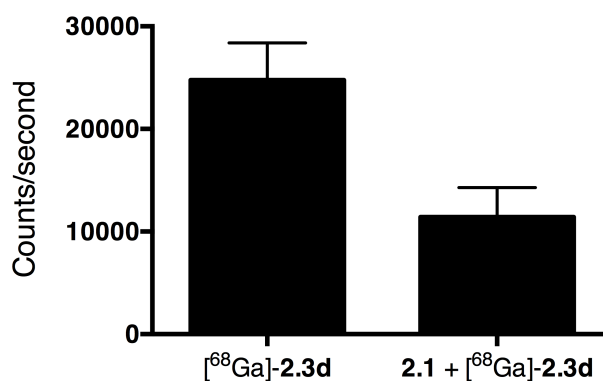


**Figure 2.4** Uptake of  $[^{68}\text{Ga}]\text{-2.3d}$  in HEK293/GHS-R1a cell with and without blocking of GHS-R1a with **2.1**.

### 2.2.5 *In Vivo* Evaluation of $^{68}\text{Ga}$ -Ghrelin (1-19)

To evaluate the effectiveness of the ghrelin-based PET imaging probe, an *in vivo* preclinical study was performed with two cell lines, HT1080/GHS-R1a and HT1080. These chosen cells lines will demonstrate the uptake of the radioligand in a xenograft overexpressing the receptor of interest compared to a xenograft with normal expression. [ $^{68}\text{Ga}$ ]-**2.3d** was studied *in vivo* in NOD/SCID male mice bearing a HT1080/GHS-R1a xenograft tumour. As a negative control model, mice bearing HT1080 xenografts were also studied. Each mouse was administered 7-10 MBq of [ $^{68}\text{Ga}$ ]-**2.3d** in a saline solution and immediately underwent a 60 minute  $\mu\text{PET}$  dynamic scan. The dynamic scans were processed into 10 minute intervals to monitor the uptake and accumulation of [ $^{68}\text{Ga}$ ]-**2.3d** in the tumour and other organs and tissues. A coronal  $\mu\text{PET}$  image (Figure 2.5A) and a three-dimensional projection (Figure 2.5C) from the small animal PET scanner was taken at the 30 to 40 minute time interval in the negative control HT1080 mice. The most notable uptake is visualized in the kidneys (k) and bladder (b). The tumour (t) is present on the right flank and accumulated a small amount of residual radioactivity. The residual radioactivity can be attributed to circulation of the [ $^{68}\text{Ga}$ ]-**2.3d** and its metabolites through the highly vascularized tumour rather than association to receptors in the HT1080 cell line. A coronal  $\mu\text{PET}$  image (Figure 2.5B) and a three-dimensional projection (Figure 2.5D) from the small animal  $\mu\text{PET}$  scanner was also taken at the 30 to 40 minute time interval in the positive HT1080/GHS-R1a mice. Similar to the control, there is high uptake in the kidneys (k) and the bladder (b). More radioactivity has now been localized and retained in the tumour (t) on the left flank. The retention of the probe is believed to be due to the active binding of [ $^{68}\text{Ga}$ ]-**2.3d** to GHS-R1a in the xenograft. The high localization of radioactivity to the kidneys is a common trait seen in radiolabelled peptides as through tubular reabsorption. Radiolabelled peptides often become trapped causing undesirable effects such as nephrotoxicity and this can be combated by reducing the presence of charged side chains within the peptide or administering a cationic amino acid prior to injection of the radiolabelled peptide.<sup>28</sup>

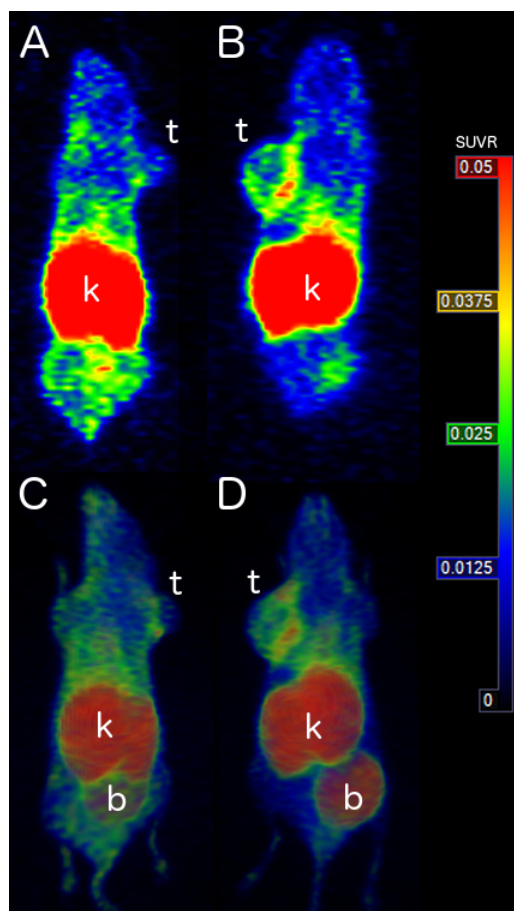


**Figure 2.5** A 60 minute dynamic uPET scan showing uptake of [ $^{68}\text{Ga}$ ]-**2.3d** from 30-40 minutes in HT1080 and HT1080/GHS-R1a xenografts. (A) HT1080 – coronal. (B) HT1080/GHS-R1a – coronal, (C) HT1080 – 3D projection and (D) HT1080/GHS-R1a – 3D projection.

To more accurately compare the uptake of [ $^{68}\text{Ga}$ ]-**2.3d** in both tumour models, standard uptake values (SUV) were calculated by designating volumes of interest (VOI) for each xenografts over the 60 minute scan using AsiPro software. The SUVs were calculated using Equation 2.1 (supplemental materials) and graphed in Figure 2.6. The SUV for HT1080/GHS-R1a xenograft mice is approximately 5 times greater than the HT1080 xenografts. These results show [ $^{68}\text{Ga}$ ]-**2.3d** is selective to xenografts that contain GHS-R1a receptors compared to those with limited receptor expression, such as the control HT1080 cell line.

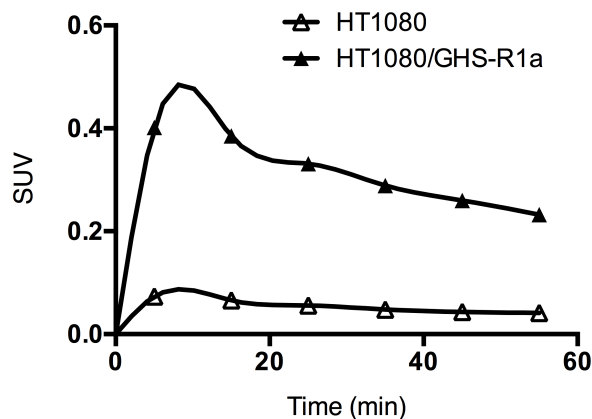


**Figure 2.6** Graphical representation of SUVs for [ $^{68}\text{Ga}$ ]-**2.3d** in HT1080/GHS-R1a and HT1080 xenographs over 60 minutes.

## 2.2.6 Conclusions

The objective of this work was to develop a ghrelin-based PET imaging probe capable of targeting the endogenous GHS-R1a with comparable affinities to the natural ligand. Truncating ghrelin (**1**) to the first 19 N-terminal amino acids and modifying positions 3 and 19 not only increased the stability and introduced a bifunctional chelator, these modifications provided a high affinity ligand to GHS-R1a.  $\text{IC}_{50}$  studies determined that the  $^{69/71}\text{Ga}$ -ghrelin complex had an improved  $\text{IC}_{50}$  value compared to the non-coordinated **2.3d**. When evaluated *in vivo*, [ $^{68}\text{Ga}$ ]-**2.3d** shows localization in HT1080/GHS-R1a xenografts within the first 30 minutes of circulation that is not present in the HT1080 negative control. Examining the SUV values over 60 minutes in each xenograft results in approximately 5 times greater uptake [ $^{68}\text{Ga}$ ]-**2.3d** in the presence of GHS-R1a. The high localization of [ $^{68}\text{Ga}$ ]-**2.3d** in the kidneys raises a concern for nephrotoxicity and suggests the need for further optimization of this analogue. Smaller ghrelin analogues are currently being developed in hopes of decreasing kidney retention and optimizing pharmacokinetic behaviour.

## 2.3 Experimental

### 2.3.1 Materials and Methods

All common solvents were purchased from Fisher Scientific. All protected amino acids, coupling reagents and resins were purchased from Novabiochem, Peptides International and Chem-Impex and were used without further purification unless otherwise stated. All reagents were obtained from Sigma-Aldrich with the exception of gallium (III) nitrate hydrate that was obtained from Strem Chemicals, HEPES free acid that was obtained from AMRESCO and tris-t-butyl DOTA that was obtained from CheMatech. RP-tC18 Sep-Pak SPE cartridges were purchased from Waters. [<sup>125</sup>I]-ghrelin was purchased from Perkin Elmer. The germanium/gallium generator and all its corresponding parts were purchased from Eckert and Ziegler Strahlen- und Medizintechnik AG. For analytical HPLC-MS, a Sunfire RP-C18 4.6 x 250 mm, 5 μm column was used. For preparative HPLC-MS work, a Sunfire RP-C18 19 x 150 mm, 5 μm column was used. A gradient solvent system was used containing 0.1% TFA in acetonitrile (solvent A) and 0.1% TFA in water (solvent B). For analytical UHPLC-MS, studies were performed on a Waters, Inc. Acquity UHPLC H-Class system, combined with a Xevo QToF mass spectrometer (ESI+, cone voltage = 30 V). For analytical UHPLC-MS studies, a Waters Acquity UHPLC BEH C18 2.1 x 50 mm, 1.7 μm column was used with a gradient solvent system consisting of 0.1% formic acid in acetonitrile (solvent C) and 0.1% formic acid in water (solvent D). Analytical radio-RP-HPLC (Sunfire™ RP-C18 column 4.6 x 150 mm, 5 μm) was performed on a Waters 1525 Binary HPLC pump containing a Waters 2487 dual λ absorbance detector, Waters in-line degasser, a gamma detector and Breeze software (version 3.30).

### 2.3.2 Synthesis of **2.3d**

Peptide synthesis was carried out manually using Fmoc-based solid-phase peptide chemistry. Peptides were synthesized at a 0.1 mmol scale on Rink Amide MBHA resin (0.51 mmol/g). The resin was initially swelled with *N,N*-dimethylformamide (DMF), followed by Fmoc deprotection using 2 mL of 20% piperidine in *N,N*-dimethylformamide (DMF) for two cycles (10 minutes, 5 minutes). Amino acids were

preactivated by combining 3 eq. of Fmoc-protected amino acid, 3 eq. of HCTU and 6 eq. of *N,N*-diisopropylethylamine (DIPEA) in 2 mL of DMF. The mixture was added to the resin and coupled for 30 minutes and repeated again for 60 minutes. These cycles were repeated until all 19 N-terminal amino acids were coupled to the resin.

Methyl trityl deprotection was carried out by mixing the resin with 2 mL of 2% trifluoroacetic acid (TFA) + 5% triisopropylsilane (TIS) in dichloromethane (DCM) solution for 2 minutes and repeating for 8 cycles, or until the yellow colour no longer persisted. To neutralize residual TFA, the resin was treated with 200  $\mu$ L of DIPEA in DMF for 5 minutes. Octanoic acid was coupled to the resulting free amine using 3 eq. octanoic acid, 3 eq. HCTU and 3 eq. of DIPEA in DMF. The mixture was left to couple overnight.

Allyloxycarbonyl deprotection was performed under inert atmospheric  $N_2$  conditions. DCM was dried over sieves for 24 hours before adding 1 mL to the resin. 2 eq. of phenylsilane in 1 mL dry DCM was then added to the peptide resin followed by 0.045 eq. of tetrakis(triphenylphosphine) palladium (0) in 1 mL dry DCM. The peptide vessel was removed from inert conditions and allowed to react for 30 minutes. The resulting free amine was coupled to the chelator using 2 eq. of tris-*t*-butyl DOTA, 2 eq. of HCTU and 6 eq. of DIPEA in DMF. The reaction mixture was left to couple overnight.

Full deprotection of the synthesized peptide was performed by adding a 2 mL mixture of 95% TFA, 2.5% TIS and 2.5% water to the resin and allowed it to mix for 5 hours. The cleaved peptide was precipitated from solution using ice-cold *tert*-butyl methyl ether (TBME) and centrifuged (3000 rpm, 10 minutes) resulting in a crude peptide pellet. The supernatant was decanted and the resulting peptide pellet was dissolved in 20% acetonitrile in water, frozen at  $-78$   $^{\circ}$ C and lyophilized to a white crude powder. Purification was performed using preparative HPLC-MS on a gradient of 20% to 60% solvent A in B over 10 minutes. Purity of the resulting peptide was analyzed using analytical UHPLC on a gradient of 10% to 60% solvent C in D over 4 minutes. Pure peptide was isolate in a 21% yield. HRMS (ESI<sup>+</sup>):  $m/z$  calculated for  $C_{118}H_{195}N_{38}O_{37}$ ,  $[M+2H]^{2+} = 1370.2927$ , observed  $[M+2H]^{2+} = 1370.1941$

### 2.3.3 Synthesis of [<sup>69/71</sup>Ga]-**2.3d**

Purified **2.3d** (5 mg) was dissolved in 1 mL of distilled water in a 5 mL pear-shaped round bottom flask. Ga(NO<sub>3</sub>)<sub>3</sub> (20 eq., 8 mg) was added to the flask and stirred at 60 °C for one hour. The reaction mixture was diluted with 3 mL of distilled water and loaded onto a tC18 Sep Pak SPE cartridge. The cartridge was rinsed with 2 mL of distilled water to remove excess gallium, and [<sup>69/71</sup>Ga]-**2.3d** was eluted from the cartridge with 3 mL of 50% ACN/H<sub>2</sub>O (3 x 1 mL aliquots). Each aliquot was analyzed by RP-UHPLC to confirm the identity and purity of [<sup>69/71</sup>Ga]-**2.3d**. Pure [<sup>69/71</sup>Ga]-**2.3d** was isolated in 86% yield. HRMS (ESI+): m/z calculated for C<sub>118</sub>H<sub>193</sub>N<sub>38</sub>O<sub>37</sub><sup>69</sup>Ga, [M+2H]<sup>2+</sup> = 1403.6979, observed [M+2H]<sup>2+</sup> = 1403.8301.

### 2.3.4 Radiochemistry

A sterile 10 mL reaction vial was loaded with **2.3d** (10 – 100 µg) in HEPES buffer (0.5 – 1 M, pH 4); all conditions can be found in Table 1. Fresh radioactive <sup>68</sup>Ga<sup>3+</sup> was eluted from a <sup>68</sup>Ge/<sup>68</sup>Ga generator using 0.1 M hydrochloric acid (HCl) and trapped on a Strata X C cation exchange column. The column was eluted with 0.1 M HCl in acetone to transfer <sup>68</sup>Ga<sup>3+</sup> to the reaction vial. In all cases, the solution was heated to 90 °C for 15 minutes followed by dilution with 3 mL of milliQ water. The diluted mixture was loaded onto a precondition tC18 sep pak SPE cartridge to remove unchelated <sup>68</sup>Ga<sup>3+</sup>. The radiolabelled peptide was eluted with 1 mL of ethanol into a sterile product vial. Specific activities were calculated by assuming all unlabelled **2.3d** remains present in the product vial. The optimal manual labelling conditions were obtained with 20 µg of **2.3d** in 1 M HEPES buffer. The radiolabelled peptide was obtained in a 54-83% decay corrected yield and specific activity of 10.2 – 22.8 GBq/µmol. Radiochemical purity was assessed using RP-HPLC coupled to a gamma detector, prior to use in *in vitro* and *in vivo* assays.

### 2.3.5 Competitive Binding Assays (IC<sub>50</sub>)

The affinity for GHS-R1a was determined using a radioligand binding assay. Assays were performed using GHS-R1a transfected HEK293 cells as receptor source and human [<sup>125</sup>I]-ghrelin(1-28) (PerkinElmer Inc.) as radioligand. Human ghrelin(1-28) was used as reference to ensure the validity of the results. [<sup>69/71</sup>Ga]-**3d** and **3d** (at concentrations of 10<sup>-</sup>



$5 \text{ M}$ ,  $10^{-6} \text{ M}$ ,  $10^{-7} \text{ M}$ ,  $10^{-8} \text{ M}$ ,  $10^{-9} \text{ M}$ ,  $10^{-10} \text{ M}$  and  $10^{-11} \text{ M}$ ) and [ $^{125}\text{I}$ ]-ghrelin (15 pM per assay tube) were mixed in binding buffer (25 mM HEPES, 5 mM magnesium chloride, 1 mM calcium chloride, 2.5 mM EDTA, and 0.4% BSA, pH 7.4). A suspension of membrane from HEK293S cells (50,000 cells per assay tube) was added to the assay tube containing test peptides and [ $^{125}\text{I}$ ]-ghrelin(1-28). The resulting suspension was incubated for 20 minutes under shaking (550 rpm). Unbound [ $^{125}\text{I}$ ]-ghrelin was removed and the amount of [ $^{125}\text{I}$ ]-ghrelin bound to the membranes was measured on a gamma counter.  $\text{IC}_{50}$  values were determined by nonlinear regression analysis to fit a 4 parameter dose response curve using GraphPad Prism (Version 6.0c) and summarized in Table 2.2. All binding assays were performed in triplicate.<sup>29</sup>

### 2.3.6 *In Vitro* Evaluation of [ $^{68}\text{Ga}$ ]-**2.3d**

[ $^{68}\text{Ga}$ ]-**2.3d** was incubated with 1 million HEK293/GHS-R1a cells (n=6) in 1 mL of binding buffer (25 mM HEPES, 5 mM  $\text{MgCl}_2$ , 1 mM  $\text{CaCl}_2$ , 2.5 mM EDTA, 0.4% BSA) for 1 hour at 37 °C. After 1 hour, the cells were pelleted, washed thoroughly with binding buffer (3 x 1 mL) and the radioactivity was measured using a gamma counter. Blocking studies were performed by administering 20 equivalents (20  $\mu\text{g}$ ) of human ghrelin to 1 million HEK293/GHS-R1a cells (n=6) in 1 mL of binding buffer and immediately before administering [ $^{68}\text{Ga}$ ]-**2.3d**. The mixture was incubated for 1 hour at 37°C, pelleted, washed and the radioactivity measured using a gamma counter. Measurements were recorded in counts/second and used to calculate the mean and standard deviation.

### 2.3.7 *In Vivo* Evaluation

*In vivo* imaging studies were carried out in two cell lines, HT1080/GHS-R1a (receptor positive) and HT1080 (natural expression). HT1080 xenografts were grown on the right upper flank of male NOD/SCID mice by injecting two million cells of HT1080 (n=1) while HT1080/GHS-R1a xenografts were grown on the left flank by injecting two million cells of HT1080/GHS-R1a (n=1). Tumours of approximately 1 centimeter in diameter, were present two weeks post injection. Each mouse was administered 7-10 MBq of [ $^{68}\text{Ga}$ ]-**2.3d** via tail vein injection. A 60-minute dynamic small animal PET scan was performed on both cell lines (Figure 5A-D).

$\mu$ PET scans were reconstructed using Carimas<sup>TM</sup> software developed at the Turku PET Centre (Turku, Finland).<sup>30</sup> To reduce variability due to mouse size and injected dose, all radiotracer accumulation was quantified with respect to standard uptake values (SUV) and normalized to the kidney uptake, therefore  $\mu$ PET scans are represented as SUV ratio (SUV<sub>r</sub>) values. SUVs were determined using AsiPro software (Concorde Microsystems, Knoxville, Tenn, USA). Volumes of interest (VOI) were contoured by hand resulting in 3D reconstruction of the tumour. The image derived radioactivity concentration (Bq/cc) was determined for each VOI based on the injected dose. Standard uptake values (SUV) are then calculated using equation 2.1 (supplemental materials) where SUV(t) is the standard uptake value at time t, C(t) is the imaged derived radioactivity concentration in Bq/cc, ID(t) is the injected dose at time t, and W is the weight of the mouse in grams.

## 2.4 Acknowledgements

HEK293/GHS-R1a cells were provided by Dr. Savita Dhanvantari of Lawson Health Research Institute and HT1080/GHS-R1a cells were provided by Dr. Hon Leong of the London Region Cancer Program. Funding from the Canadian Institutes for Health Research (CIHR), Prostate Cancer Canada and the London Regional Cancer Program.

## 2.5 References

1. M. Kojima, H. Hosoda, Y. Date, M. Nakazato, H. Matsuo and K. Kangawa, *Nature*, 1999, **402**, 656-660.
2. P. L. Jeffery, A. C. Herington and L. K. Chopin, *Cytokine Growth Factor Rev*, 2003, **14**, 113-122.
3. A. Pedretti, M. Villa, M. Pallavicini, E. Valoti and G. Vistoli, *J. Med. Chem.*, 2006, **49**, 3077-3085.
4. S. Gnanapavan, B. Kola, S. A. Bustin, D. G. Morris, P. McGee, P. Fairclough, S. Bhattacharya, R. Carpenter, A. B. Grossman and M. Korbonits, *J Clin Endocrinol Metab*, 2002, **87**, 2988.

5. L. Chopin, C. Walpole, I. Seim, P. Cunningham, R. Murray, E. Whiteside, P. Josh and A. Herington, *Mol Cell Endocrinol*, 2011, **340**, 65-69.
6. A. H. Yeh, P. L. Jeffery, R. P. Duncan, A. C. Herington and L. K. Chopin, *Clin Cancer Res*, 2005, **11**, 8295-8303.
7. P. Cassoni, E. Allia, T. Marrocco, C. Ghe, E. Ghigo, G. Muccioli and M. Papotti, *J Endocrinol Invest*, 2006, **29**, 781-790.
8. F. Gaytan, C. Morales, M. L. Barreiro, P. Jeffery, L. K. Chopin, A. C. Herington, F. F. Casanueva, E. Aguilar, C. Dieguez and M. Tena-Sempere, *J Clin Endocrinol Metab*, 2005, **90**, 1798-1804.
9. F. Gaytan, M. L. Barreiro, J. E. Caminos, L. K. Chopin, A. C. Herington, C. Morales, L. Pinilla, R. Paniagua, M. Nistal, F. F. Casanueva, E. Aguilar, C. Dieguez and M. Tena-Sempere, *J Clin Endocrinol Metab*, 2004, **89**, 400-409.
10. R. Wasko, M. Jaskula, M. Kotwicka, M. Andrusiewicz, A. Jankowska, W. Liebert and J. Sowinski, *Neuro Endocrinol Lett*, 2008, **29**, 929-938.
11. N. Diaz-Lezama, M. Hernandez-Elvira, A. Sandoval, A. Monroy, R. Felix and E. Monjaraz, *Biochem Biophys Res Commun*, 2010, **403**, 24-29.
12. J. N. Fung, I. Seim, D. Wang, A. Obermair, L. K. Chopin and C. Chen, *Horm Cancer*, 2010, **1**, 245-255.
13. M. S. Duxbury, T. Waseem, H. Ito, M. K. Robinson, M. J. Zinner, S. W. Ashley and E. E. Whang, *Biochem. Biophys. Res. Commun.*, 2003, **309**, 464-468.
14. T. Waseem, R. Javaid Ur, F. Ahmad, M. Azam and M. A. Qureshi, *Peptides*, 2008, **29**, 1369-1376.
15. D. Rosita, M. A. DeWit and L. G. Luyt, *J Med Chem*, 2009, **52**, 2196-2203.

16. M. Matsumoto, H. Hosoda, Y. Kitajima, N. Morozumi, Y. Minamitake, S. Tanaka, H. Matsuo, M. Kojima, Y. Hayashi and K. Kangawa, *Biochem. Biophys. Res. Commun.*, 2001, **287**, 142-146.
17. M. A. Bednarek, S. D. Feighner, S.-S. Pong, K. K. McKee, D. L. Hreniuk, M. V. Silva, V. A. Warren, A. D. Howard, L. H. Y. Van der Ploeg and J. V. Heck, *J Med Chem*, 2000, **43**, 4370-4376.
18. M. Van Craenenbroeck, F. Gregoire, P. De Neef, P. Robberecht and J. Perret, *Peptides*, 2004, **25**, 959-965.
19. R. McGirr, M. S. McFarland, J. McTavish, L. G. Luyt and S. Dhanvantari, *Regul. Peptides*, 2011, **172**, 69-76.
20. C. Lu, M. S. McFarland, R.-L. Nesbitt, A. K. Williams, S. Chan, J. Gomez-Lemus, A. M. Autran-Gomez, A. Al-Zahrani, J. L. Chin, J. I. Izawa, L. G. Luyt and J. D. Lewis, *The Prostate*, 2012, **72**, 825-833.
21. G. A. F. Douglas, R. McGirr, C. L. Charlton, D. B. Kagan, L. M. Hoffman, L. G. Luyt and S. Dhanvantari, *Peptides*, 2014, **54**, 81-88.
22. C. Chollet, R. Bergmann, J. Pietzsch and A. G. Beck-Sickinger, *Bioconjug Chem*, 2012, **23**, 771-784.
23. P. Koźmiński and E. Gniazdowska, *Nucl. Med. Biol.*, 2015, **42**, 28-37.
24. M. A. Green and M. J. Welch, *Int J Rad Appl Instrum B*, 1989, **16**, 435-448.
25. M. Henze, J. Schuhmacher, P. Hipp, J. Kowalski, D. W. Becker, J. Doll, H. R. Macke, M. Hofmann, J. Debus and U. Haberkorn, *J. Nucl. Med.*, 2001, **42**, 1053-1056.
26. H. R. Maecke, M. Hofmann and U. Haberkorn, *J Nucl Med*, 2005, **46 Suppl 1**, 172S-178S.
27. S. R. Banerjee and M. G. Pomper, *Appl Radiat Isot*, 2013, **76**, 2-13.

28. A. Choudhary and R. T. Raines, *Chem Biochem*, 2011, **12**, 1801-1807.
29. B. Behnam Azad, V. A. Rota, D. Breadner, S. Dhanvantari and L. G. Luyt, *Bioorg. Med. Chem.*, 2010, **18**, 1265-1272.
30. S. V. Nesterov, C. Han, M. Maki, S. Kajander, A. G. Naum, H. Helenius, I. Lisinen, H. Ukkonen, M. Pietila, E. Joutsiniemi and J. Knuuti, *Eur J Nucl Med Mol Imaging*, 2009, **36**, 1594-1602.

## Chapter 3

### 3 Structural-Activity Study of Ghrelin(1-8) Resulting in Potent Fluorine-bearing Ligands for GHS-R1a

#### 3.1 Introduction

The recent advances in the field of molecular imaging have vastly influenced disease monitoring, staging and diagnosis. Molecular imaging techniques, such as optical imaging (OI), positron emission tomography (PET) and single-photon emission computed tomography (SPECT), have been used to develop a better understanding of specific molecular events occurring within a disease state.<sup>1</sup> The field of oncology has greatly benefitted from developments in molecular imaging. Classical methods of cancer diagnosis, such as histology, are slowly being replaced by new non-invasive methods developed through molecular imaging. One approach to developing these methodologies is identifying molecular receptors involved in the proliferation, migration and cell invasion processes associated with cancer progression and using them as a marker for the disease.<sup>2</sup> For example, somatostatin receptors are highly expressed on the cell surface of specific neoplastic tissues. Considerable research effort has been dedicated to targeting this receptor using its endogenous peptide ligand, somatostatin. Unfortunately, the naturally occurring 28-mer and 14-mer somatostatin ligands are known to have poor *in vivo* stability. In an effort to improve metabolic stability, collections of modified somatostatin analogues were developed by structure-activity studies. From these analogues, a cyclic octapeptide, known as octreotide, was found to be more stable than somatostatin. Using a pendant design approach, chelating moieties were appended to the cyclic peptide to incorporate various radiometals such as <sup>64</sup>Cu, <sup>68</sup>Ga and <sup>111</sup>In. These analogues are now capable of detecting neuroendocrine tumours using scintigraphy and have been evaluated in preclinical and clinical studies.<sup>3-5</sup> This approach to designing stable, high affinity peptide ligands for tumour receptors has led to many new peptide ligands based off of integrin, gastrin-releasing peptide, cholestokinin and alpha-melanocyte stimulating hormone and continues to be an area of focus for designing new receptor-binding peptide ligands.

An exciting new receptor holding potential relevance to certain cancers is the growth-hormone secretagogue receptor (GHS-R). GHS-R has been detected in two isoforms. GHS-R1a is a G-protein coupled receptor known to induce growth-hormone release, as well as various other functions, mediated by its endogenous ligand ghrelin. GHS-R1b is a truncated 5-transmembrane receptor found to be functionally inactive and possessing no known endogenous ligands.<sup>6</sup> Initially, it was proposed that GHS-R1a was solely expressed in the pituitary and hypothalamus but more intensive studies show that although GHS-R1a is predominately expressed in the pituitary, it is also present in low levels in peripheral tissues including the thyroid, pancreas, spleen, myocardium and adrenal gland.<sup>6</sup> More importantly, GHS-R1a is differentially expressed in healthy human tissues and several tumour types such as prostate, breast, testicular and ovarian carcinomas.<sup>7-11</sup>

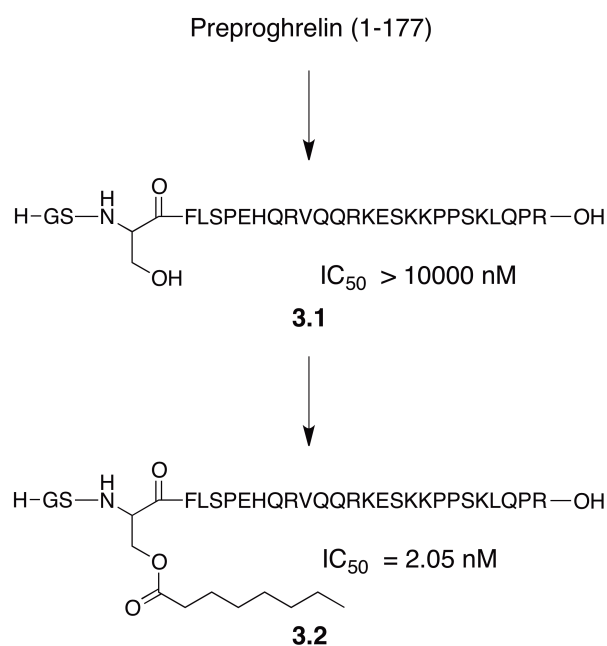


**Figure 3.1** Preproghrelin undergoes proteolytic cleavage resulting in desacyl ghrelin (3.1) which undergoes acylation by ghrelin O-acyl transferase resulting in ghrelin(1-28) (3.2).

The endogenous ligand for GHS-R1a is ghrelin (3.2), a 28 amino acid peptide hormone (GSS(octanoyl)FLSPEHQQRVQQRKESKKPPAKLQPR) that possesses a unique octanoyl chain on the serine side chain at position 3. Human ghrelin originates from preproghrelin, a 177-amino acid protein that undergoes proteolytic cleavage to a 28

amino acid peptide known as desacyl ghrelin (**3.1**). Compound **3.1** possesses the same amino acid sequence as **3.2**, but lacks the octanoyl chain present at position 3.<sup>12</sup> Without the octanoyl chain, **3.1** has virtually no affinity ( $IC_{50} > 10000$  nM) affinity to GHS-R1a as determined by a competitive binding assay. **3.1** then undergoes acylation by the ghrelin O-acyl transferase (GOAT) to yield the unique octanoyl modification. It is this unique modification that significantly increases the affinity to GHS-R1a to 2.05 nM (Figure 3.1).<sup>13</sup>

Ghrelin provides a high affinity template as a starting point to further develop into a radiopeptide. Like many other peptides, ghrelin lacks *in vivo* stability and requires modifications such as truncation and amino acid substitution in order to resist *in vivo* degradation and maintain affinity to GHS-R1a. Much like somatostatin, a methodical structural activity study of ghrelin will help to better understand the role each amino acid plays in the interaction with GHS-R1a. We propose that truncation of ghrelin to the first eight *N*-terminal amino acids will result in high affinity ghrelin analogues by selectively modifying amino acids important for receptor interaction. We will also incorporate a radionuclide into the ghrelin scaffold that is integral for receptor interaction. This requires the development of a new fluorine-18 prosthetic group and results in a high affinity ghrelin(1-8) analogue capable of targeting GHS-R1a.

## 3.2 Results and Discussion

### 3.2.1 Design of Ghrelin Analogues for Positron Emission Tomography (PET)

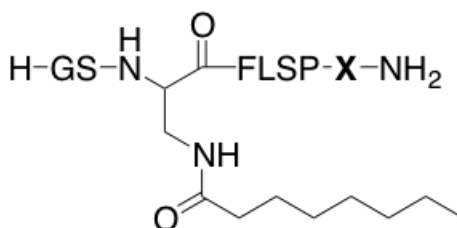
A significant quantity of literature has focused on describing studies where the ghrelin(1-28) structure is modified in order to determine the portions necessary for activity, the role of the octanoyl chain, as well as determining the shortest peptide fragment to activate the receptor.<sup>14, 15</sup> Matsumoto *et al.* determined that the *C*-terminal region of the peptide, ghrelin(16-28), has no affinity to the GHS-R1a. The *N*-terminal region of the peptide was then investigated to determine how many amino acids must be maintained to ensure affinity to GHS-R1a. When truncated to the first 14 *N*-terminal amino acids, ghrelin(1-14), affinity to GHS-R1a remained respectable with an  $IC_{50}$  of 9.6 nM. As further



truncation occurred, there was an increasing loss of affinity for the receptor. For example, ghrelin(1-10) has an  $IC_{50}$  of 19 nM while ghrelin(1-4) has an  $IC_{50}$  of 480 nM. When ghrelin was truncated to less than 4 amino acids, all affinity to the receptor was lost suggesting the first 4 amino acids play an integral role in the affinity to GHS-R1a.<sup>14</sup>

When VanCraenenbroeck *et al.* studied ghrelin(1-14) analogues, they discovered that placing an alanine or tyrosine in position 8 resulted in the most potent ghrelin(1-14) analogues. These findings suggest that the negatively charged glutamic acid found in natural ghrelin is not the optimal choice for this position. Synthesizing several ghrelin(1-8) analogues that replace glutamic acid with various hydrophobic or polar-uncharged side chains could result in an optimal amino acid capable of targeting GHS-R1a with equal or greater affinity than ghrelin(1-28).<sup>16</sup> Modifications were made to positions 3 and 8 while the other amino acids remained the same as the natural ghrelin sequence. At position 3, serine was replaced with the unnatural amino acid diaminopropionic acid (Dpr) to replace the ester linkage with a more synthetically facile and stable amide linkage.<sup>17, 18</sup> Octanoic acid was added to the side chain of Dpr using standard coupling conditions. Position 8 was modified to contain all the hydrophobic aromatic side chain amino acids; phenylalanine (F), tyrosine (Y) and tryptophan (W), and compared to the natural sequence bearing glutamic acid (E). The binding affinity to GHS-R1a was determined using a previously reported competitive binding assay.<sup>18</sup> As summarized in Table 3.1, E as residue 8 resulted in an  $IC_{50}$  of 200 nM but replacing this residue with hydrophobic aromatic side chain greatly increased the binding affinity. W and Y were less effective substitutions resulting in 86.3 nM (**3.3c**) and 65.0 nM (**3.3a**), respectively, while the binding affinity substantially increased with F to 6.67 nM (**3.3b**). Position 8 was also substituted with amino acids bearing polar-uncharged side chains; serine (S), asparagine (N), glutamine (Q) and threonine (T). These substitutions lead to higher affinity analogues than the hydrophobic aromatic side chains. The best analogue **3.3f** (Figure 3.2A), with T in the 8<sup>th</sup> position, had a 3.26 nM  $IC_{50}$ , while N (**3.3d**), S (**3.3g**) and Q (**3.3e**) were less effective with 31.9 nM, 28.8 nM and 21.7 nM respectively.

**Table 3.1** : Substitution of residue 8 with various natural and unnatural amino acids and the resulting IC<sub>50</sub> (nM) for GHS-R1a.



Amino Acid X	Unnatural Amino Acid X	Compound No.	IC <sub>50</sub> (nM)
E		3.3	200
Y		3.3a	65.0
F		3.3b	6.67
W		3.3c	86.3
N		3.3d	31.9
Q		3.3e	21.7
T		3.3f	3.26
S		3.3g	28.8
	t	3.3h	66.2
	β-homo-Thr	3.3i	45.0
	2-Nal	3.3j	24.8

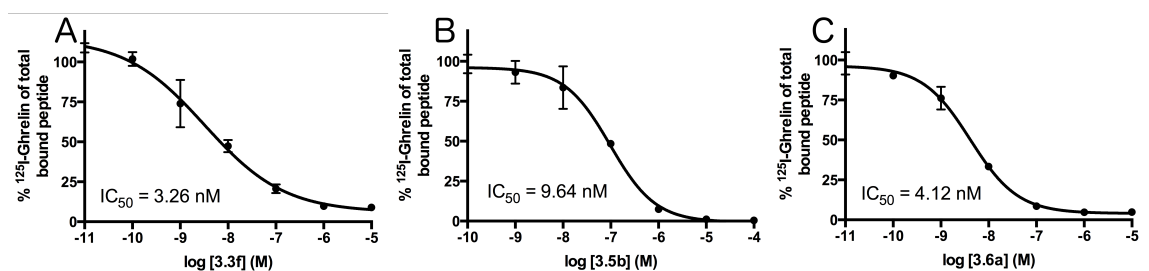


**Figure 3.2** IC<sub>50</sub> curves of lead analogues 3.3f (A), 3.5b (B) and 3.6a (C) after modifications were made to positions 8, 1 and 4, respectively.

One drawback to using peptides as targeting entities is the *in vivo* stability of peptides. For example, natural human ghrelin(1-28) has a biological half-life on the scale of 9-12 minutes.<sup>19</sup> In order to increase the stability of the developed ghrelin(1-8) analogues,

bioisosteres can be added to reduce degradation by endopeptidases and exopeptidases. Bioisosteres are chemical groups that possess similar physical and chemical properties to another chemical compound as well as elicit similar biological properties.<sup>20</sup> Bioisosteres of F and T, the two lead modifications to position 8, were incorporated into the peptide sequence in hopes of maintaining the affinity to GHS-R1a of the natural amino acid as well as increasing the overall stability of the peptide. As summarized in Table 3.1, two bioisosteres of T were introduced, D-threonine (**3.3h**) and  $\beta$ -homo-threonine (**3.3i**). These modifications had a negative effect on binding affinity by increasing the IC<sub>50</sub> to 66.0 nM and 45.0 nM, respectively. 2-Naphthylalanine (2-Nal, **3.3j**) was also introduced as a non-classical bioisostere for F and also had a negative effect on IC<sub>50</sub>, increasing it 24.8 nM. Overall, two amino acids were found to more effectively increase binding affinity than E. These two amino acids are F (**3.3b**) and T (**3.3f**).

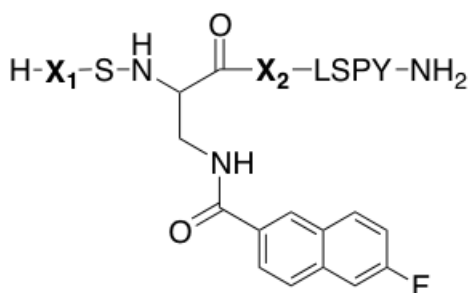
Bednarek, *et al.* investigated the importance of the octanoyl chain by evaluating several analogues where serine-3 was acylated with different aliphatic and aromatic acids. When serine-3 is acylated with large aliphatic groups, such as 11-undecanoic acid, the affinity to GHS-R1a is as effective as natural human ghrelin. Yet, when small, less hydrophobic acids are present, such as formic acid, all affinity to GHS-R1a is lost. This investigation demonstrates that ghrelin is able to tolerate large lipophilic groups at position 3 and possibly provides the opportunity to create a short ghrelin analogue with a radioisotope integrated into the side chain at position 3.<sup>13</sup> To test this hypothesis, Rosita *et al.* integrated lipophilic groups bearing fluorine-19 and rhenium-185/187 in position 3 of ghrelin(1-14)-amide to investigate the potential as PET imaging agents for GHS-R1a. The most promising fluorine-19 group contained a 12-carbon chain, the IC<sub>50</sub> was 27.9 nM and the most promising rhenium-185/187 contained a cyclopentadienyl-rhenium complex after a 3-carbon chain that resulted in a 35 nM affinity. These analogues were not further developed into PET imaging agents but acted as inspiration for further development of ghrelin(1-8) analogues that require a radioisotope for association to the native receptor.<sup>21</sup>

**Table 3.2** Substitution of Dpr side chain with various fluorine-bearing aromatic prosthetic groups and the resulting IC<sub>50</sub> (nM) for GHS-R1a.

Prosthetic Group R	Compound No.	IC <sub>50</sub> (nM)
	<b>3.4a</b>	65
	<b>3.4b</b>	9.9
	<b>3.4c</b>	3.5

Since it was demonstrated that large lipophilic groups were tolerated in position 3, we chose to integrate a well-known fluorine-18 prosthetic group, 4-fluorobenzoic acid (4-FBA), at the end of the Dpr side chain. 4-[<sup>18</sup>F]FBA has been used to radiolabel various peptides such as RGD and bombesin, and has well developed radiochemical procedures.<sup>22, 23</sup> Shown in Table 3.2, integration of 4-FBA (**3.4a**) onto residue 3 resulted in a less than optimal IC<sub>50</sub>, of 65 nM. In order to increase the lipophilicity of the prosthetic group, another aromatic ring was added by introducing 6-fluoronaphthoic acid (6-FNA, **3.4b**) and 4'-fluoro-[1,1'-biphenyl]-4-carboxylic acid (4'-FBC, **3.4c**) using standard coupling conditions. The increased lipophilicity had a positive effect on binding affinity to 9.9 nM and 3.5 nM, respectively, and led us to develop a new fluorine-18 prosthetic group. Unfortunately nucleophilic aromatic substitution with the biphenyl scaffold proved to be low yielding and therefore, 6-FNA was further developed into a prosthetic group rather than 4'-FBC.

**Table 3.3** Substitution of residue 1 and 4 with various unnatural amino acids and the resulting IC<sub>50</sub> (nM) for GHS-R1a.



Amino Acid X <sub>1</sub>	Amino Acid X <sub>2</sub>	Compound No.	IC <sub>50</sub> (nM)
G	F	3.4b	9.9
Aib	F	3.5a	9.28
Inp	F	3.5b	9.64
Sar	F	3.5c	262
G	Nal-1	3.6a	4.12
G	Nal-2	3.6b	1068

Following the choice of a suitable prosthetic group for position 3, further modifications were made to the *N*-terminal residue 1 and residue 4 in hopes of further increasing *in vivo* stability and GHS-R1a affinity using more unnatural amino acids. The *N*-terminal glycine was replaced with one of three unnatural amino acids; aminoisobutyric acid (Aib), isonipecotic acid (Inp) or sarcosine (Sar). The secondary amine found in Sar (**3.5c**) had a large negative effect on IC<sub>50</sub> causing it to rise to 262 nM, while the secondary amine found in Inp (**3.5b**, Figure 3.2B) had the opposite effect decreasing it to a desirable IC<sub>50</sub> of 9.64 nM. Aib, a primary amine, also had a positive effect on IC<sub>50</sub> decreasing it to 9.26 nM (Table 3.3). When choosing the most suitable candidate for residue 1, Inp was chosen in order to reduce the presence of primary amines during the radiochemical prosthetic group labelling. VanCraenenbroeck performed an alanine scan on ghrelin(1-14) and determined that the Phe present at residue 4 was integral for interaction with GHS-R1a. Replacement of this residue with alanine or tyrosine caused a decrease in binding affinity.<sup>16</sup> Therefore, we hypothesized that replacing Phe with a larger, more lipophilic side chain may create a stronger interaction between the ligand and receptor. Substitution of Phe with Nal-1 and Nal-2 had varied success (Table 3.3). Nal-1 was able

to increase the affinity to GHS-R1a greatly from 65 nM (**3.4a**) to 4.12 nM (**3.6a**, Figure 3.2C) while Nal-2 had a detrimental effect result in a large loss of affinity.

A thorough investigation into the amino acid sequence of ghrelin(1-8)-amide has led to many analogues with binding affinities comparable to ghrelin(1-28). Combining the most successful substitutions has led to a lead peptide analogue (Figure 3.3) to be further developed into a fluorine-18 PET imaging agent. The best substitutions were Inp, Nal-1 and Thr in positions 1, 4 and 8, respectively and coupling 4-FNA to the side chain of Dpr at position 3. Compound **3.7** resulted in the best IC<sub>50</sub> of all ghrelin analogues at 0.16 nM and supported the further development of this peptide into a PET radiopeptide by incorporating fluorine-18.

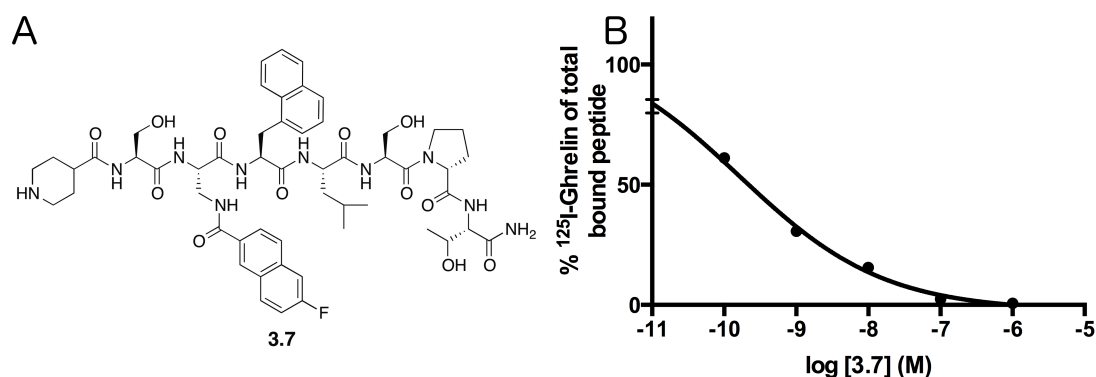
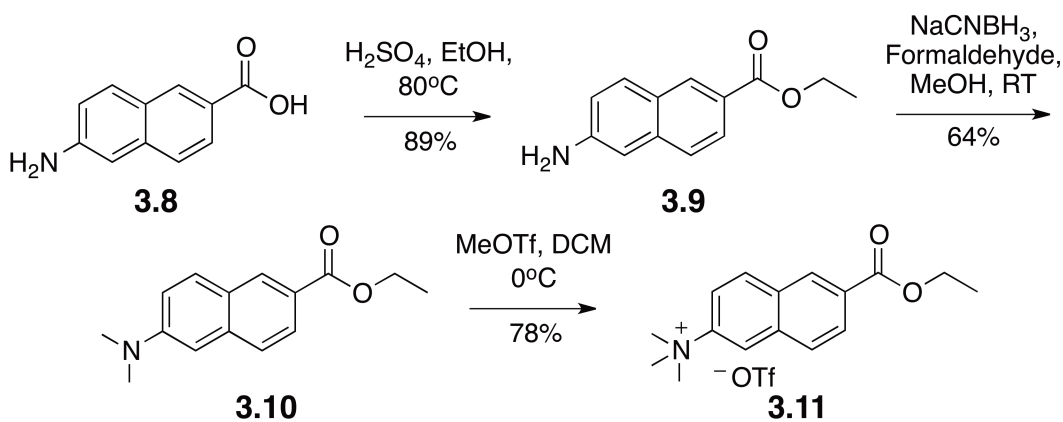


**Figure 3.3** Amino acid structure (A) and IC<sub>50</sub> curve (B) of the the ghrelin (1-8) analogue bearing lead modifications to all positions 1, 3, 4 and 8.

### 3.2.2 Synthesis of Prosthetic Groups and Standards

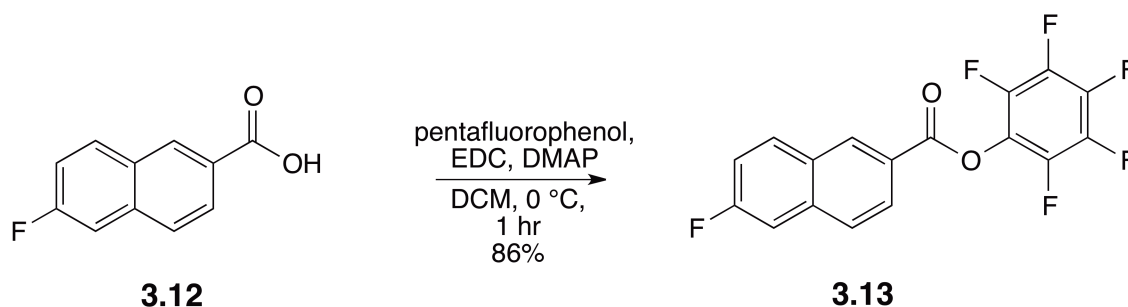
The synthesis of the new prosthetic group precursor **3.11** is outlined in scheme 3.1. Prosthetic group precursor **3.11** was obtained in good yield following a 3-step synthesis. The commercially available starting material, 6-amino-2-naphthoic acid (**3.8**), was dissolved in ethanol and acidified with sulfuric acid (pH 4) to produce 6-amino-2-ethyl naphthoate (**3.9**). Following purification by flash column chromatography, **3.9** was dimethylated by an Eschweiler-Clarke reaction using sodium cyanoborohydride and formaldehyde to produce **3.10**. The final synthetic step requires methylation of the

dimethylamine with the strong methylating agent, methyl trifluoromethanesulfonate (MeOTf). The resulting 6-trimethylamino-2-ethylnaphthoate trifluoromethanesulfonate (**3.11**) was obtained as a pure white powder after precipitation and recrystallization. The identity of the product was confirmed by proton and carbon NMR spectroscopy as well as mass spectrometry. This prosthetic group was designed to undergo nucleophilic aromatic substitution in the presence nucleophilic fluorine. The electron withdrawing nature of the ethyl ester at carbon-2 activates the ring for nucleophilic attack by fluorine at carbon-6. The trimethylammonium acts as a better quality leaving group resulting in a substitution with fluorine. Therefore, employment of the standard radiofluorination protocols using potassium carbonate and kryptofix 2.2.2 was expected to be suitable for radiolabelling of this prosthetic group.



**Scheme 3.1** Synthesis of 6-trimethylamino-2-ethyl-naphthoate triflate (**3.11**)

Most fluorine-18-labelled prosthetic groups reported in the literature are designed as activated esters for facile acylation to peptide targeting entities. The most common activated ester reported is the N-hydroxysuccinimide ester used for 4- $^{18}\text{F}$ -fluorobenzoic acid to result in N-succinimidyl-4- $^{18}\text{F}$ -fluorobenzoate. Unfortunately, acylation of our lead peptide analogue with an N-hydroxysuccinimide ester of 6-fluoro-2-naphthoic acid resulted in degradation of the active ester due to harsh conditions. The sluggish and low yielding reactions therefore led us to seek out a different active ester. Pentafluorophenyl (PFP) esters are becoming recognized for the increased stability and reaction rate when compared to NHS esters.<sup>24, 25</sup>



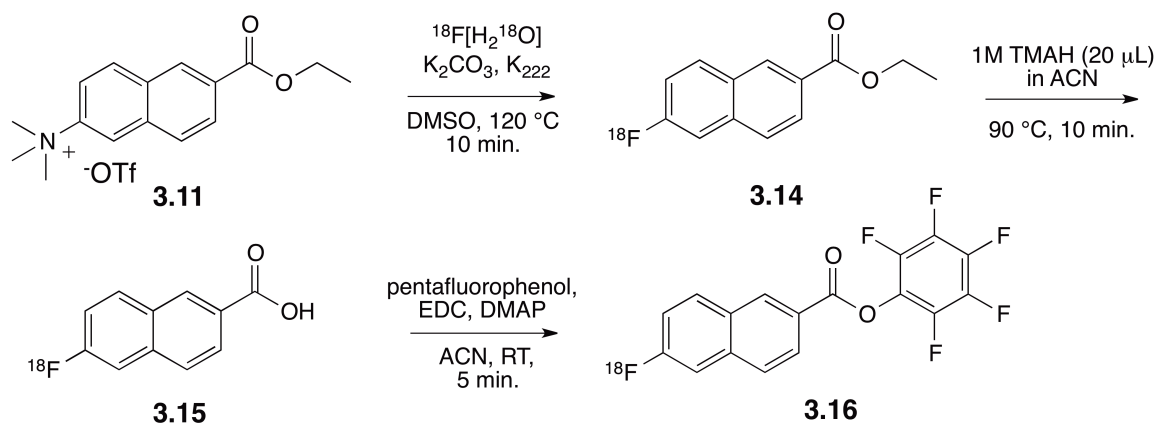
**Scheme 3.2** Synthesis of the non-radioactive standard 6-fluoro-2-pentafluorophenyl naphthoate (PFPN, **3.13**)

A non-radioactive 6-fluoro-2-pentafluorophenylnaphthoate ( $[^{19}\text{F}]$ -PFPN) standard was synthesized using 6-fluoro-2-naphthoic acid, pentafluorophenol and DMAP. The desired activated ester was purified by flash column chromatography in an 86% yield and verified by  $^1\text{H}$  NMR,  $^{13}\text{C}$  NMR spectroscopy and high-resolution mass spectrometry (HRMS). A peptide precursor of **3.7** was synthesized to possess a free amine at the Dpr residue in position 3. This peptide was synthesized on Rink Amide MBHA resin with all amino acids bearing standard protecting groups. Upon cleavage from the resin using strong acid, all the protecting groups were removed leaving one primary amine at position 3 and a secondary amine on the *N*-terminus. This peptide precursor (**3.17**) is capable to coupling to PFPN in the presence of a weak base producing the desired radiolabelled ghrelin(1-8) peptide.

### 3.2.3 Radiochemistry

Full synthesis of  $[^{18}\text{F}]$ -**3.7** was carried out in 4 synthetic steps summarized in scheme 3.3. The first two steps were carried out on the automated Tracer Lab FX<sub>FN</sub> synthesis box. Shown in Figure 4, the configuration of the synthesis box was slightly modified to accommodate the first two synthetic steps. Valve 14 (V14) was directly attached to a product output line to bypass the rest of the synthesis system and transfer the crude reaction material from the reaction vial to a product vial outside the synthesis box for further manipulation.





**Scheme 3.3** The radiosynthetic pathway for the synthesis of [ $^{18}\text{F}$ ]-PFPN by automated and manual synthesis.

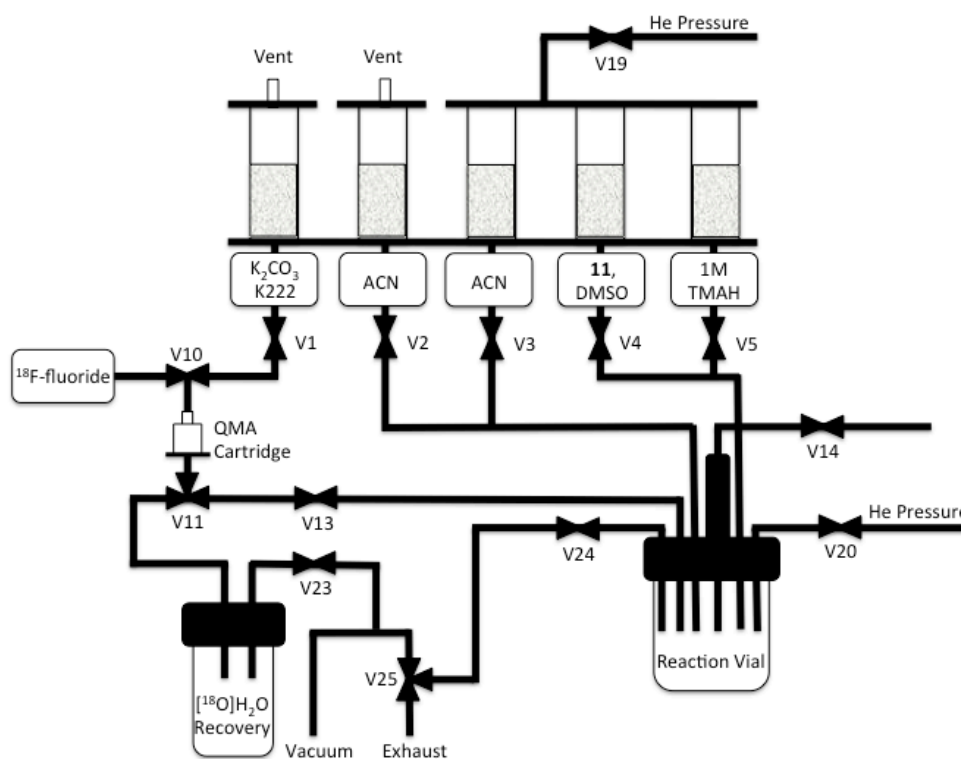
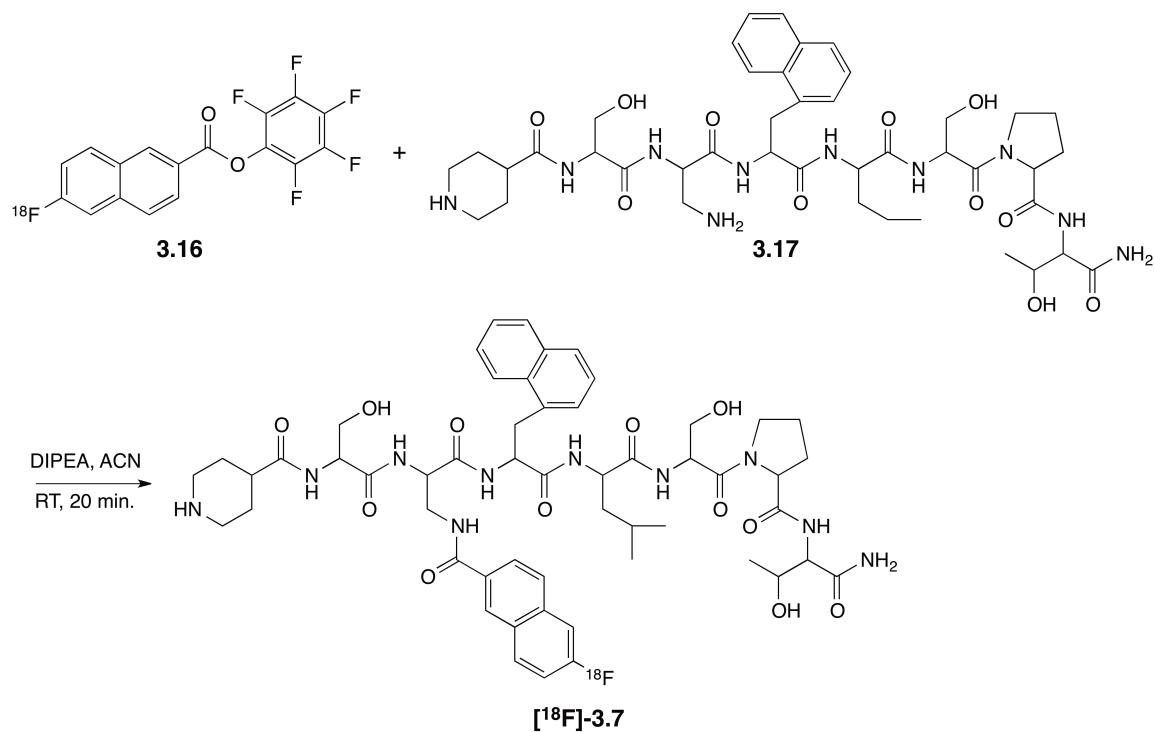


**Figure 3.4** The modified schematic of Tracer Lab  $\text{FX}_{\text{FN}}$  for the synthesis of 6- $^{18}\text{F}$ -fluoro-2-naphthoic acid (**3.15**).

The TracerLab  $\text{FX}_{\text{FN}}$  was prepared for synthesis by filling vial 1 with a solution of 2 mg potassium carbonate and 7 mg of kryptofix 2.2.2 in 200  $\mu\text{L}$  of milliQ water and 800  $\mu\text{L}$  of

acetonitrile (ACN). Vials 2 and 3 were filled with 1 mL of dry ACN each, used to azeotropically dry the nucleophilic fluoride-18. 2 mg of precursor **3.11** was added to vial 4 in 750  $\mu$ L of dry dimethylsulfoxide (DMSO). Finally, vial 5 contained 20  $\mu$ L of 1M tetramethylammonium hydroxide (in water, TMAH) in 1 mL of ACN for deprotection of the ethyl ester.

Fluorine-18 was delivered to the synthesis box in  $\text{H}_2[^{18}\text{O}]$  and trapped on a Waters QMA Carbonate Sep Pak. The activity was then eluted into the reaction vial by the solution in vial 1. The solution was then azeotropically dried for 5 minutes at 75°C with the solution in vial 2 and repeated for vial 3. Following drying, precursor **3.11** was introduced to the reaction vial from vial 4 and allowed to react at 110°C for 10 minutes resulting in 6- $[^{18}\text{F}]$ -2-ethylnaphoate (**3.14**). 1M TMAH (20  $\mu$ L) in 1 mL of ACN was then added to the reaction mixture from vial 5 and heated to 90 °C for 10 minutes. After cooling the reaction mixture to 40 °C, the reaction crude was then transferred from the reaction vial to a product vial containing 7 mL of milliQ water and 0.1% TFA in the side chamber *via* valve 14. The following steps were carried out manually. The diluted reaction crude was loaded onto a tC18 Sep Pak to remove any unreacted nucleophilic fluorine-18. 6- $[^{18}\text{F}]$ -4-Naphthoic acid (**3.15**) was eluted from the tC18 Sep Pak with 1 mL of acetonitrile into a reaction vial containing 20 mg of pentafluorophenol, 10 mg 1-ethyl-3-(3-dimethylaminopropyl)carbodiimide (EDC) and 1 mg 4-dimethylaminopyridine (DMAP). The reaction mixture was allowed to sit at room temperature for 5 minutes at which time 1 mL of milliQ water was added to the crude reaction mixture. The diluted mixture is then purified by semi-preparative HPLC (55 – 95% acetonitrile in water) to collect the pure 6- $[^{18}\text{F}]$ -2-pentafluorophenylnaphthoate in 6.5% decay corrected yield. The purified **3.16** was redissolved in 1 mL of acetonitrile containing 1.5 mg of peptide precursor (**3.17**) (Scheme 3.4). After administration of 30  $\mu$ L of diisopropylethylamine (DIPEA), the reaction mixture was warmed at 40 °C for 20 minutes before being diluted with 500  $\mu$ L milliQ water and purified by semi-preparative HPLC (20 – 80% acetonitrile in water). HPLC purified  $[^{18}\text{F}]$ **3.7** was collected at 5 minutes in a 3.1% decay corrected yield. The identity of **3.18** was confirmed by co-injection with the non-radioactive standard **3.7** (Figure 3.5).



**Scheme 3.4** Coupling of  $[^{18}\text{F}]\text{-PFPN}$  to the lead ghrelin(1-8) analogue resulting in  $[^{18}\text{F}]\text{-3.7}$ .

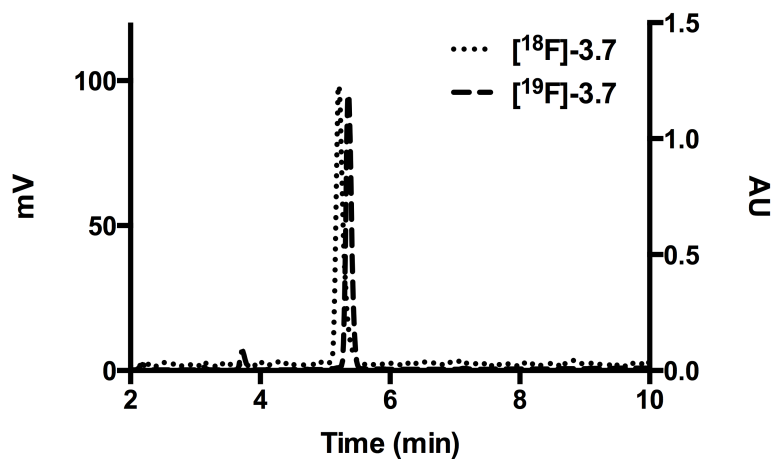


**Figure 3.5** Overlaid C18 reverse-phase HPLC chromatograms of  $[^{19}\text{F}]\text{-3.7}$  (AU) and  $[^{18}\text{F}]\text{-3.7}$  (mV).

### 3.2.4 Conclusions

Ghrelin has shown it is capable of distinguishing between cancerous and benign prostate tissue that has shown to be a difficult task with other clinical PET imaging agents, such as  $[^{18}\text{F}]\text{-fluorodeoxyglucose}$ . This emphasizes the need for new ghrelin-based PET

probes. The natural ghrelin(1-8) sequence was methodically altered to increase the affinity to GHS-R1a from 200 nM to 0.16 nM. Modifications made at positions 1, 3, 4 and 8 resulted in various analogues with  $IC_{50}$  values equal or better than ghrelin(1-28). Compiling all the lead modifications into one peptide analogue resulted in [Inp<sup>1</sup>, Dpr<sup>3</sup>(6-fluoro-2-naphthoate), 1-Nal<sup>4</sup>, Thr<sup>8</sup>] ghrelin(1-8) which possessed a fluorine for further development into a PET radiopeptide. **3.7** resulted in a 1250-fold increase of affinity to GHS-R1a than **3.3** based off their  $IC_{50}$  values. In order to incorporate fluorine-18, a new prosthetic group, [<sup>18</sup>F]-PFPN, was developed using a combination of automated and manual synthesis with a TracerLab FX<sub>FN</sub> synthesis box. Coupling of [<sup>18</sup>F]-PFPN to the lead peptide analogue with a free amine at residue 3 resulted in the first fluorine-18 labelled, high affinity ghrelin (1-8) analogue for GHS-R1a in an overall 3.1% radiochemical yield (d.c.). Therefore, this reports the successful radiolabelling of the first fluorine-18 labelled ghrelin(1-8) analogue. This is not only the highest affinity ghrelin analogue reported in the literature, it is also the shortest ghrelin analogue capable of binding GHS-R1a with better affinity than ghrelin(1-28).

Preclinical evaluation of this PET probe is currently underway in prostate cancer models although [<sup>18</sup>F]-**3.7** can be a valuable tool for visualizing various tissues and disease states that are known for GHS-R1a expression beyond the field of oncology.

### 3.3 Experimental

#### 3.3.1 Materials and Methods

All common solvents were purchased from Fisher Scientific. All protected amino acids, coupling reagents and resins were purchased from Novabiochem, Peptides International and Chem-Impex and were used without further purification unless otherwise stated. All reagents were obtained from Sigma-Aldrich. RP-tC18 Sep-Pak SPE and QMA carbonate SPE cartridges were purchased from Waters. [<sup>125</sup>I]-Ghrelin was purchased from Perkin Elmer. Cyclotron produced [<sup>18</sup>F]H<sub>2</sub><sup>18</sup>O was obtained from Dr. Mike Kovacs at the Cyclotron & PET Radiochemistry Facility at St. Josephs Hospital in London, Ontario, Canada. For analytical HPLC-MS, a Agilent RP-C18 4.6 x 250 mm, 5 μm column was used. For semi-preparative HPLC-MS work, an Agilent RP-C18 19 x 150 mm, 5 μm

column was used. A gradient solvent system was used containing 0.1% TFA in acetonitrile (solvent A) and 0.1% TFA in water (solvent B). For analytical UHPLC-MS, studies were performed on a Waters, Inc. Acquity UHPLC H-Class system, combined with a Xevo QToF mass spectrometer (ES+, cone voltage = 30 V). For analytical UHPLC-MS studies, a Waters Acquity UHPLC BEH C18 2.1 x 50 mm, 1.7  $\mu\text{m}$  column was used with a gradient solvent system consisting of 0.1% formic acid in acetonitrile (solvent C) and 0.1% formic acid in water (solvent D). Analytical radio-RP-HPLC (Agilent<sup>TM</sup> RP-C18 column 4.6 x 150 mm, 5  $\mu\text{m}$ ) was performed on a Waters 1525 Binary HPLC pump containing a Waters 2487 dual  $\lambda$  absorbance detector, Waters In-Line degasser, a gamma detector and Breeze software (version 3.30).

### 3.3.2 General Fmoc Synthesis of Ghrelin(1-8) Peptides

Peptide synthesis was carried out manually using Fmoc-based solid-phase peptide chemistry. Peptides were synthesized at a 0.1 mmol scale on Rink Amide MBHA resin (0.52 mmol/g). The resin was initially swelled with *N,N*-dimethylformamide (DMF), followed by Fmoc deprotection using 2 mL of 20% piperidine in *N,N*-dimethylformamide (DMF) for two cycles (10 minutes, 5 minutes). Amino acids were preactivated by combining 3 eq. of Fmoc-protected amino acid, 3 eq. of O-(6-chlorobenzotriazol-1-yl)-*N,N,N',N'*-tetramethyluronium hexafluorophosphate (HCTU) and 6 eq. of *N,N*-diisopropylethylamine (DIPEA) in 2 mL of DMF. The mixture was added to the resin and vortexed for 60 minutes. These cycles were repeated until all 8 N-terminal amino acids were coupled to the resin.

Allyloxycarbonyl deprotection of diaminopropionic acid was performed under inert atmospheric  $\text{N}_2$  conditions. DCM was dried over sieves for 24 hours before adding 1 mL to the resin. 2 eq. of phenylsilane in 1 mL dry DCM was then added to the peptide resin followed by 0.045 eq. of tetrakis(triphenylphosphine) palladium (0) in 1 mL dry DCM. The peptide vessel was removed from inert conditions and allowed to react for 30 minutes. The resulting free amine was acylated using 2 eq. of the corresponding acid (octanoic acid, 4-fluorobenzoic acid, 6-fluoronaphthoic acid or 4'-fluoro-[1,1'-biphenyl]-4-carboxylic acid), 2 eq. of HCTU and 6 eq. of DIPEA in DMF. The reaction mixture was left to couple overnight.

Full deprotection of the synthesized peptide was performed by adding a 2 mL mixture of 95% trifluoroacetic acid (TFA), 2.5% triisopropylsilane (TIS) and 2.5% water to the resin and allowed it to mix for 5 hours. The cleaved peptide was precipitated from solution using ice-cold *tert*-butyl methyl ether (TBME) and centrifuged (3000 rpm, 10 minutes) resulting in a crude peptide pellet. The supernatant was decanted and the resulting peptide pellet was dissolved in 20% acetonitrile in water, frozen at -78 °C and lyophilized to a white crude powder. Purification was performed using preparative HPLC-MS and purity of the resulting peptides were analyzed using analytical UHPLC, these results are summarized in table 3.4.

**Table 3.4** Analytical data of ghrelin analogues 3.3-3.3j, 3.4a-3.4b, 3.5a-3.5c, 3.6a-3.6b and 3.7

Compound Number	Compound	[M+H] <sup>+</sup> Calculated	[M+H] <sup>+</sup> Found	Purity (%)	Yield (%)
3.3	GS-Dpr(octanoyl)-FLSPE	946.5123	946.4376	96%	22%
3.3a	GS-Dpr(octanoyl)-FLSPY	980.5330	980.2072	98%	20%
3.3b	GS-Dpr(octanoyl)-FLSPF	965.5459	965.3738	99%	23%
3.3c	GS-Dpr(octanoyl)-FLSPW	1004.5568	1004.4395	95%	19%
3.3d	GS-Dpr(octanoyl)-FLSPN	932.5204	932.8724	99%	25%
3.3e	GS-Dpr(octanoyl)-FLSPQ	946.5361	946.4215	88%	14%
3.3f	GS-Dpr(octanoyl)-FLSPT	919.5252	919.8689	99%	24%
3.3g	GS-Dpr(octanoyl)-FLSPS	905.5095	905.3037	99%	19%
3.3h	GS-Dpr(octanoyl)-FLSPt	918.5174	921.4526	97%	15%
3.3i	GS-Dpr(octanoyl)-FLSP-β-homoT	932.5341	935.4747	99%	11%
3.3j	GS-Dpr(octanoyl)-FLSP-2-Nal	1014.5537	1014.3309	99%	27%
3.4a	GS-Dpr(4-FB)-FLSPY	1027.4688	1027.5223	99%	25%
3.4b	GS-Dpr(6-FN)-FLSPY	1055.5012	1055.3751	98%	25%
3.5a	Aib-S-Dpr(6-FN)-FLSPY	1080.5079	1080.4139	97%	18%
3.5b	Inp-S-Dpr(6-FN)-FLSPY	1041.4844	1041.4180	99%	21%
3.5c	Sar-S-Dpr(6-FN)-FLSPY	1077.4844	1077.3226	96%	23%
3.6a	GS-Dpr(6-FN)-Nal-1-LSPY	1077.4844	1077.3178	98%	20%
3.6b	GS-Dpr(6-FN)-Nal-2-LSPY	1018.4923	1018.3571	99%	26%
3.7	Inp-S-Dpr(6-FN)-Nal-1-LSPT				

### 3.3.3 Competitive Binding Assay (IC<sub>50</sub>)

The affinity for GHS-R1a was determined using a radioligand competitive binding assay. Assays were performed using GHS-R1a transfected HEK293 cells as receptor source and human [<sup>125</sup>I]-ghrelin(1-28) (PerkinElmer Inc.) as the radioligand. Human ghrelin(1-28) was used as reference to ensure the validity of the results. A suspension of membrane from HEK293/GHS-R1a cells (50,000 cells per assay tube) were incubated with ghrelin(1-8) peptide analogues (at concentrations of 10<sup>-5</sup> M, 10<sup>-6</sup> M, 10<sup>-7</sup> M, 10<sup>-8</sup> M, 10<sup>-9</sup>

M,  $10^{-10}$  M and  $10^{-11}$  M) and [ $^{125}$ I]-ghrelin (15 pM per assay tube) in binding buffer (25 mM HEPES, 5 mM magnesium chloride, 1 mM calcium chloride, 2.5 mM EDTA, and 0.4% BSA, pH 7.4). The resulting suspension was incubated for 20 minutes under shaking (550 rpm) at 37 °C. Unbound [ $^{125}$ I]-ghrelin was removed and the amount of [ $^{125}$ I]-ghrelin bound to the membranes was measured by gamma counter. IC<sub>50</sub> values were determined by nonlinear regression analysis to fit a 4 parameter dose response curve using Prism 6 (Version 6.0c). All binding assays were performed in triplicate.

### 3.3.4 Synthesis of 6-amino-2-ethylnaphthoate (**3.9**)

6-Amino-2-naphthoic acid (300 mg, 1.60 mmol) was dissolved in 50 mL of ethanol and heated to 80 °C while stirring in a 100 mL round bottom. Sulfuric acid was added dropwise until pH 6 was reached. The reaction was left to reflux overnight. Ethanol was removed by rotary evaporation and the crude oil was redissolved in dichloromethane and transferred to a separatory funnel. Compound **3.9** was extracted with 0.1 M sodium bicarbonate (50 mL) and dichloromethane (3 x 50 mL). The organic fractions were combined and dried with MgSO<sub>4</sub>. MgSO<sub>4</sub> was removed by gravity filtration and the resulting solution was removed by rotary evaporation. The crude solid was dissolved in 1 mL of dichloromethane with 0.1 % triethylamine. The crude solution was purified by flash column chromatography (dichloromethane, 0.1% triethylamine) and tracked by TLC. The spot at R<sub>f</sub> = 0.4 was collected into a 100 mL round bottom and rotary evaporated to dryness. Pure **3.9** was isolated as a brown solid in 86% yield (295 mg, 1.37 mmol). HRMS: m/z calculated for C<sub>13</sub>H<sub>13</sub>O<sub>2</sub>N, 215.0946; observed 215.0942. <sup>1</sup>H-NMR Spectrum (400 MHz, CDCl<sub>3</sub>, δ): 8.46 (1H, s, H<sub>arom</sub>), 7.96 (1H, d, H<sub>arom</sub>, J = 8 Hz), 7.77 (1H, d, H<sub>arom</sub>, J = 12 Hz), 7.60 (1H, d, H<sub>arom</sub>, J = 12 Hz), 7.00-6.97 (2H, m, H<sub>arom</sub>), 4.42 (2H, q, CH<sub>2</sub>CH<sub>3</sub>, J = 8 Hz), 1.43 (3H, t, CH<sub>2</sub>CH<sub>3</sub>).

### 3.3.5 Synthesis of 6-dimethylamino-2-ethylnaphthoate (**3.10**)

Compound **3.9** (295 mg, 1.37 mmol) was dissolved in 60 mL of methanol in a 250 mL round bottom and stirred at room temperature. While stirring, 37 %wt formaldehyde (2.0 mL, 27.4 mmol) was added dropwise followed by sodium cyanoborohydride (0.86 g, 13.7 mmol) and was left to stir at room temperature for 12 hours. After 12 hours, starting



material was still present by thin layer chromatography (TLC) (100% dichloromethane), therefore the reaction was heated to 40 °C for 4 hours. The reaction mixture was diluted with 50 mL of fresh dichloromethane and transferred to a separatory funnel. The crude product was extracted with distilled water (50 mL) and dichloromethane (3 x 50 mL). The organic fractions were combined and dried with MgSO<sub>4</sub>. MgSO<sub>4</sub> was removed by gravity filtration and the resulting solution was removed by rotary evaporation to a yellow solid and dried under high vacuum. The crude solid was dissolved in 1 mL of 10% hexanes in dichloromethane and purified by flash column chromatography (10% hexanes in dichloromethane) and tracked by TLC. Fractions containing the spot at R<sub>f</sub> = 0.55 were combined into a 100 mL round bottom and rotary evaporated. Pure **3.10** was obtained in 64% yield (213 mg, 0.87 mmol). HRMS: m/z calculated for C<sub>15</sub>H<sub>17</sub>O<sub>2</sub>N, 243.1259; observed 243.1255. <sup>1</sup>H-NMR Spectrum (400 MHz, CDCl<sub>3</sub>, δ): 8.40 (1H, s, C<sub>arom</sub>), 7.92 (1H, d, J= 8 Hz, C<sub>arom</sub>), 7.81 (1H, d, J= 8 Hz, C<sub>arom</sub>), 7.70 (1H, d, J= 8 Hz, C<sub>arom</sub>), 7.28 (1H, d, J= 8 Hz, C<sub>arom</sub>) 6.96 (1H, s, C<sub>arom</sub>), 4.33 (2H, q, J = 8 Hz, CH<sub>2</sub>CH<sub>3</sub>), 3.06 (6H, s, (CH<sub>3</sub>)<sub>2</sub>), 1.35 (3H, t, J = 8 Hz, CH<sub>2</sub>CH<sub>3</sub>).

### 3.3.6 Synthesis of 6-trimethylamino-2-ethylnaphthoate triflate (**3.11**)

Compound **3.10** (200 mg, 0.82 mmol) was dissolved in 30 mL of anhydrous dichloromethane dried over sieves. The round bottom was evacuated and charged with N<sub>2</sub>. The reaction mixture was then cooled to 0 °C in an ice bath and methyl trifluoromethanesulfonate (370 μL, 3.28 mmol) was added dropwise using an oven dried needle and syringe. The reaction was left to stir. Pure **3.11** precipitated out of solution after 1 hour. The precipitate was collected with a Hirsch funnel and rinsed thoroughly with cold anhydrous dichloromethane. The resulting white solid was dried under high vacuum, with **3.11** being isolated in a 78% yield (260 mg, 0.64 mmol). <sup>1</sup>H-NMR Spectrum (400 MHz, DMSO, δ): 8.77 (1H, s, C<sub>arom</sub>), 8.62 (1H, s, C<sub>arom</sub>), 8.47 (1H, d, J= 8 Hz, C<sub>arom</sub>), 8.17-8.26 (3H, m, C<sub>arom</sub>), 4.40 (2H, q, J= 8 Hz, CH<sub>2</sub>CH<sub>3</sub>) 3.72 (9H, s, (CH<sub>3</sub>)<sub>3</sub>), 1.38 (3H, t, J = 8 Hz, CH<sub>2</sub>CH<sub>3</sub>). <sup>13</sup>C-NMR Spectrum (100 MHz, DMSO, δ): 223.0 (C<sub>arom</sub>-N(CH<sub>3</sub>)<sub>3</sub>), 165.9 (C=O), 134.7 (C<sub>arom</sub>), 132.3 (C<sub>arom</sub>), 132.1 (C<sub>arom</sub>), 130.0 (C<sub>arom</sub>), 130.0



(C<sub>arom</sub>), 127.0 (C<sub>arom</sub>), 120.0 (C<sub>arom</sub>), 120.0 (C<sub>arom</sub>), 110.0 (C<sub>arom</sub>), 62.9 (N-(CH<sub>3</sub>)<sub>3</sub>), 61.6 (CH<sub>2</sub>CH<sub>3</sub>), 21.4 (CH<sub>2</sub>CH<sub>3</sub>).

### 3.3.7 Synthesis of [<sup>19</sup>F]-PFPN

6-Fluoronaphthoic acid (200 mg, 1.05 mmol) and pentafluorophenol (211 mg, 1.15 mmol) were dissolved in 100 mL of dichloromethane and cooled to 0 °C in an ice bath. EDC (30.2 mg, 1.58 mmol) and DMAP (25 mg, 0.21 mmol) were added to the reaction and stirred. The reaction was tracked by thin-layer chromatography (5% ethyl acetate in hexanes, R<sub>f</sub> = 0.69). After 1 hour, no starting material was visible by TLC. The reaction was quenched with 30 mL of saturated ammonium chloride (NH<sub>4</sub>Cl) and transferred to a 250 mL separatory funnel. [<sup>19</sup>F]-PFPN was extracted with 50 mL of ethyl acetate and repeated 3 times. The organic layers were combined and dried with magnesium sulphate (MgSO<sub>4</sub>). MgSO<sub>4</sub> was removed by gravity filtration and the solution was dried using rotary evaporation. The crude solid was dissolved in 1 mL of 5% ethyl acetate in hexanes and loaded onto a silica plug and eluted with 5% ethyl acetate in hexanes. [<sup>19</sup>F]-PFPN was isolated as a white solid in 86% yield (322 mg, 0.90 mmol). HRMS: m/z calculated for C<sub>17</sub>H<sub>6</sub>O<sub>2</sub>F<sub>6</sub>, 356.0272; observed 356.0279. <sup>1</sup>H-NMR Spectrum (400 MHz, CDCl<sub>3</sub>, δ): 8.81 (1H, s, H<sub>arom</sub>), 8.19 (1H, d, H<sub>arom</sub>, J = 8 Hz), 8.04 (1H, dd, H<sub>arom</sub>, J = 8 Hz, 2 Hz), 7.93 (1H, d, H<sub>arom</sub>, J = 8 Hz), 7.57 (1H, d, H<sub>arom</sub>, J = 8 Hz), 7.41 (1H, dd, H<sub>arom</sub>, J = 8 Hz, 2 Hz) <sup>13</sup>C-NMR Spectrum (100 MHz, CDCl<sub>3</sub>, δ): 163.9 (C=O), 162.7 (F-C<sub>naphthyl</sub>), 161.4 ((C=O)O-C<sub>6</sub>F<sub>5</sub>), 137.5 (C<sub>6</sub>F<sub>5</sub>), 137.4 (C<sub>6</sub>F<sub>5</sub>), 132.9 (C<sub>6</sub>F<sub>5</sub>), 132.4 (C<sub>6</sub>F<sub>5</sub>), 132.3 (C<sub>6</sub>F<sub>5</sub>), 129.4 (C<sub>naphthyl</sub>), 128.2 (C<sub>naphthyl</sub>), 128.1 (C<sub>naphthyl</sub>), 126.4 (C<sub>naphthyl</sub>), 123.5 (C<sub>naphthyl</sub>), 118.0 (C<sub>naphthyl</sub>), 117.7 (C<sub>naphthyl</sub>), 111.5 (C<sub>naphthyl</sub>), 111.2 (C<sub>naphthyl</sub>).

### 3.3.8 Radiolabelling Procedure of [<sup>18</sup>F]-PFPN

To prepare **3.11**, Tracerlab FX<sub>FN</sub> (GE Healthcare) was configured as shown in figure 4. Vials were loaded as follows: Vial 1: potassium carbonate (2.0 mg), krytofix 2.2.2 (7.0 mg) in 200 μL H<sub>2</sub>O and 800 μL ACN; Vial 2: 1000 μL anhydrous ACN; Vial 3: 1000 μL anhydrous ACN; Vial 4: 2 mg of **3.11** in 750 μL DMSO; Vial 5: 20 μL TMAH (1M) in 1000 μL ACN.

Fluorine-18 was produced on a GE Healthcare PETtrace 880 cyclotron (16.5 MeV) via a  $^{18}\text{O}(\text{p},\text{n})$  nuclear reaction on a high yield Nb25 fluorine-18 target. Fluoride-18 was delivered in a 2 mL aliquot to a QMA carbonate Sep-Pak to isolate the  $[\text{}^{18}\text{O}]\text{H}_2\text{O}$  from fluoride-18. The fluoride was then eluted into the reaction vial using the potassium carbonate/kryptofix solution in Vial 1. The fluoride-18 was azeotropically dried by heating the reaction vial to 75 °C under full vacuum for 5 minutes. This repeated 2 more times using the anhydrous ACN in Vials 2 and 3. Once dried, the radiolabelling precursor **3.11** was added to the reaction vial from Vial 4, heated to 120 °C and allowed to react for 10 minutes. Following this reaction, Vial 5 was added to the reaction vial to hydrolyze the ester, heated to 90 °C for 5 minutes before being cooled to 40 °C and completing the automated portion of the synthesis. The reactor needle was injected down into the reaction mixture and helium was pumped into the reaction vial for 3 minutes to transfer the crude mixture from the reaction vial to a product vial *via* V14. The crude mixture was collected into 20 mL scintillation vial containing 7 mL of 0.1% TFA in MilliQ water in the side chamber and removed for manual synthesis.

The diluted mixture was loaded onto a conditioned tC18 Sep Pak to remove unreacted fluoride-18. Radiolabelled **3.16** was eluted from the Sep-Pak with 1000  $\mu\text{L}$  of ACN into a new reaction vial containing 20 mg pentafluorophenol, 10 mg EDC and 1 mg of DMAP. The mixture was allowed to react at room temperature for 5 minutes before being diluted with 500  $\mu\text{L}$  of 0.1% TFA in  $\text{H}_2\text{O}$  and injected onto the HPLC for semi-preparative purification (55% to 95% acetonitrile in water with 0.1% TFA). Purified **3.16** was collected at 9 minutes into a scintillation vial and subsequently evaporated to dryness using a Biotage Speed Rotary Evaporator for 5 minutes. After evaporation, **3.17** in 750  $\mu\text{L}$  of ACN was added to the scintillation vial followed by 30  $\mu\text{L}$  of DIPEA. The reaction mixture was left at 40 °C for 20 minutes, diluted to 1500  $\mu\text{L}$  with 0.1% TFA in  $\text{H}_2\text{O}$  and injected on to the HPLC for semi-preparative purification (20% to 80% acetonitrile in water with 0.1% TFA). Purified **3.18** was collected at 5 minutes for 1.5 minutes into a 10 mL sterile vial resulting in approximately 8 mL of solvent.

### 3.3.9 Quality Control of [<sup>19</sup>F]-PFPN

Using an analytical radio-RP-HPLC equipped with a gamma detector, the radiochemical purity and identity of **3.18** was confirmed by co-injection with a non-radioactive standard **3.7**. Retention times were consistent at 5.0 minutes. **3.18** was obtained in 3.1% decay correct radiochemical yield and 95% radiochemical purity with a complete synthesis time of 1.5 hours.

## 3.4 Acknowledgments

Thank you to the Nordal Cyclotron & PET Radiochemistry Facility at St. Josephs Hospital in London, Ontario, Canada for generously donating [<sup>18</sup>F]H<sub>2</sub>[<sup>18</sup>O] for these procedures.

## 3.5 References

1. P. Ray, *J Biosci*, 2011, **36**, 499-504.
2. S. Lee, J. Xie and X. Chen, *Chem Rev*, 2010, **110**, 3087-3111.
3. M. Gabriel, C. Decristoforo, D. Kendler, G. Dobrozemsky, D. Heute, C. Uprimny, P. Kovacs, E. Von Guggenberg, R. Bale and I. J. Virgolini, *J Nucl Med*, 2007, **48**, 508-518.
4. E. P. Krenning, D. J. Kwekkeboom, W. H. Bakker, W. A. Breeman, P. P. Kooij, H. Y. Oei, M. van Hagen, P. T. Postema, M. de Jong, J. C. Reubi and et al., *Eur J Nucl Med*, 1993, **20**, 716-731.
5. C. J. Anderson, F. Dehdashti, P. D. Cutler, S. W. Schwarz, R. Laforest, L. A. Bass, J. S. Lewis and D. W. McCarthy, *J Nucl Med*, 2001, **42**, 213-221.
6. S. Gnanapavan, B. Kola, S. A. Bustin, D. G. Morris, P. McGee, P. Fairclough, S. Bhattacharya, R. Carpenter, A. B. Grossman and M. Korbonits, *J Clin Endocrinol Metab*, 2002, **87**, 2988.
7. P. L. Jeffery, A. C. Herington and L. K. Chopin, *J Endocrinol*, 2002, **172**, R7-11.

8. A. H. Yeh, P. L. Jeffery, R. P. Duncan, A. C. Herington and L. K. Chopin, *Clin Cancer Res*, 2005, **11**, 8295-8303.
9. P. Cassoni, M. Papotti, C. Ghe, F. Catapano, A. Sapino, A. Graziani, R. Deghenghi, T. Reissmann, E. Ghigo and G. Muccioli, *J Clin Endocrinol Metab*, 2001, **86**, 1738-1745.
10. F. Gaytan, M. L. Barreiro, J. E. Caminos, L. K. Chopin, A. C. Herington, C. Morales, L. Pinilla, R. Paniagua, M. Nistal, F. F. Casanueva, E. Aguilar, C. Dieguez and M. Tena-Sempere, *J Clin Endocrinol Metab*, 2004, **89**, 400-409.
11. F. Gaytan, C. Morales, M. L. Barreiro, P. Jeffery, L. K. Chopin, A. C. Herington, F. F. Casanueva, E. Aguilar, C. Dieguez and M. Tena-Sempere, *J Clin Endocrinol Metab*, 2005, **90**, 1798-1804.
12. M. Kojima, H. Hosoda, Y. Date, M. Nakazato, H. Matsuo and K. Kangawa, *Nature*, 1999, **402**, 656-660.
13. M. A. Bednarek, S. D. Feighner, S.-S. Pong, K. K. McKee, D. L. Hreniuk, M. V. Silva, V. A. Warren, A. D. Howard, L. H. Y. Van der Ploeg and J. V. Heck, *J. Med. Chem.*, 2000, **43**, 4370-4376.
14. M. Matsumoto, H. Hosoda, Y. Kitajima, N. Morozumi, Y. Minamitake, S. Tanaka, H. Matsuo, M. Kojima, Y. Hayashi and K. Kangawa, *Biochem. Biophys. Res. Commun.*, 2001, **287**, 142-146.
15. M. Matsumoto, Y. Kitajima, T. Iwanami, Y. Hayashi, S. Tanaka, Y. Minamitake, H. Hosoda, M. Kojima, H. Matsuo and K. Kangawa, *Biochem. Biophys. Res. Commun.*, 2001, **284**, 655-659.
16. M. Van Craenenbroeck, F. Gregoire, P. De Neef, P. Robberecht and J. Perret, *Peptides*, 2004, **25**, 959-965.

17. C. Lu, M. S. McFarland, R.-L. Nesbitt, A. K. Williams, S. Chan, J. Gomez-Lemus, A. M. Autran-Gomez, A. Al-Zahrani, J. L. Chin, J. I. Izawa, L. G. Luyt and J. D. Lewis, *The Prostate*, 2012, **72**, 825-833.
18. R. McGirr, M. S. McFarland, J. McTavish, L. G. Luyt and S. Dhanvantari, *Regul. Peptides*, 2011, **172**, 69-76.
19. T. Akamizu, K. Takaya, T. Irako, H. Hosoda, S. Teramukai, A. Matsuyama, H. Tada, K. Miura, A. Shimizu, M. Fukushima, M. Yokode, K. Tanaka and K. Kangawa, *Eur J Endocrinol*, 2004, **150**, 447-455.
20. A. M. Wassermann and J. Bajorath, *MedChemComm*, 2011, **2**, 601-606.
21. D. Rosita, M. A. DeWit and L. G. Luyt, *J. Med. Chem.*, 2009, **52**, 2196-2203.
22. S. Richter, M. Wuest, S. S. Krieger, B. E. Rogers, M. Friebe, R. Bergmann and F. Wuest, *Nucl Med Biol*, 2013, **40**, 1025-1034.
23. D. Thonon, D. Goblet, E. Goukens, G. Kaisin, J. Paris, J. Aerts, S. Lignon, X. Franci, R. Hustinx and A. Luxen, *Mol Imaging Biol*, 2011, **13**, 1088-1095.
24. D. E. Olberg, J. M. Arukwe, D. Grace, O. K. Hjelstuen, M. Solbakken, G. M. Kindberg and A. Cuthbertson, *J Med Chem*, 2010, **53**, 1732-1740.
25. M. R. Lockett, M. F. Phillips, J. L. Jarecki, D. Peelen and L. M. Smith, *Langmuir*, 2008, **24**, 69-75.
26. McFarland, M., "The Design and Synthesis of Ghrelin as Molecular Imaging Probes" (2011). Electronic Thesis and Dissertation Repository.

## Chapter 4

### 4 Synthesis of Monomeric and Dimeric Dye Labelled Ghrelin(1-8) Analogues for Evaluation in GHS-R1a Expressing Cells by Fluorescence Microscopy

#### 4.1 Introduction

The growth hormone secretagogue receptor-1a (GHS-R1a) is a G-protein coupled receptor (GPCR) that is activated by peptidic growth hormone secretagogues to release growth hormone from the pituitary. This receptor is not solely expressed in the pituitary and can be found in various other tissues such as the hypothalamus, heart, lung, pancreas, intestine and adipose.<sup>1, 2</sup> When activated by its endogenous ligand, ghrelin, this receptor performs important roles such as energy homeostasis, body weight control, aging and cardiac contractility. The endogenous ligand for GHS-R1a was isolated from the rat stomach in 1990 by Kojima *et. al.*<sup>2</sup> Ghrelin is a 28 amino acid peptide containing a unique octanoylated serine at residue 3 of the amino acid sequence.

Several peptides, such as neuropeptide Y, cholestokinin and ghrelin, are capable of stimulating feeding and maintaining a positive energy balance through central or peripheral administered doses.<sup>3-5</sup> What is most intriguing about ghrelin, is its ability to have a longer acting regulation of body weight rather than a short-term, meal related regulation found with other peptides, such as cholestokinin. The ghrelin-GHSR-1a axis has also been implicated in aging. Studies have shown the GHS-R1a regulates the timing and amplitude of growth hormone release in human subjects and as subjects age, the amplitude of growth hormone release begins to regress. Administration of ghrelin agonist analogues to elderly human subjects was shown to increase amplitude of GH release, increase lean mass in shoulder and knee strength, accelerate the healing process following a hip fracture as well as increase bone mineral density in postmenopausal women.<sup>6-10</sup> From a therapeutic standpoint, targeting GHS-R1a receptors using ghrelin-based analogues can hold promise for treatment of anorexia, cachexia or other diseases that cause involuntary weight loss as well as age-dependent functions caused by suppression of growth hormone.<sup>11</sup> Targeting of GHS-R1a is also advantageous for

diagnosis of cardiomyopathy and cancer. Studies have shown that GHS-R1a is upregulated in the left ventricular tissue of patients that previously suffered congestive heart failure. These areas of higher GHS-R1a concentration were visualized using dye-labelled ghrelin analogues and fluorescence microscopy.<sup>12-14</sup> GHSR-1a and ghrelin have also been implicated in many cancer progression processes such as cell proliferation, migration and apoptosis. GHSR-1a has been identified in a wide range of human cancers such as pituitary, prostate, breast, and ovarian tumours as well as astrocytoma.<sup>15</sup> The GHS-R1a/ghrelin axis plays an important role in various biological issues that require therapeutic and diagnostic pharmaceuticals. Development of ghrelin-based ligands with affinity and specificity to GHS-R1a would have a wide range of applications in both therapeutic and diagnostic fields.

There are several approaches to increasing the affinity and specificity of a targeting ligand, one method that has proven to be successful is multimerization. Several examples of multimerization have been demonstrated with RGD to target the integrin receptor  $\alpha_v\beta_3$ . When compared to monomeric RGD, dimeric and tetrameric analogues have shown to possess improved *in vivo* kinetics and target affinity.<sup>16,17</sup> The increase in affinity has been attributed to a higher local concentration of the targeting peptide in the immediate surroundings of the receptor. Once one unit of the multimer ligand has been bound, the other units are more likely to have a higher rate of binding and lower rate of dissociation. This phenomenon leads to higher uptake and longer retention of targeting ligands at the receptor.<sup>18</sup> These aspects of multimerization are valuable when visualizing receptors of interest and therefore have been applied to various peptides used in optical imaging and scintillation imaging.<sup>16-22</sup>

Optical imaging (OI) is a useful tool to visualize molecular targets in living systems without using radioactive materials required for other imaging modalities, such as positron emission tomography (PET) and single-photon emission computed tomography (SPECT). This method of imaging is known to be a cost-effective and robust but difficulties arise when photons are absorbed or scattered by surrounding tissues. These difficulties can be addressed by using near-infrared (NIR) light (700-1000 nm) that has better photon penetration in and out of tissues and therefore more less absorption and

scattering is caused by tissues. OI can be used to better understand the biology of various disease states as well as monitor therapy and other biological process.

There are two examples in which fluorescently labelled ghrelin analogues have been used to detect the GHS-R1a receptor as a biomarker of prostate cancer and cardiomyopathy.<sup>13, 23</sup> In the first example, a fluorescein-ghrelin(1-19) analogue was incubated with prostate core biopsy samples of 13 patients with ranging conditions from normal, benign hyperplasia (BPH), prostatic interneoplasia (PIN) and prostate cancer. Using OI, the fluorescent signal of fluorescein-ghrelin(1-19) was 4.7-fold higher in prostate cancer than BPH and normal prostate tissue. The signal was also 1.9-fold higher in prostate cancer than PIN. This not only demonstrates the value OI agents have for biomarker screening of *ex vivo* biopsy samples using a facile and low cost method of detection, but also demonstrates the usefulness of ghrelin for accurate detection of prostate cancer from other states of prostate tissue health. The second example uses a Cyanine5-ghrelin(1-19) analogue to detect the presence of GHS-R1a during the differentiation of P19-derived cardiomyocytes through using OI in *in vitro* and *ex vivo* assays.

In this study, we propose to synthesize high affinity monomeric and dimeric ghrelin(1-10) analogues bearing a NIR Cyanine5 dye. These NIR-analogues can be used to visualize GHS-R1a using fluorescence microscopy and holds promise for monitoring therapies and diagnosis of the various biological processes effected by the GHS-R1a receptor.

## 4.2 Results and Discussion

### 4.2.1 Synthesis and Characterization of a NIR Ghrelin(1-10) Monomer and Dimer

As discussed in Chapter 3, ghrelin can be truncated to the first 8 *N*-terminal amino acids and maintain affinity to GHS-R1a. Through modification of various positions in the 8 amino acid sequence, several analogues were able to selectively target GHS-R1a with remarkable affinity. Replacing phenylalanine-4 with 1-naphthylalanine (Nal-1) lead to a 48-fold increase in affinity to GHS-R1a while replacing glutamic acid-8 with threonine lead to a 61-fold increase in affinity than the natural ghrelin(1-8) sequence. These two

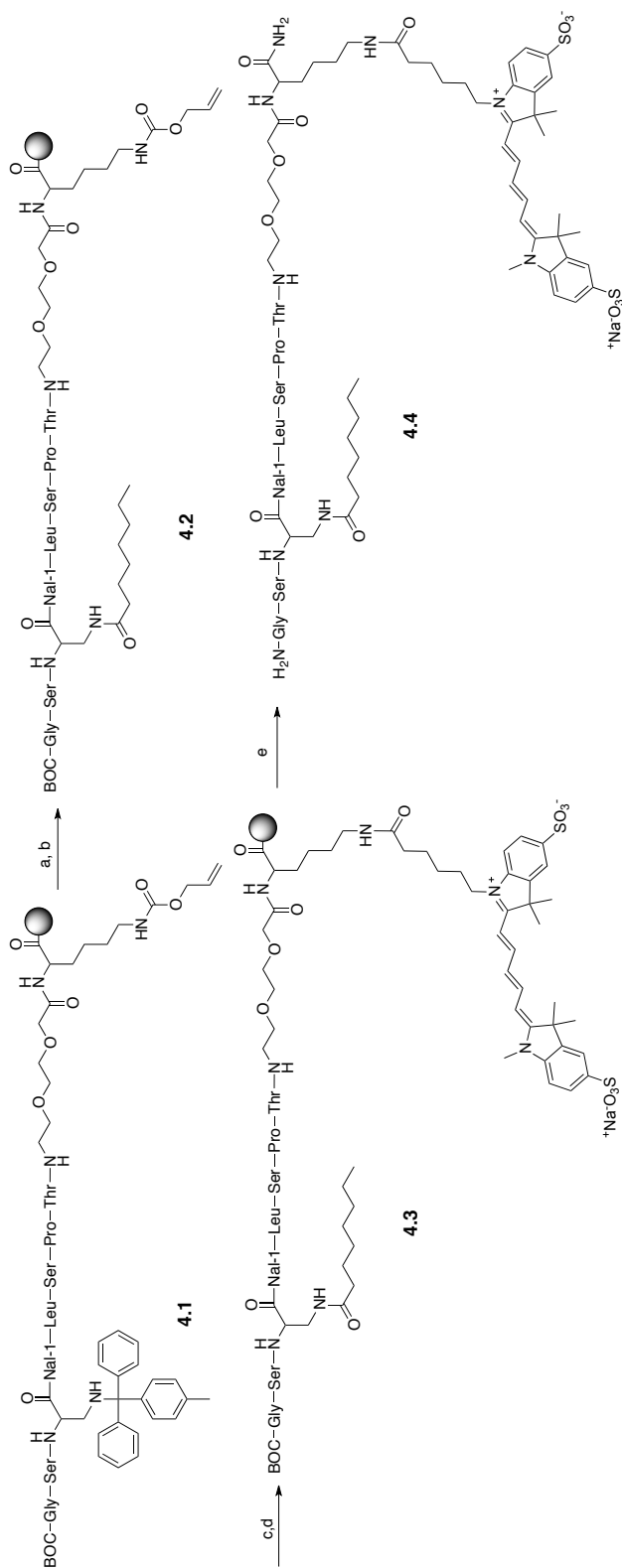


modifications were incorporated into a ghrelin(1-10) monomer and a ghrelin (1-10) dimer to target GHS-R1a. All the other amino acids were left unchanged except for residue 3, which was substituted for diaminopropionic acid (Dpr) acylated with octanoic acid. This substitution replaces the labile ester moiety with an amide for better stability and facile chemical synthesis. Therefore, the ghrelin(1-8) peptide chosen to be further developed into a fluorescent ghrelin(1-10) monomer and dimer was; H-GS-Dpr(octanoyl)-(Nal-1)-LSPT-NH<sub>2</sub>.

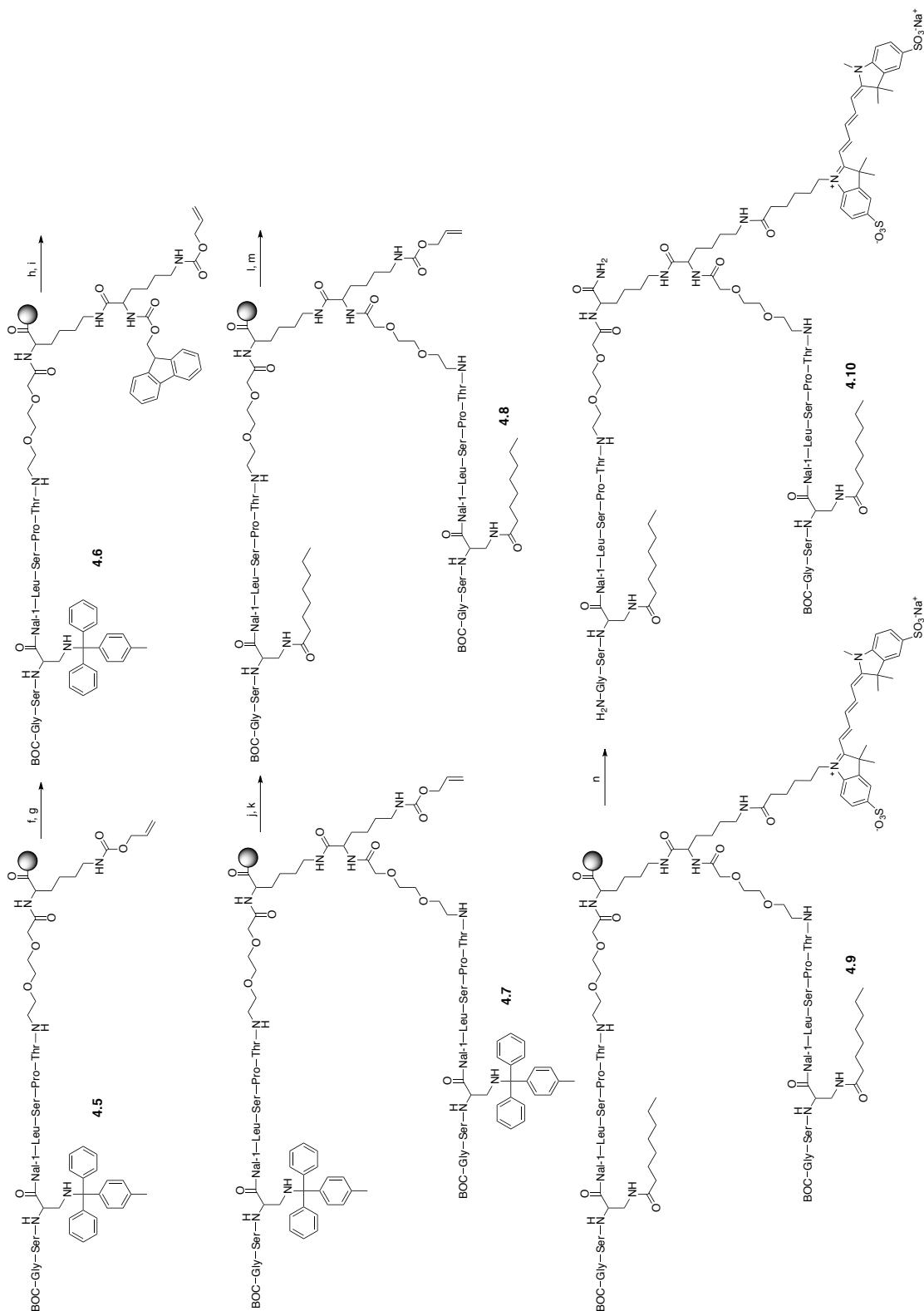
In order to maintain affinity to GHS-R1a, ghrelin analogues can only be modified at the C-terminus due to the importance of the N-terminal amine for receptor binding.<sup>24</sup> The Cy5-Ghrelin (1-10) monomer (Scheme 4.1) and dimer (Scheme 4.2) were synthesized using standard Fmoc peptide chemistry on a solid support. They were synthesized with amino acids bearing standard protecting groups, with the exception of Dpr and Lys, that contained the orthogonal protecting groups methytrityl (Mtt) and allyloxycarbonyl (Alloc). After automated peptide synthesis of the core amino acid sequence, the orthogonal protecting groups were selectively removed to acylate Dpr with octanoic acid and to incorporate the cyanine-5 (Cy5) on the lysine side chain, resulting in the **4.4**. To synthesize the ghrelin dimer, the first ghrelin unit was synthesized on solid support using automated peptide synthesis followed by selective deprotection of the lysine alloc protecting group to couple another Fmoc-lysine(alloc)-OH using standard coupling conditions. The second lysine introduces another Fmoc-protected N-terminal amine for the second targeting ghrelin unit to be synthesized using automated peptide synthesis. Once both ghrelin units were added to the solid support, the Mtt protecting group is selectively deprotected from both Dpr side chains and the resulting free amines are acylated with octanoic acid. The final deprotection of alloc on the second lysine side chain leaves a free amine to couple Cy5 resulting in **4.10**. To reduce the negative steric effects the Cy5 may cause on receptor affinity, the ghrelin(1-8) targeting peptides were separated from the lysine by a [2-(2-(Fmoc-amino)ethoxy)ethoxy]acetic acid (AEEA) spacer and are therefore ghrelin(1-10) analogues. Both peptides were cleaved from the resin and all standard protecting groups removed using strong acid before being purified by reverse-phase preparative HPLC. The yields and purities are summarized in Table 1.

**Table 4.1** Analytical data for 4.4 and 4.10

<b>Ghrelin Analogue</b>	<b>[M+2H]<sup>2+</sup> Expected</b>	<b>[M+2H]<sup>2+</sup> Observed</b>	<b>Yield</b>	<b>Purity</b>
<b>4.4</b>	934.4612	934.1838	26%	98%
<b>4.10</b>	1547.3027	1547.9197	25%	91%



**Scheme 4.1** Synthesis of monomer (4.4). a. 2% TFA, 5% TIS in DCM, b. octanoic acid (3 eq.), HCTU (3eq.), DIPEA (6 eq.) c. Pd(PPh<sub>3</sub>)<sub>4</sub> (0.035 eq.), PhSiH<sub>3</sub> (2 eq.), DCM, d. sulfo-Cy5 NHS ester (1 eq.), DIPEA (2 eq.) in DMF, e. 95% TFA, 2.5% H<sub>2</sub>O, 2.5% TIS



**Scheme 4.2** Synthesis of dimer (**4.10**). f. Pd(PPh<sub>3</sub>)<sub>4</sub> (0.035 eq.), PhSiH<sub>3</sub> (2 eq.), DCM, g. Fmoc-Lys(alloc)-OH (3 eq.), HCTU (3 eq.), DIPEA (6 eq.) in DMF, h. 20% piperidine in DMF (3 mL), i. Automated peptide synthesis, j. 2% TFA, 2% TIS in DCM, k. octanoic acid (6 eq.), HCTU (6 eq.), DIPEA (12 eq.) l. Pd(PPh<sub>3</sub>)<sub>4</sub> (0.035 eq.), PhSiH<sub>3</sub> (2 eq.), DCM, m. sulfo-Cy5 NHS ester (1 eq.), DIPEA (2 eq.) in DMF, n. 95% TFA, 2.5% H<sub>2</sub>O, 2.5% TIS

#### 4.2.2 Binding Affinity of **4.4** and **4.10** to GHS-R1a

The binding affinity of each peptide was measured using a competitive binding assay against  $^{125}\text{I}$ -Ghrelin(1-28). Varying concentrations of the monomer and dimer were incubated with HEK293 cells transfected with GHS-R1a in the presence of  $^{125}\text{I}$ -ghrelin(1-28). As the concentration of the monomer and dimer was increased,  $^{125}\text{I}$ -ghrelin(1-28) was competitively displaced and quantified into sigmoidal curve (Figure 4.2). The half-maximal concentration ( $\text{IC}_{50}$ ) can be extracted from these curves and used to quantify the binding affinity to GHS-R1a.

From the  $\text{IC}_{50}$  curves, the monomer (**4.4**) had 26.3 nM affinity while the dimer (**4.10**) had 50.0 nM affinity. As reported in Chapter 2, the  $\text{IC}_{50}$  of the unmodified ghrelin(1-8) sequence is 200 nM. The monomer and dimer were able to achieve 7.6 and 4.0-fold increase in affinity, respectively. This is the opposite trend than expected. Dijkgraaf *et al.* studied the multimerization of [ $^{68}\text{Ga}$ ]-RDG peptides by synthesizing a homomonomer, dimer and tetramer. The binding affinity to integrin  $\alpha_v\beta_3$  became stronger as more RGD units were added. The monomer, dimer and tetramer had  $\text{IC}_{50}$  values of 23.9 nM, 8.99 nM and 1.74 nM respectively. Multimerization of ghrelin did not produce the same trend although tetrameric analogues were not studied.<sup>21</sup>

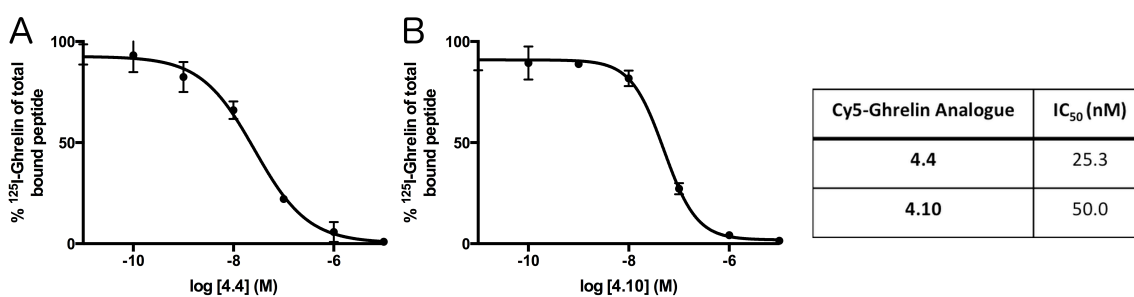


**Figure 4.1** Competitive binding curves in HEK293/GHS-R1a cells and  $\text{IC}_{50}$  (nM) values for **4.4** (A) and **4.10** (B)

### 4.2.3 *In Vitro* Fluorescence Imaging in HT1080 and HT1080/GHS-R1a

The subcellular localization of **4.4** and **4.10** were evaluated in the HT1080 (GHS-R1a negative) cell line and the HT1080/GHS-R1a (GHS-R1a positive) cell line. Each peptide was diluted with DMSO into a 0.5  $\mu$ M solution and incubated with each cell line for 1 hour at 37 °C. The cells were then rinsed with serum-free media and PBS before fixed to microscope slides with 4% paraformaldehyde. Cyanine5 has an excitation maximum of 646 nm and emission maximum of 662 nm, therefore the slides were irradiated with 636 nm light for excitation and emissions were collected using a 663-738 nm filter to visualize the dye-labelled fluorescence. DAPI stained nuclei were irradiated with 402 nm light and emissions were collected using a 425 – 475 nm filter. The images were then overlaid into the merge images.

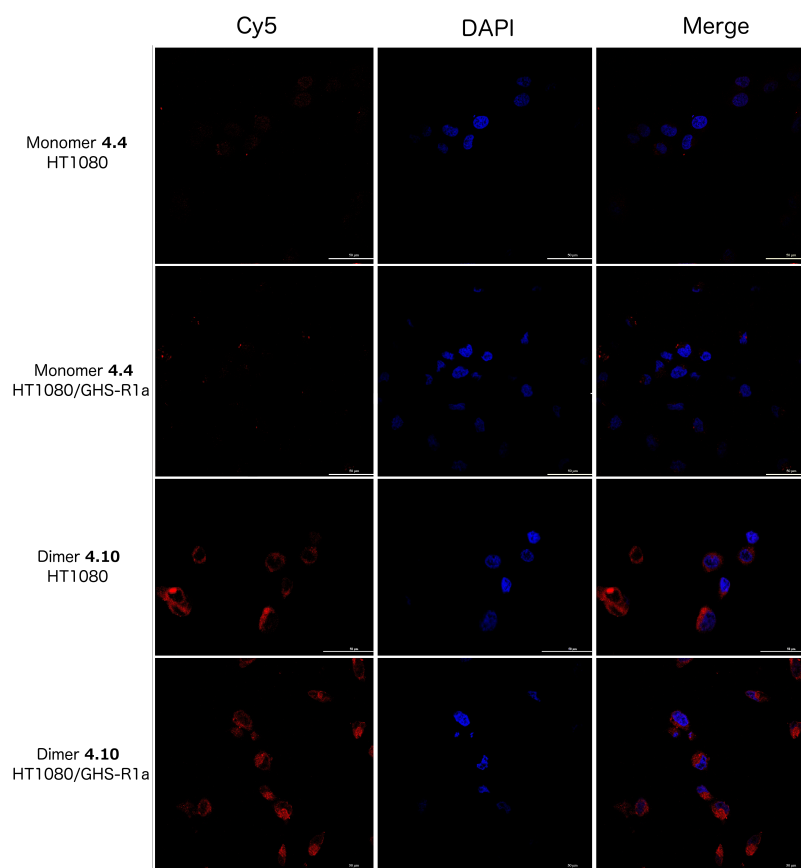


**Figure 4.2** Confocal microscopy results of 4.4 and 4.10 with HT1080 (GHS-R1a negative) and HT1080/GHS-R1a (GHS-R1a positive) (magnification x 60).

The obtained fluorescence images are shown in Figure 4.2. Contrary to the  $IC_{50}$  results, **4.4** had little localization in both cell lines. Within the HT1080/GHS-R1a images, it appears that there are areas of highly concentrated fluorescence on the cell surface that are not present in the HT1080 cell line. This could be due the higher expression of the target receptor although the difference of fluorescence in each cell line was hypothesized to be much greater. **4.10**, which possessed the lower affinity to GHS-R1a based off the  $IC_{50}$  had high fluorescence in both cell lines. The fluorescence in HT1080 cells appears uniform along the cell surface while the fluorescence appears less uniform and more concentrated into specific areas on the cell surface of the HT1080/GHS-R1a cells. This is the same trend seen with **4.4**. The high fluorescence of **4.10** in HT1080 cells suggest that creating a dimer of ghrelin has effect the *in vitro* properties of peptide and lead the peptide to non-preferentially binding to the cell surface. This is undesirable as the peptide can no longer be used to distinguish between GHS-R1a expression. Western blot analysis is underway with HT1080 and HT1080/GHS-R1a cells to confirm the expression of GHS-R1a in each cell line. These results will provide an explanation regarding the low uptake of the monomer **4.4** that is unexpected with an  $IC_{50}$  of 25.3 nM.

### 4.3 Conclusions

The many biological roles effected by GHS-R1a make this a beneficial pharmacological target for various therapeutic and diagnostic applications that require specific and prolonged interaction of a targeting entity with the receptor. As mentioned in Chapter 2, ghrelin(1-8) analogues are capable of targeting GHS-R1a with high affinity and using the emerging field of multimerization, held promise to become higher affinity and longer acting ghrelin targeting entities. Unfortunately, dimerizing a high affinity ghrelin(1-8) analogue and introducing a NIR dye caused detrimental effects on binding affinity. The dimerized peptide also developed non-preferential cell surface binding when dimerized and therefore were not ideal OI agents for GHS-R1a. Liu *et al.* compared the pharmacokinetic properties of two RGD dimers with differing chain lengths between the homodimeric units. One RGD dimer contained 15 atom linker while the other RGD dimer contained a 47 atom linker. The extra chain length increased the *in vitro* binding affinity, but more importantly, resulted in better tumour to background ratios.<sup>19</sup>

Therefore, it is advantageous to further investigate the optimal chain length between ghrelin units in order to obtain better binding affinity and *in vitro* kinetics of these dimers. Other structural changes such as using a different ghrelin(1-8) sequence, or another NIR dye may also have a positive effect on these dimer properties.

## 4.4 Experimental

### 4.4.1 Materials and Methods

All common solvents were purchased from Fisher Scientific. All protected amino acids, coupling reagents and resins were purchased from Novabiochem, Peptides International and Chem-Impex and were used without further purification unless otherwise stated. All reagents were obtained from Sigma-Aldrich. [<sup>125</sup>I]-Ghrelin(1-28) was purchased from Perkin Elmer. For analytical HPLC-MS, an Agilent RP-C18 4.6 x 250 mm, 5 μm column was used. For semi-preparative HPLC-MS work, an Agilent RP-C18 19 x 150 mm, 5 μm column was used. A gradient solvent system was used containing 0.1% TFA in acetonitrile (solvent A) and 0.1% TFA in water (solvent B). For analytical UHPLC-MS, studies were performed on a Waters, Inc. Acquity UHPLC H-Class system, combined with a Xevo QToF mass spectrometer (ES+, cone voltage = 30 V). For analytical UHPLC-MS studies, a Waters Acquity UHPLC BEH C18 2.1 x 50 mm, 1.7 μm column was used with a gradient solvent system consisting of 0.1% formic acid in acetonitrile (solvent C) and 0.1% formic acid in water (solvent D).

### 4.4.2 Automated Peptide Synthesis of **4.4**

Automated peptide synthesis was carried out using a Biotage Syrowave synthesizer and all amino acids contained standard protecting groups with the exception of Dpr and Lys that contained methyltrityl (Mtt) and allyloxycarbonyl (Alloc) orthogonal protecting groups, respectively. The N-terminal glycine contained a BOC protecting group rather than Fmoc. **4.4** was synthesized at a 0.1 mmol scale on Rink Amide MBHA resin (0.52 mmol/g). The resin was initially swelled with *N,N*-dimethylformamide (DMF) followed by two cycles (10 minutes, 5 minutes) of Fmoc deprotection using 2 mL of 20% piperidine in *N,N*-dimethylformamide (DMF). Amino acids were preactivated by combining 3 eq. of Fmoc-protected amino acid, 3 eq. of HCTU and 6 eq. of *N,N*-



diisopropylethylamine (DIPEA) in 2 mL of DMF. The mixture was added to the resin and coupled for 60 minutes. These cycles were repeated until all 10 N-terminal amino acids were coupled to the resin in the following sequence; H-GS-Dpr(mtt)-Nal-1-LSPT-AEEA-Lys(Alloc)-Rink Amide MBHA Resin.

Mtt deprotection of diaminopropionic acid was performed using vortexing the resin with 2 mL of 2% TFA and %5 TIS in dichloromethane for 2 minutes. The resin was then rinsed well with dichloromethane. This method was repeated 8 times, or until the solution no longer appeared yellow. Following the deprotection, the resin was vortexed with 200  $\mu$ L of DIPEA in DMF to neutralize any residual TFA. Octanoic acid (3 eq.) was coupled to the Dpr free amine using HCTU (3 eq.) and DIPEA (6 eq.) in DMF. The resin was vortexed for 1 hour.

Allyloxycarbonyl deprotection of lysine was performed under inert atmospheric N<sub>2</sub> conditions. DCM was dried over sieves for 24 hours before adding 1 mL to the resin. 2 eq. of phenylsilane in 1 mL dry DCM was then added to the peptide resin followed by 0.045 eq. of tetrakis(triphenylphosphine) palladium (0) in 1 mL dry DCM. The peptide vessel was removed from inert conditions and allowed to react for 30 minutes. The resin was thoroughly rinsed with dichloromethane and subsequently dried by passing air over the resin. The dried resin was weighed and 10% of the total resin was transferred to a new peptide vessel to couple to the NIR dye. The lysine free amine was coupled to sulfo-cyanine5 NHS ester (1 eq.) using 50  $\mu$ L of DIPEA in 0.5 mL of DMF. The peptide vessel was covered in foil and allowed to vortex overnight. The resin was thoroughly washed with DMF and dichloromethane.

Full deprotection and cleavage from solid support was performed by adding a 1 mL mixture of 95% TFA, 2.5% TIS and 2.5% water to the resin and allowed it to mix for 5 hours in the dark. The cleaved peptide was precipitated from solution using ice-cold *tert*-butyl methyl ether (TBME) and centrifuged (3000 rpm, 10 minutes) resulting in a crude peptide pellet. The supernatant was decanted and the resulting peptide pellet was dissolved in 20% acetonitrile in water, frozen at -78 °C and lyophilized to a blue crude powder. Purification was performed using preparative HPLC-MS and purity of the

resulting peptides were analyzed using analytical UHPLC. HRMS (ESI<sup>+</sup>): m/z calculated for C<sub>91</sub>H<sub>131</sub>N<sub>15</sub>O<sub>23</sub>S<sub>2</sub>, [M+2H]<sup>2+</sup> = 934.4612, observed [M+2H]<sup>2+</sup> = 934.1838.

#### 4.4.3 Automated Peptide Synthesis of **4.10**

Automated peptide synthesis was carried out using Biotage Syrowave and all amino acids contained standard protecting groups with the exception of Dpr and Lys that contained methyltrityl (Mtt) and allyloxycarbonyl (Alloc) orthogonal protecting groups, respectively. The N-terminal glycine contained a BOC protecting group rather than Fmoc. **4.10** was synthesized at a 0.1 mmol scale on Rink Amide MBHA resin (0.52 mmol/g). The resin was initially swelled with *N,N*-dimethylformamide (DMF) followed by two cycles (10 minutes, 5 minutes) of Fmoc deprotection using 2 mL of 20% piperidine in *N,N*-dimethylformamide (DMF). Amino acids were preactivated by combining 3 eq. of Fmoc-protected amino acid, 3 eq. of HCTU and 6 eq. of *N,N*-diisopropylethylamine (DIPEA) in 2 mL of DMF. The mixture was added to the resin and coupled for 60 minutes. These cycles were repeated until all 10 N-terminal amino acids were coupled to the resin in the following sequence; H-GS-Dpr(mtt)-Nal-1-LSPT-AEEA-Lys(Alloc)-Rink Amide MBHA Resin.

Allyloxycarbonyl deprotection of lysine was performed under inert atmospheric N<sub>2</sub> conditions. DCM was dried over sieves for 24 hours before adding 1 mL to the resin. 2 eq. of phenylsilane in 1 mL dry DCM was then added to the peptide resin followed by 0.045 eq. of tetrakis(triphenylphosphine) palladium (0) in 1 mL dry DCM. The peptide vessel was removed from inert conditions and allowed to react for 30 minutes. The resin was thoroughly washed with dichloromethane and DMF before being manually coupled to Fmoc-Lys(alloc)-OH (3 eq.) using HCTU (3 eq.) and DIPEA (6 eq.) in 2 mL of DMF. The resin was vortexed for 1 hour and thoroughly rinsed with DMF before being placed on the Biotage Syrowave to continue the automated synthesis of the second ghrelin unit of the dimer. Upon completion of automated synthesis, the second Dpr(Mtt) was deprotected using the same Mtt deprotection protocol explained above and couple to octanoic acid using the same coupling conditions. The second Lys(alloc) was deprotected using the same method listed above and thoroughly rinsed with dichloromethane before drying the resin by passing air over it. The resin was also weighed and 10% of the resin

was transferred to a new peptide vessel. The free amine was coupled to sulfo-cyanine5 NHS ester (Lumiprobe, 1 eq.) with 200  $\mu$ L of DIPEA in 1 mL of DMF. The resin was vortexed in the dark overnight before being thoroughly rinsed with DMF and dichloromethane.

Full deprotection and cleavage from solid support was performed by adding a 1 mL mixture of 95% TFA, 2.5% TIS and 2.5% water to the resin and allowed it to mix for 5 hours in the dark. The cleaved peptide was precipitated from solution using ice-cold *tert*-butyl methyl ether (TBME) and centrifuged (3000 rpm, 10 minutes) resulting in a crude peptide pellet. The supernatant was decanted and the resulting peptide pellet was dissolved in 20% acetonitrile in water, frozen at -78  $^{\circ}$ C and lyophilized to a blue crude powder. Purification was performed using preparative HPLC-MS and purity of the resulting peptides were analyzed using analytical UHPLC. HRMS (ESI<sup>+</sup>): m/z calculated for C<sub>150</sub>H<sub>233</sub>N<sub>27</sub>O<sub>39</sub>S<sub>2</sub>, [M+2H]<sup>2+</sup> = 1547.3027, observed [M+2H]<sup>2+</sup> = 1547.9197.

#### 4.4.4 Competitive Binding Assay (IC<sub>50</sub>)

The affinity for GHS-R1a was determined using a radioligand competitive binding assay. Assays were performed using GHS-R1a transfected HEK293 cells as receptor source and human [<sup>125</sup>I]-ghrelin(1-28) (PerkinElmer Inc.) as the radioligand. Human ghrelin(1-28) was used as reference to ensure the validity of the results. A suspension of membrane from HEK293/GHS-R1a cells (50,000 cells per assay tube) were incubated with ghrelin(1-8) peptide analogues (at concentrations of 10<sup>-5</sup> M, 10<sup>-6</sup> M, 10<sup>-7</sup> M, 10<sup>-8</sup> M, 10<sup>-9</sup> M, 10<sup>-10</sup> M and 10<sup>-11</sup> M) and [<sup>125</sup>I]-ghrelin (15 pM per assay tube) in binding buffer (25 mM HEPES, 5 mM magnesium chloride, 1 mM calcium chloride, 2.5 mM EDTA, and 0.4% BSA, pH 7.4). The resulting suspension was incubated for 20 minutes under shaking (550 rpm) at 37  $^{\circ}$ C. Unbound [<sup>125</sup>I]-ghrelin was removed and the amount of [<sup>125</sup>I]-ghrelin bound to the membranes was measured by Gamma counter. IC<sub>50</sub> values were determined by nonlinear regression analysis to fit a 4 parameter dose response curve using GraphPad Prism 6 (Version 6.0c). All binding assays were performed in triplicate.

#### 4.4.5 Fluorescence Microscopy of **4.4** and **4.10** with GHS-R1a

Monomer **4.4** and dimer **4.10** were dissolved in DMSO for a concentration of 1 mM. Dye stocks were subsequently diluted in serum-free Dulbecco's modified Eagle's medium media (DMEM) supplemented with Penicillin-Streptomycin (Pen-Strep) to a final concentration of 0.5  $\mu$ M.

Affinity of dye-labelled peptide was tested towards HT1080 fibrosarcoma cells (ATCC) and HT1080 fibrosarcoma cells stably transfected with GHS-R, transcript variant 1a (OriGene Technologies Inc.). HT1080 and HT1080/GHSR1a cell lines were seeded onto coverslips at 50,000 cells per well in a 12-well plate format. Cells were incubated overnight in DMEM supplemented with 10% fetal bovine serum (FBS) and Pen-Strep at 37 °C in a 5% CO<sub>2</sub> atmosphere. Media was removed and cells washed once with serum-free media and twice with phosphate buffer saline (PBS). Cells were then incubated with 1 mL of 0.5  $\mu$ M **4.4** or **4.10** in serum-free media for 1 hour at 37°C in a 5% CO<sub>2</sub> atmosphere. Cells were washed once with serum free media and twice with phosphate buffer saline (PBS), fixed with 4% paraformaldehyde for 15 minutes and mounted onto slides containing Pro-Long Antifade® mounting medium with 4',6-diamino-2-phenylindole (DAPI). Images were obtained using a Nikon A1R confocal microscope. **4.4** and **4.10** were visualized with excitation at 636 nm and emission collected between 663–738 nm. DAPI was visualized with excitation at 402 nm and emission collected between 425-475 nm.

## 4.5 References

1. S. Gnanapavan, B. Kola, S. A. Bustin, D. G. Morris, P. McGee, P. Fairclough, S. Bhattacharya, R. Carpenter, A. B. Grossman and M. Korbonits, *J Clin Endocrinol Metab*, 2002, **87**, 2988.
2. H. H. Masayasu Kojima, Yukari Date, Masamitsu Nakazato, Hisayuki Matsuo, Kenji Kangawa, *Nature*, 1999, **402**, 656-660.
3. A. Asakawa, A. Inui, O. Kaga, H. Yuzuriha, T. Nagata, N. Ueno, S. Makino, M. Fujimiya, A. Niijima, M. A. Fujino and M. Kasuga, *Gastroenterol.*, 2001, **120**, 337-345.

4. S. Chearskul, E. Delbridge, A. Shulkes, J. Proietto and A. Kriketos, *Am. J. Clin. Nutri.*, 2008, **87**, 1238-1246.
5. E. Painsipp, M. J. Kofer, A. Farzi, U. S. Dischinger, F. Sinner, H. Herzog and P. Holzer, *Br J Pharmacol*, 2013, **170**, 1014-1026.
6. M. A. Bach, K. Rockwood, C. Zetterberg, G. Thamsborg, R. Hebert, J. P. Devogelaer, J. S. Christiansen, R. Rizzoli, J. L. Ochsner, N. Beisaw, O. Gluck, L. Yu, T. Schwab, J. Farrington, A. M. Taylor, J. Ng, V. Fuh and M. K. H. F. S. Group, *J Am Geriatr Soc*, 2004, **52**, 516-523.
7. M. G. Murphy, S. Weiss, M. McClung, T. Schnitzer, K. Cerchio, J. Connor, D. Krupa, B. J. Gertz and M. K.-A. S. Group, *J Clin Endocrinol Metab*, 2001, **86**, 1116-1125.
8. R. G. Smith, L. H. Van der Ploeg, A. D. Howard, S. D. Feighner, K. Cheng, G. J. Hickey, M. J. Wyvrat, Jr., M. H. Fisher, R. P. Nargund and A. A. Patchett, *Endocr Rev*, 1997, **18**, 621-645.
9. I. M. Chapman, M. A. Bach, E. Van Cauter, M. Farmer, D. Krupa, A. M. Taylor, L. M. Schilling, K. Y. Cole, E. H. Skiles, S. S. Pezzoli, M. L. Hartman, J. D. Veldhuis, G. J. Gormley and M. O. Thorner, *J Clin Endocrinol Metab*, 1996, **81**, 4249-4257.
10. R. G. Smith, Y. Sun, H. Jiang, R. Albarran-Zeckler and N. Timchenko, *Ann N Y Acad Sci*, 2007, **1119**, 147-164.
11. M. D. Klok, S. Jakobsdottir and M. L. Drent, *Obes Rev*, 2007, **8**, 21-34.
12. A. Beiras-Fernandez, S. Kreth, F. Weis, C. Ledderose, T. Pottinger, C. Dieguez, A. Beiras and B. Reichart, *Peptides*, 2010, **31**, 2222-2228.
13. G. A. F. Douglas, R. McGirr, C. L. Charlton, D. B. Kagan, L. M. Hoffman, L. G. Luyt and S. Dhanvantari, *Peptides*, 2014, **54**, 81-88.
14. R. McGirr, M. S. McFarland, J. McTavish, L. G. Luyt and S. Dhanvantari, *Regul. Peptides*, 2011, **172**, 69-76.
15. L. Chopin, C. Walpole, I. Seim, P. Cunningham, R. Murray, E. Whiteside, P. Josh and A. Herington, *Mol. Cell. Endocrinol.*, 2011, **340**, 65-69.
16. S. Liu, *Mol Pharm*, 2006, **3**, 472-487.
17. Z. Liu, S. Liu, F. Wang, S. Liu and X. Chen, *Eur J Nucl Med Mol Imaging*, 2009, **36**, 1296-1307.
18. K. Chen, W. Ma, G. Li, J. Wang, W. Yang, L. P. Yap, L. D. Hughes, R. Park and P. S. Conti, *Mol Pharm*, 2013, **10**, 417-427.

19. Z. Wu, Z. B. Li, W. Cai, L. He, F. T. Chin, F. Li and X. Chen, *Eur J Nucl Med Mol Imaging*, 2007, **34**, 1823-1831.
20. J. Shi, Y. S. Kim, S. Zhai, Z. Liu, X. Chen and S. Liu, *Bioconjug Chem*, 2009, **20**, 750-759.
21. I. Dijkgraaf, C. B. Yim, G. M. Franssen, R. C. Schuit, G. Luurtsema, S. Liu, W. J. Oyen and O. C. Boerman, *Eur J Nucl Med Mol Imaging*, 2011, **38**, 128-137.
22. P. Fournier, V. Dumulon-Perreault, S. Ait-Mohand, R. Langlois, F. Benard, R. Lecomte and B. Guerin, *EJNMMI Res*, 2012, **2**, 8.
23. C. Lu, M. S. McFarland, R.-L. Nesbitt, A. K. Williams, S. Chan, J. Gomez-Lemus, A. M. Autran-Gomez, A. Al-Zahrani, J. L. Chin, J. I. Izawa, L. G. Luyt and J. D. Lewis, *The Prostate*, 2012, **72**, 825-833.
24. M. Van Craenenbroeck, F. Gregoire, P. De Neef, P. Robberecht and J. Perret, *Peptides*, 2004, **25**, 959-965.

## Chapter 5

### 5 Conclusions

#### 5.1 Outlook and Conclusions

This thesis provides an example of how a natural receptor-ligand complex can be exploited for diagnostic and therapeutic purposes. Ghrelin, being the endogenous ligand for GHS-R1a, provided a high affinity template to begin modifying, as well as a “gold-standard” to compare the success of other ghrelin analogues.<sup>1</sup> The modifications to ghrelin were made rationally based off previous ghrelin literature and used classical approaches to increasing *in vivo* affinity and stability, as well as standard approaches to incorporating signaling sources, such as optical dyes and radionuclides. The methods led to various ghrelin analogues with high affinity to GHS-R1a and only a few were further evaluated as optical or scintigraphical imaging agents. The lead analogues are summarized in table 5.1

**Table 5.1** Summary of all ghrelin analogues synthesized and the corresponding IC<sub>50</sub>.

Chapter	Ghrelin Analogue	IC <sub>50</sub> (nM)
2	Dpr <sup>3</sup> (octanoyl), Lys <sup>19</sup> ([ <sup>69/71</sup> Ga]-DOTA)-Ghrelin(1-19)	5.67
3	Inp <sup>1</sup> ,Dpr <sup>3</sup> (6-fluoro-2-naphthyl),Nal-1 <sup>4</sup> ,Thr <sup>8</sup> -Ghrelin(1-8)	0.16
4	Dpr <sup>3</sup> (octanoyl), Nal-1 <sup>4</sup> , Thr <sup>8</sup> , AEEA <sup>9</sup> ,Lys <sup>10</sup> -Ghrelin(1-10) <sub>monomer</sub>	25.3
4	Dpr <sup>3</sup> (octanoyl), Nal-1 <sup>4</sup> , Thr <sup>8</sup> , AEEA <sup>9</sup> ,Lys <sup>10</sup> -Ghrelin(1-10) <sub>dimer</sub>	50.0

The first generation ghrelin analogue, [Dpr<sup>3</sup>(octanoyl), Lys<sup>19</sup>(<sup>68</sup>Ga-DOTA)]-ghrelin(1-19) (**2.3d**), was capable of targeting GHS-R1a with similar affinity to ghrelin(1-28) when chelated to gallium-68 and was shown to selectively target GHS-R1a in blocking studies. While **2.3d** was capable imaging GHS-R1a *in vivo*, preclinical studies in HT1080 and HT1080/GHS-R1a raised two concerns; relatively low localization to the tumour and retention of the radioactivity in kidneys. While this analogue supported the capability of ghrelin to be used as an *in vivo* PET imaging agent, there were modifications required to provide sufficient tumour uptake, optimal tumour-to-background ratios and overall

improved pharmacokinetics. These findings further developed this thesis into the second generation of ghrelin(1-8) analogues.

In an effort positively affect the pharmacokinetic properties of the next generation of ghrelin analogues, many of the C-terminal amino acids were removed. This would hypothetically remove many amino acid side chain charges and decrease retention in the kidneys. Unfortunately, this would also have a detrimental effect on binding affinity. Systematic modifications were made to residues 1, 3, 4 and 8 in order to optimize ligand-receptor interactions and increase binding affinity to GHS-R1a. Various substitutions of natural and unnatural amino acids at these residues successfully resulted in many ghrelin(1-8) analogues with equal or better binding affinity to GHS-R1a. This also introduced an unnatural element to ghrelin(1-8) useful for increasing *in vivo* stability. This generation of analogues was developed with fluorine-bearing side chain modification at residue 3 to allow translation to a fluorine-18 imaging agent. New radiochemical procedures were devised for the prosthetic group [<sup>18</sup>F]-PFPN and through synthesis of an active ester, [<sup>18</sup>F]-PFPN was successfully coupled to the lead ghrelin(1-8) analogue, H-Inp-S-Dpr-Nal-1-LSPT-NH<sub>2</sub>. This new ghrelin(1-8) fluorine-18 imaging agent ([<sup>18</sup>F]-**3.7**) was obtained in 3.6% d.c. yield. The high specificity to GHS-R1a is an exciting discovery and preclinical studies are still required to determine if these modifications had a positive affect kidney retention, *in vivo* stability and overall pharmacokinetics.

The final chapter investigated a new approach to optimizing *in vivo* pharmacokinetics of peptide-based targeting entities by employing multimerization. Other well-studied targeting peptides, such as RGD and bombesin resulted in better binding affinity and *in vivo* biodistribution profiles when dimeric and tetrameric peptides were compared to the monomeric counterparts.<sup>2, 3</sup> Two dye labelled ghrelin analogues, a monomer (**4.4**) and a dimer (**4.10**), were synthesized to determine if the same trend resulted from multimerization of ghrelin. Adding a second unit resulted in a negative effect on binding affinity and *in vitro* properties. Upon dimerization, **4.10** showed non-preferential binding in both of the studied cell lines and in turn, is not able to differentiate between GHS-R1a expression levels. These results should not deter those from developing different



dimerized ghrelin analogues as slight modifications to the structures will affect the biological properties.<sup>4</sup> An extensive look into 10 amino acid sequence and employing the methods mentioned in Chapter 1.4 could result in a more effective ghrelin dimer. It would be advantageous to investigate the chain length between ghrelin units by synthesizing longer linkers, and using variations of hydrophilic and hydrophobic linkers.<sup>5</sup> It would also be beneficial to study other multimer types of ghrelin such as trimer and tetramer analogues as the most successful of the RGD multimers is an octamer.<sup>2</sup> The positioning of the signaling source at the end of the lysine chain makes it easy to investigate other optical dyes, or to incorporate radiometals *via* chelators or other radionuclides using prosthetic group or direct group labeling.

Previous to the research stated in this thesis, little work had been done on the synthesis of ghrelin analogues as PET or SPECT imaging agents. In 2009, non-radioactive ghrelin (1-5) and ghrelin(1-14) analogues were synthesized to explore whether or not ghrelin was capable of tolerating fluorine and rhenium modifications to residue 3. The ghrelin(1-14) analogues set the stage for PET imaging potential with ghrelin, but were not further developed.<sup>6</sup> In 2014, a ghrelin(1-6) peptide was labelled with monodentate and tridentate technetium-99m complexes. These peptides had respectable  $IC_{50}$  values of 45 nM and 54 nM for GHS-R1a but biodistribution studies revealed that this analogue mainly localized to the kidneys.<sup>7</sup> The research in this thesis extended the knowledge of long and short ghrelin analogues as PET imaging agents that was an area previous under studied. It provides solid ground work for others to continue optimizing ghrelin in order to improve pharmacokinetic properties and design a strong diagnostic and therapeutic peptide molecular imaging probe.

When drawing similarities between the works, it must be noted that ghrelin has shown undesirable biodistribution profiles independent of the ghrelin length. As mentioned in the introductory material, kidney uptake can be reduced by co-administering megalin or a cationic amino acid, but these approaches do not address the issue with the peptide targeting entity directly. There is a particular characteristic about ghrelin analogues that causes this phenomenon. It would be interesting to use combinatorial methods, such as one-bead-one-compound, to synthesize a large library of unrelated peptide sequences that

could retain affinity to GHS-R1a without the attraction to kidney.<sup>8</sup> These types of combinatorial libraries have become more sophisticated and are able to incorporate non-radioactive counterparts to common radionuclides in order to create a targeting entity that requires the signaling source for affinity to the receptor, much like the analogues synthesized in Chapter 3.<sup>9</sup>

There is another family of peptides that are well-known for targeting GHS-R1a that are structurally different to natural ghrelin. The discovery of these peptides began with enkephalin (H-TGGFM-OH) in 1977 and through the work of many research groups, resulted in many more analogues synthesized by 1995.<sup>10-14</sup> These small synthetic peptides were capable of releasing growth hormone in *in vivo* studies and were grouped into a family known as growth hormone secretagogues. It was this family of peptides that helped lead to the discovery of the receptor GHS-R1a in 1996.<sup>15</sup> These peptides already have good affinity for GHS-R1a and would not require optimization by truncation. Using the classical methods to optimize peptide sequences detailed in Chapter 1, these peptides could also targeting GHS-R1a with the affinity that the synthesized truncated ghrelin analogues are capable of. Incorporating a molecular imaging signaling source, such as a radioisotope or optical dye, could result in larger scope of peptides capable of imaging GHS-R1a using imaging modalities. There is value in finding other peptide analogues capable of targeting GHS-R1a to determine what is the most reliable method for detection.

Overall, this thesis delved into the versatility of ghrelin and its ability to target its endogenous receptor, GHS-R1a. *In vitro* and *in vivo* assays clearly demonstrate that ghrelin is able to tolerate substantial truncations to the C-terminal region of the natural amino acid sequence and using well-known approaches to modifying peptides, varying lengths of ghrelin analogues effectively targeted GHS-R1a. Although more research is required to validate all these peptides, it is evident they hold potential to be effective imaging agents for the various conditions and diseases that are regulated by GHS-R1a expression.

## 5.2 References

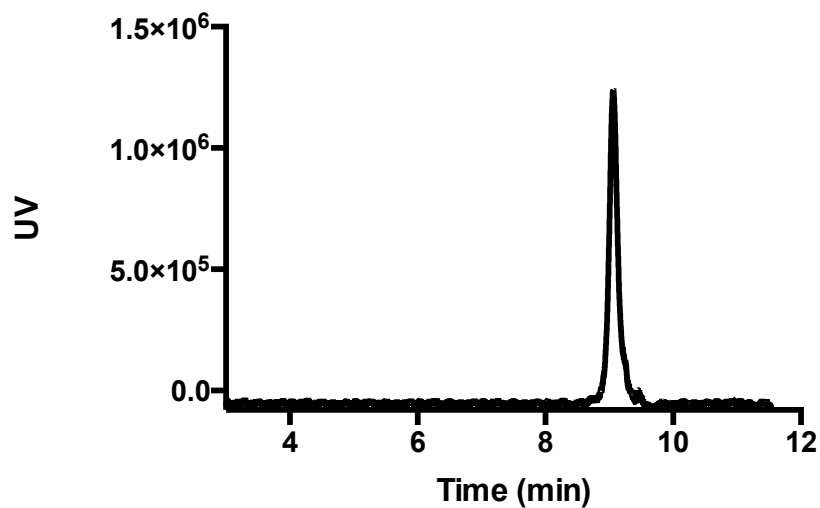
1. H. H. Masayasu Kojima, Yukari Date, Masamitsu Nakazato, Hisayuki Matsuo, Kenji Kangawa, *Nature*, 1999, **402**, 656-660.
2. Z. B. Li, K. Chen and X. Chen, *Eur J Nucl Med Mol Imaging*, 2008, **35**, 1100-1108.
3. Z. B. Li, Z. Wu, K. Chen, E. K. Ryu and X. Chen, *J Nucl Med*, 2008, **49**, 453-461.
4. Y. Yan and X. Chen, *Amino Acids*, 2011, **41**, 1081-1092.
5. Z. Liu, S. Liu, F. Wang, S. Liu and X. Chen, *Eur J Nucl Med Mol Imaging*, 2009, **36**, 1296-1307.
6. D. Rosita, M. A. DeWit and L. G. Luyt, *J. Med. Chem.*, 2009, **52**, 2196-2203.
7. P. Koźmiński and E. Gniazdowska, *Nucl. Med. Biol.*, 2014.
8. K. S. Lam, S. E. Salmon, E. M. Hersh, V. J. Hruby, W. M. Kazmierski and R. J. Knapp, *Nature*, 1991, **354**, 82-84.
9. D. R. Cruickshank and L. G. Luyt, *Can. J. Chem.*, 2014, **93**, 234-243.
10. C. Y. Bowers, J. Chang, F. Momany and K. Folkers, *Mol. Endocrinol. Proc.*, 1977, 287-292.
11. R. G. Smith, K. Cheng, W. R. Schoen, S. S. Pong, G. Hickey, T. Jacks, B. Butler, W. W. Chan, L. Y. Chaung, F. Judith and et al., *Science*, 1993, **260**, 1640-1643.
12. T. Jacks, G. Hickey, F. Judith, J. Taylor, H. Chen, D. Krupa, W. Feeney, W. Schoen, D. Ok, M. Fisher and et al., *The Journal of endocrinology*, 1994, **143**, 399-406.
13. A. A. Patchett, R. P. Nargund, J. R. Tata, M. H. Chen, K. J. Barakat, D. B. Johnston, K. Cheng, W. W. Chan, B. Butler, G. Hickey and et al., *Proceedings of the National Academy of Sciences of the United States of America*, 1995, **92**, 7001-7005.
14. E. Ghigo, E. Arvat, L. Gianotti, B. P. Imbimbo, V. Lenaerts, R. Deghenghi and F. Camanni, *The Journal of clinical endocrinology and metabolism*, 1994, **78**, 693-698.
15. A. D. Howard, S. D. Feighner, D. F. Cully, J. P. Arena, P. A. Liberator, C. I. Rosenblum, M. Hamelin, D. L. Hreniuk, O. C. Palyha, J. Anderson, P. S. Paress, C. Diaz, M. Chou, K. K. Liu, K. K. McKee, S. S. Pong, L. Y. Chaung, A. Elbrecht, M. Dashkevicz, R. Heavens, M. Rigby, D. J. Sirinathsinghji, D. C.

Dean, D. G. Melillo, A. A. Patchett, R. Nargund, P. R. Griffin, J. A. DeMartino, S. K. Gupta, J. M. Schaeffer, R. G. Smith and L. H. Van der Ploeg, *Science*, 1996, **273**, 974-977.

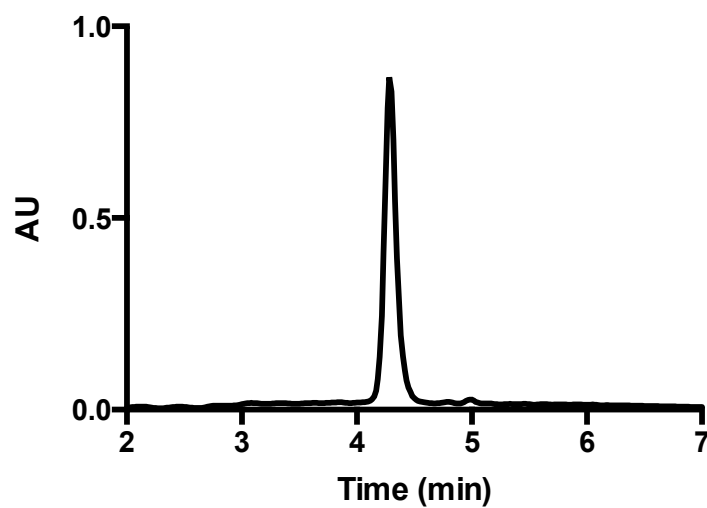
## 6 Appendix

### 6.1 Chapter 2 HPLC Traces

HPLC of **2.3d**: Analytical 20 – 60 % acetonitrile in water - 15 minutes

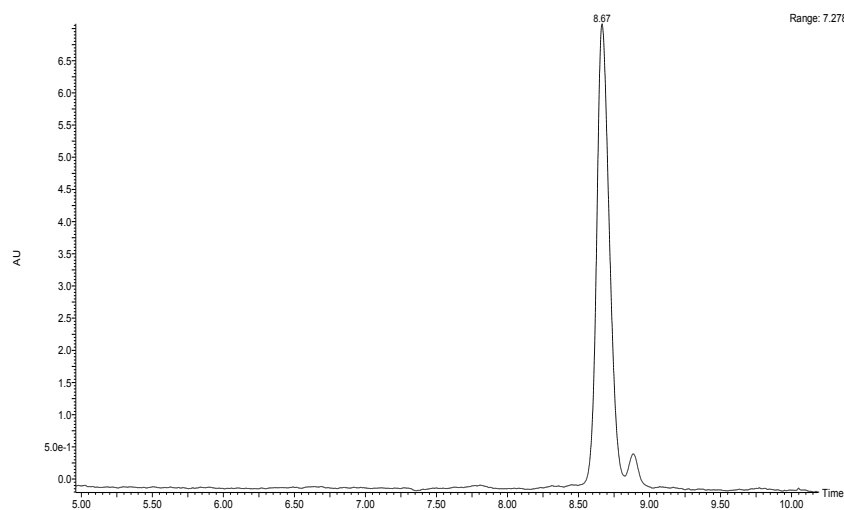


HPLC of [ $^{69/71}\text{Ga}$ ]-**2.3d**: Analytical 30 – 80 % acetonitrile in water - 15 minutes

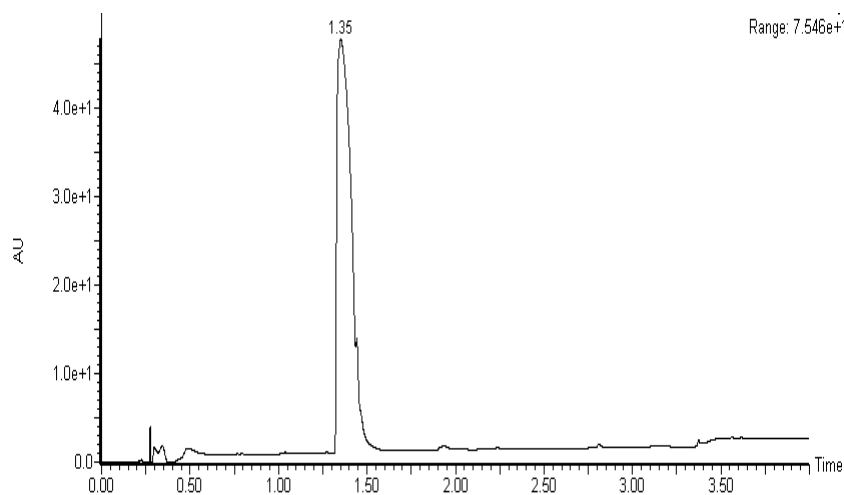


## 6.2 Chapter 3 HPLC Traces

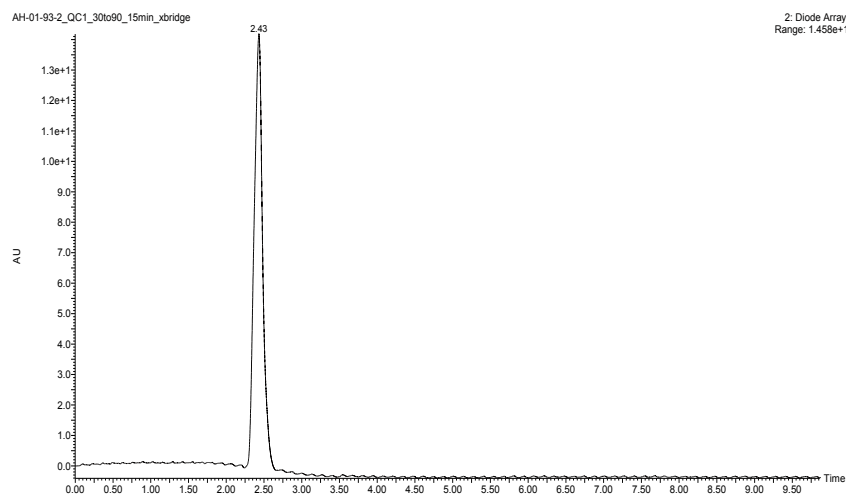
HPLC for **3.3**: Analytical 30 – 90 % acetonitrile in water – 15 minutes



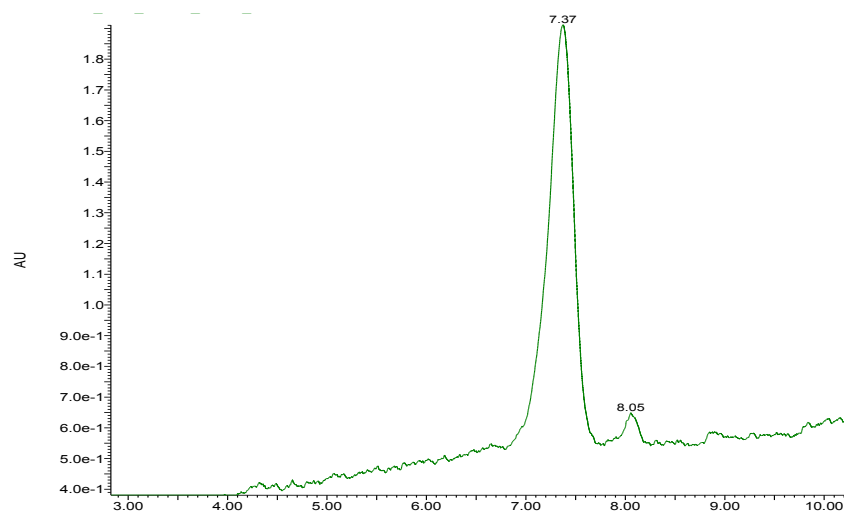
HPLC for **3.3b**: Analytical 20 – 80 % acetonitrile in water – 15 minutes



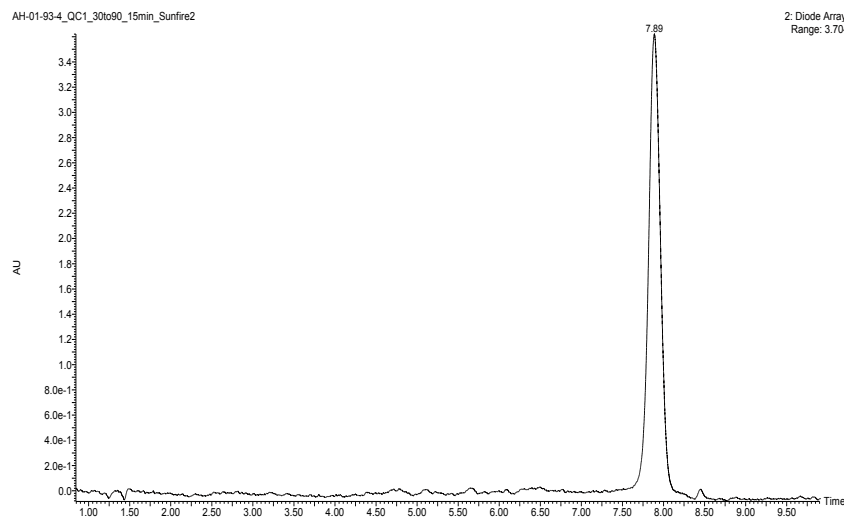
HPLC for **3.3d**: Analytical 30 – 90 % acetonitrile in water – 15 minutes



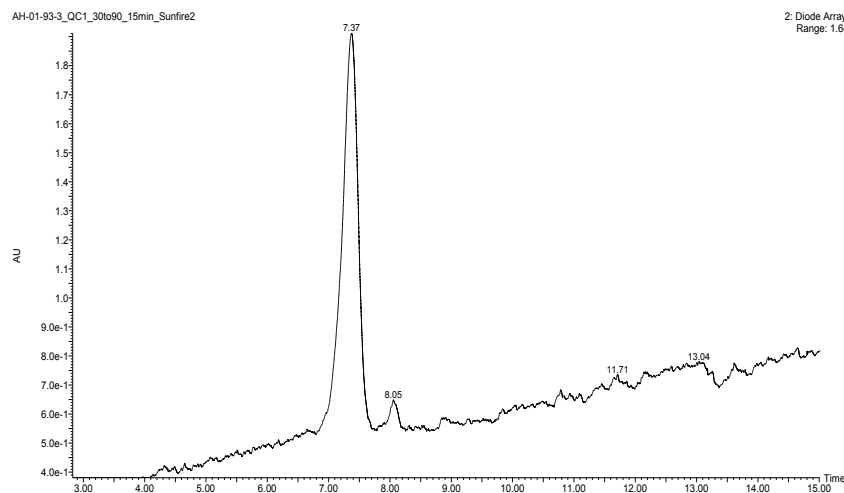
HPLC for **3.3e**: Analytical 30 – 90 % acetonitrile in water – 15 minutes



HPLC for **3.3f**: Analytical 30 – 90 % acetonitrile in water – 15 minutes

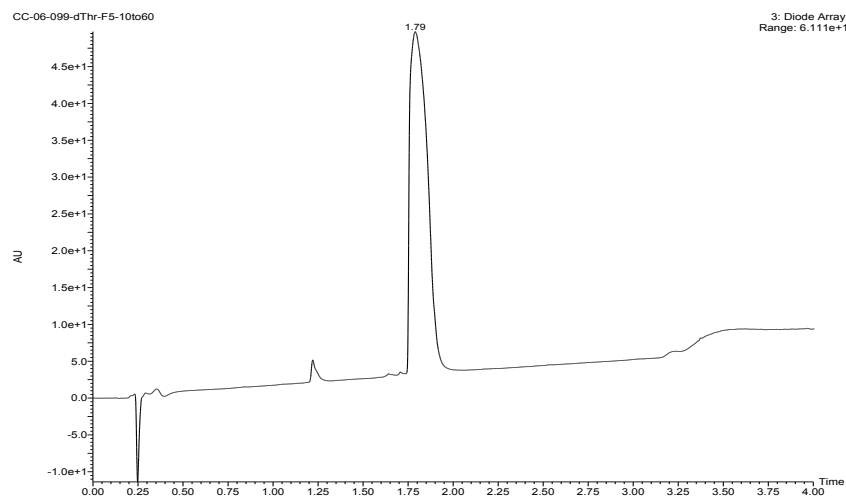


HPLC for **3.3g**: Analytical 30 – 90 % acetonitrile in water – 15 minutes

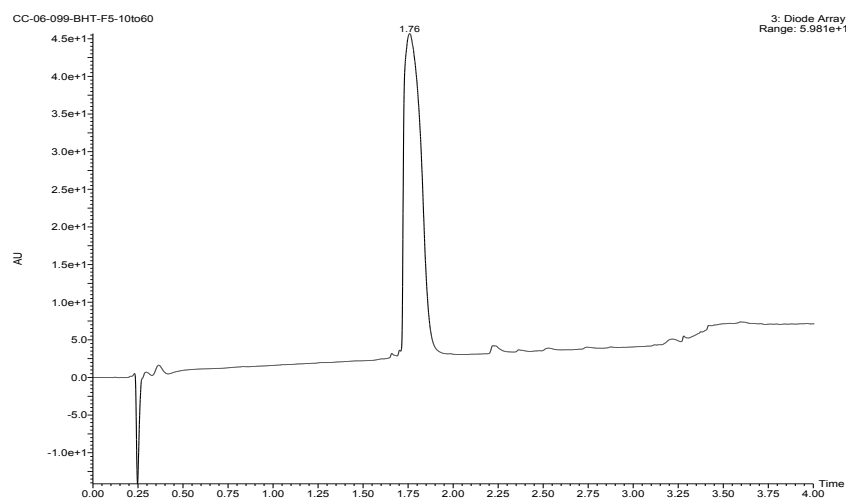




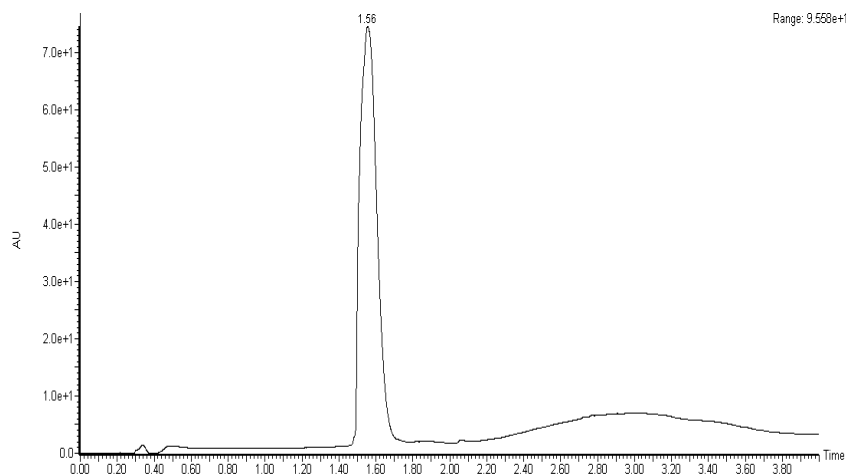
UHPLC for **3.3h**: Analytical 10 – 60 % acetonitrile in water – 4 minutes



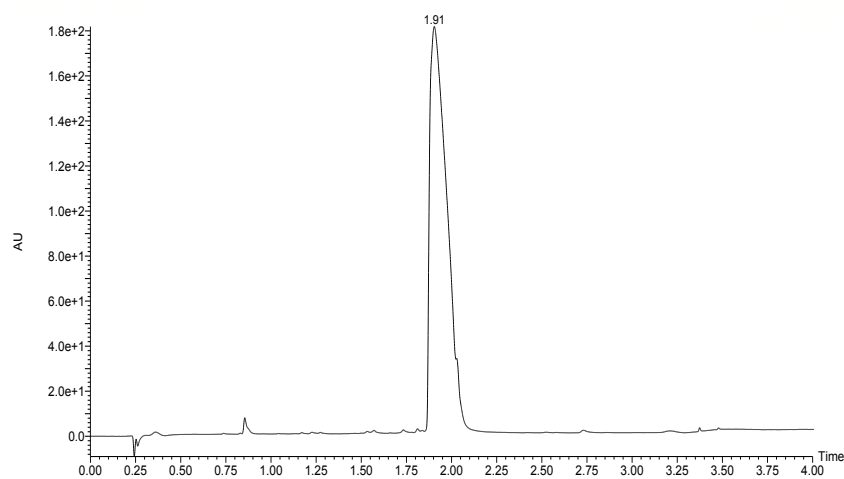
HPLC for **3.3i**: Analytical 10 – 60 % acetonitrile in water – 4 minutes



HPLC for **3.3j**: Analytical 20 – 80 % acetonitrile in water – 15 minutes

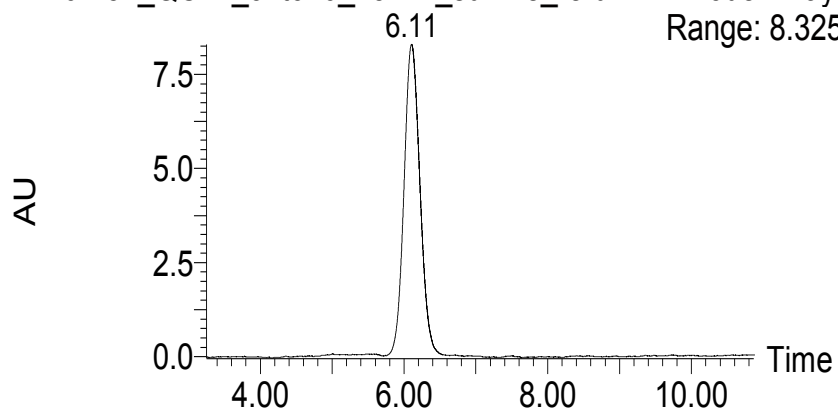


HPLC for **3.4c**: Analytical 10 – 60 % acetonitrile in water – 15 minutes

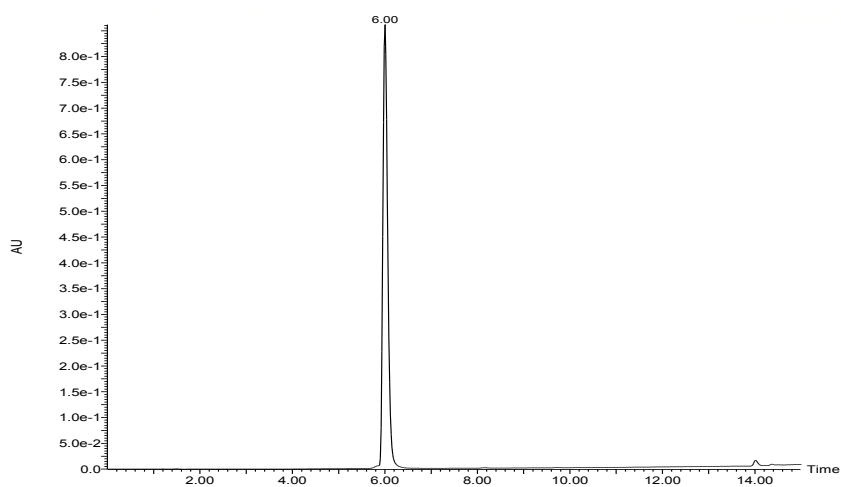


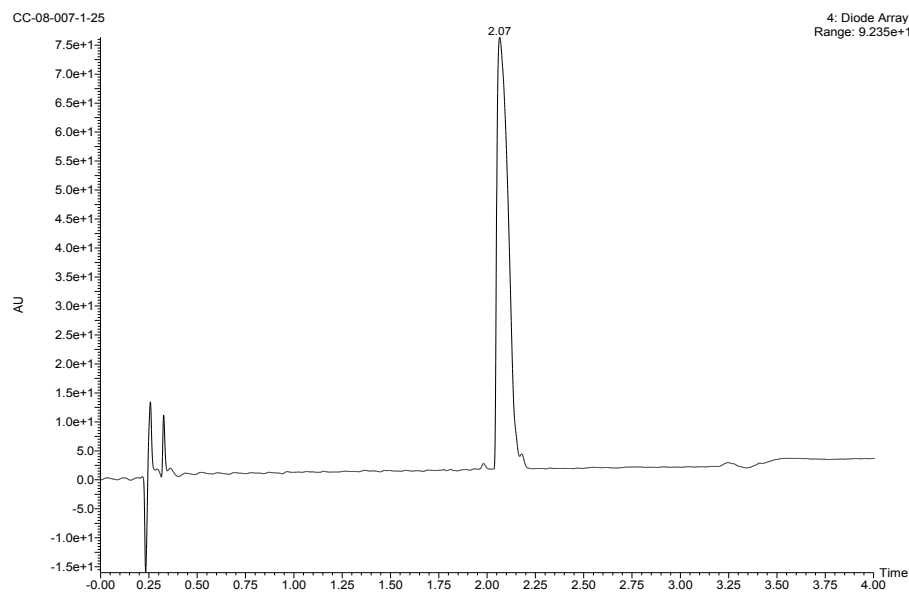
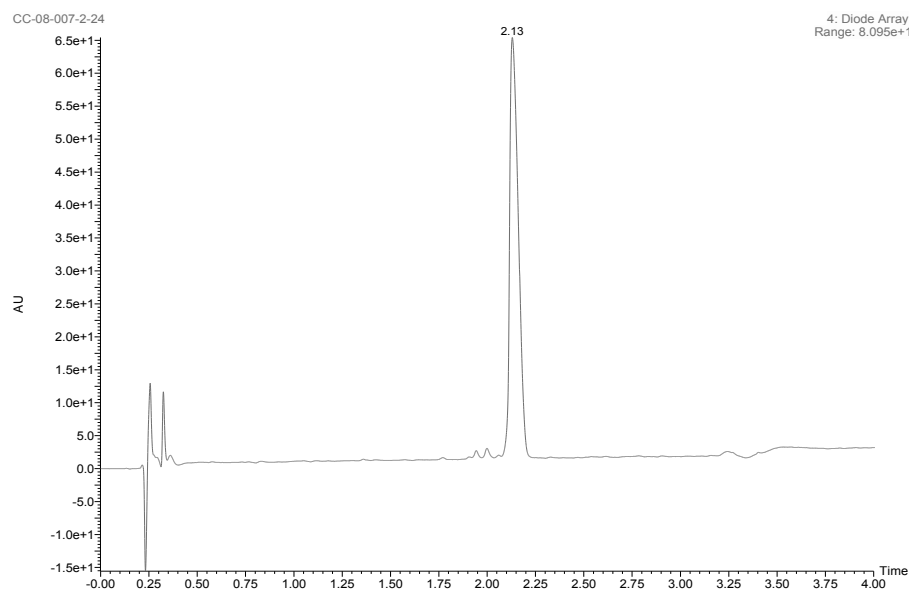
HPLC for **3.5a**: Analytical 32 – 70 % acetonitrile in water – 15 minutes

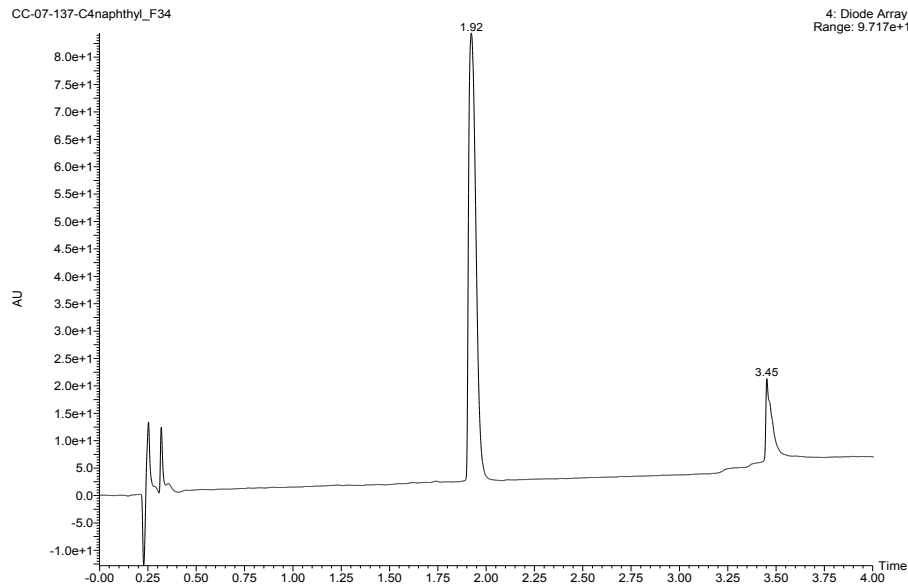
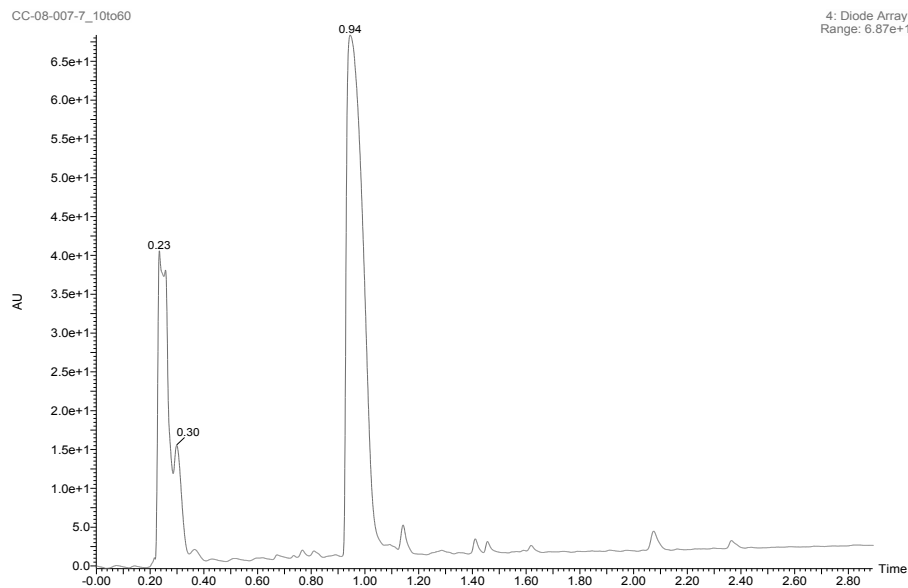
AH-01-51\_QC#4\_32to70\_15min\_sunfire\_rerun 2: Diode Array  
Range: 8.325



HPLC for **3.5c**: Analytical 32 – 80% acetonitrile in water – 15 minutes

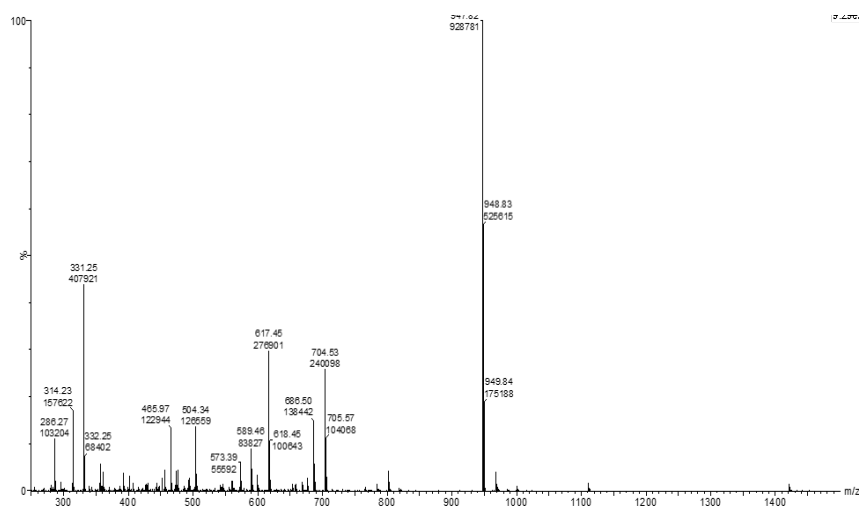


UHPLC for **3.6a**: Analytical 10 – 60 % - 4 minutesUHPLC for **3.6b**: Analytical 20 – 70 % - 4 minutes

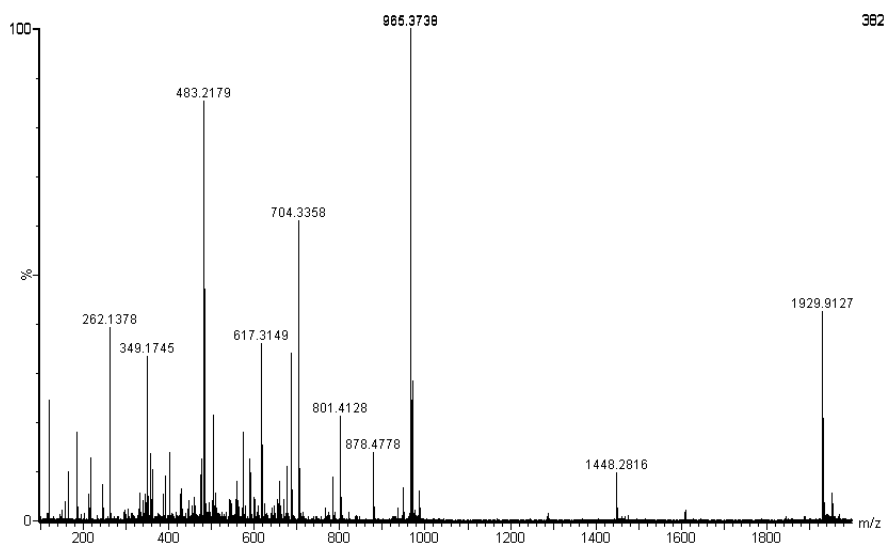
UHPLC for **3.7**: Analytical 20 – 70 % - 4 minutesUHPLC for **3.17**: Analytical 10 – 60 % - 4 minutes

## 6.3 Chapter 3 ESI<sup>+</sup> Mass Spectrums

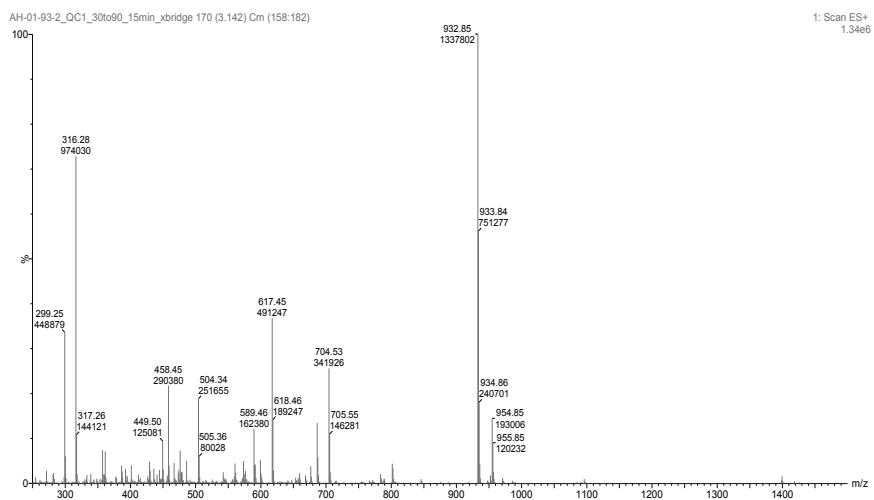
### ESI<sup>+</sup> Mass Spectrum for 3.3



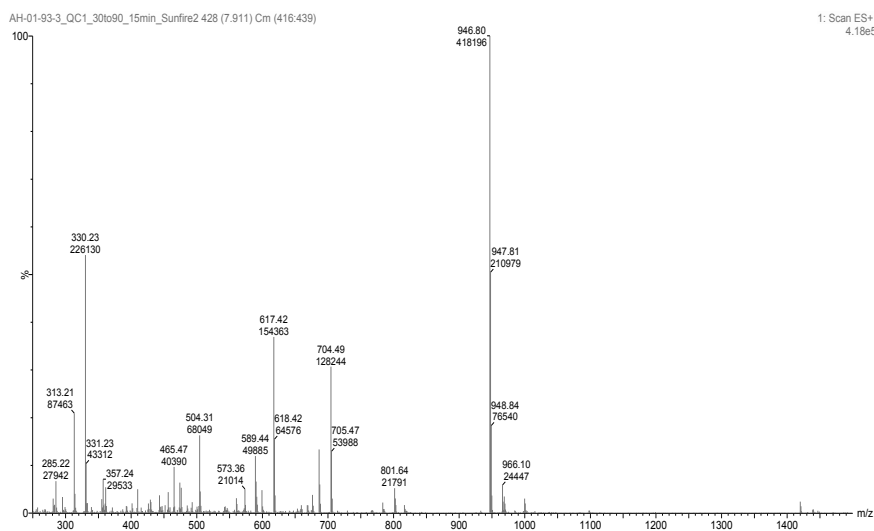
### ESI<sup>+</sup> Mass Spectrum for 3.3b

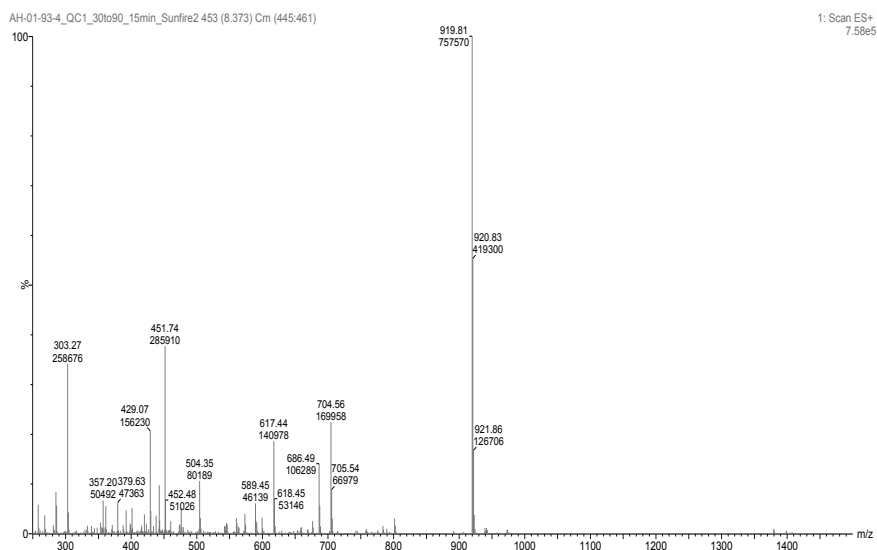
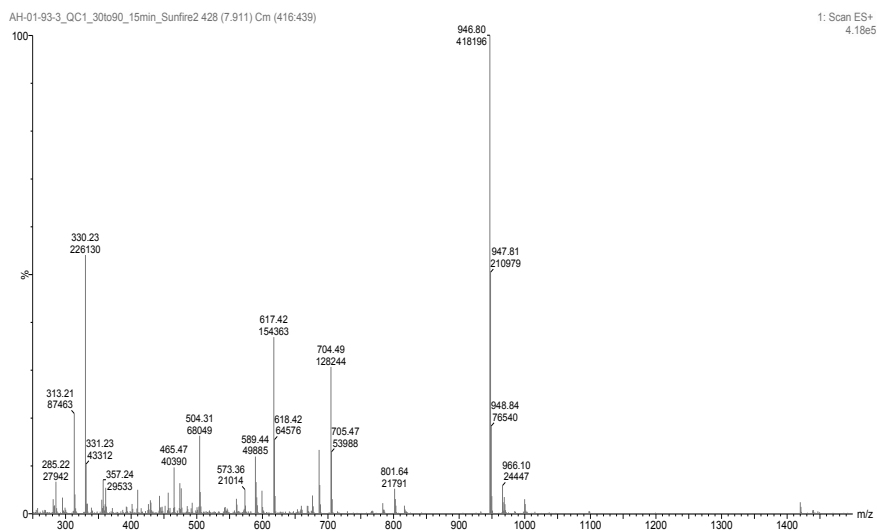


### ESI<sup>+</sup> Mass Spectrum for **3.3d**

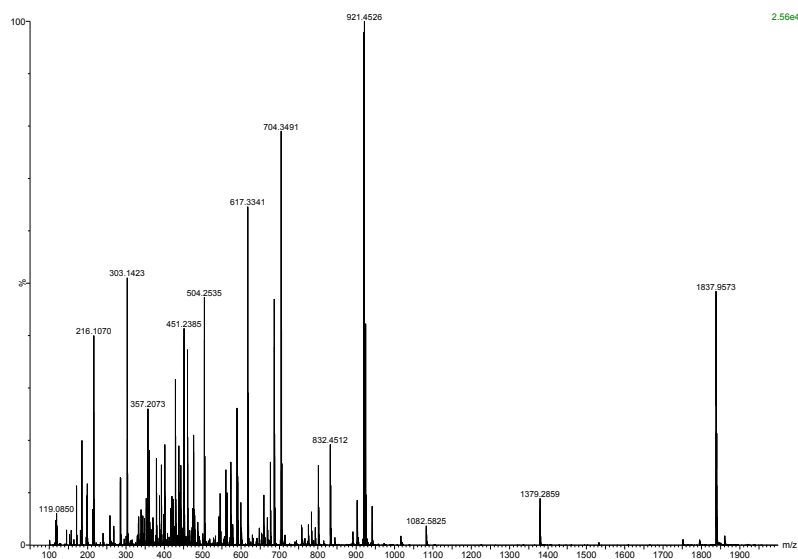
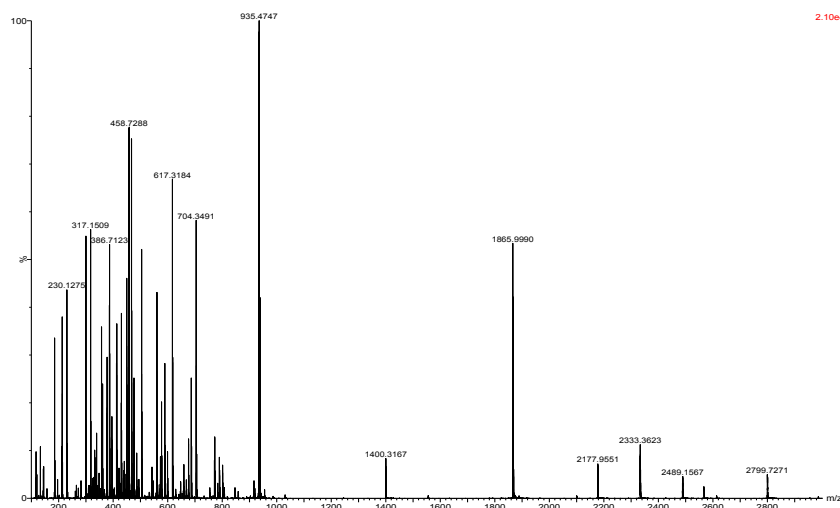


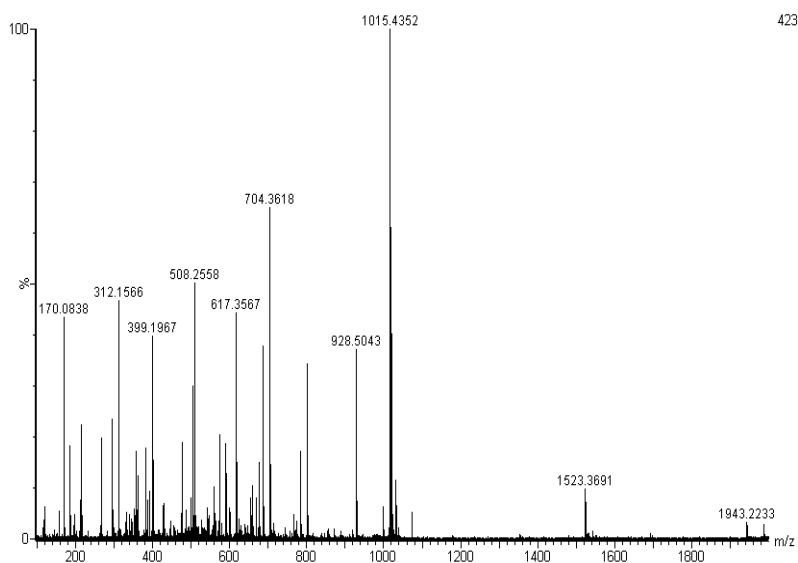
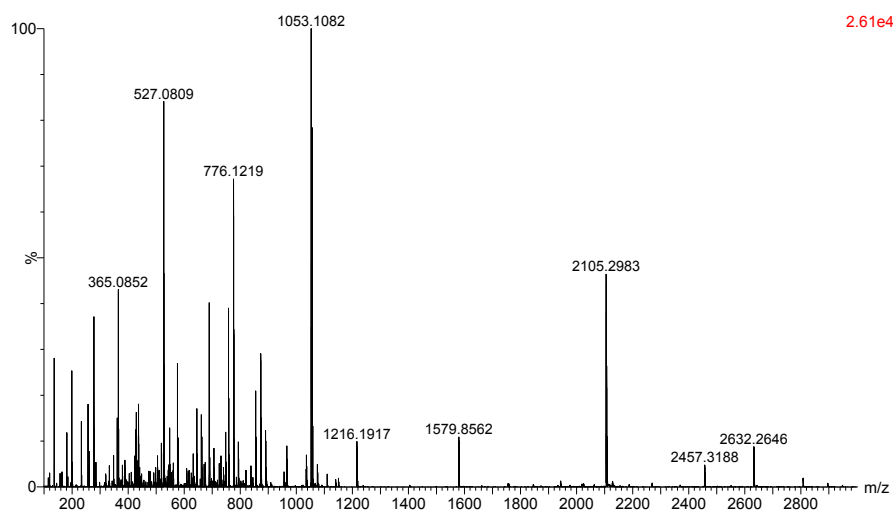
### ESI<sup>+</sup> Mass Spectrum for **3.3e**

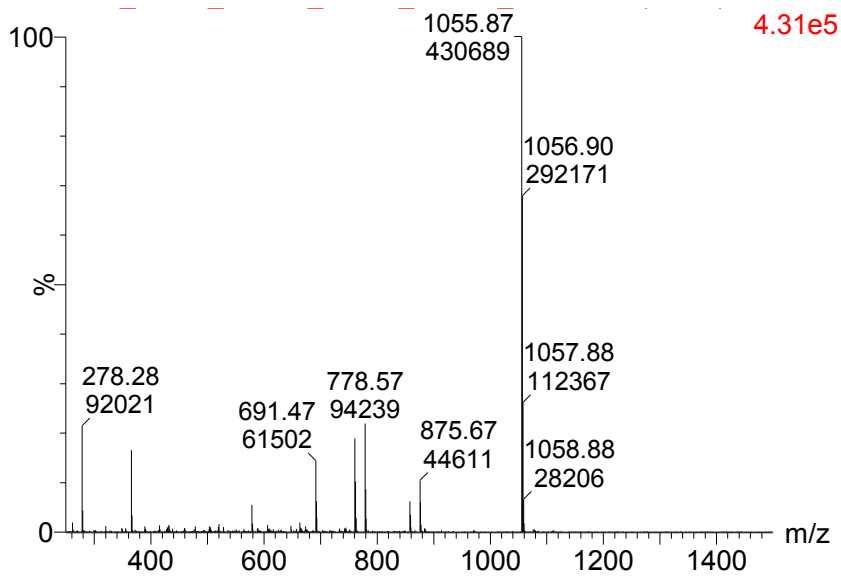
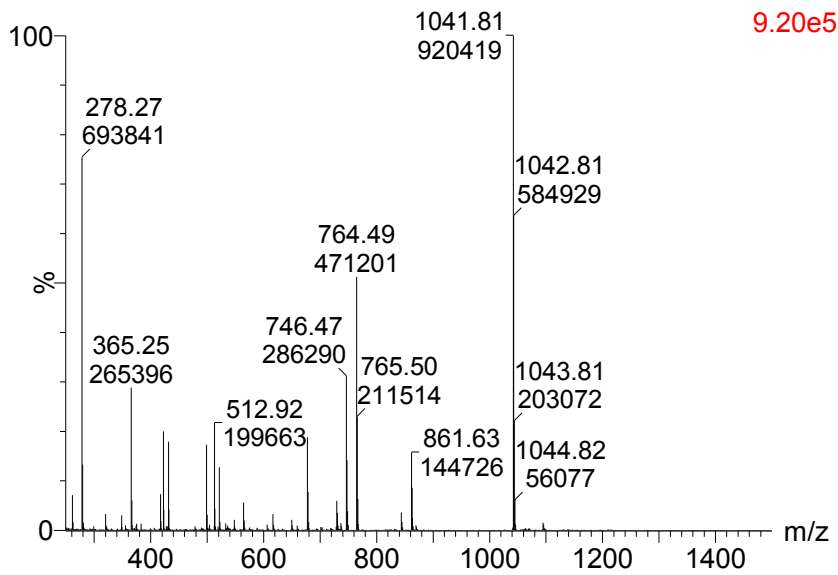


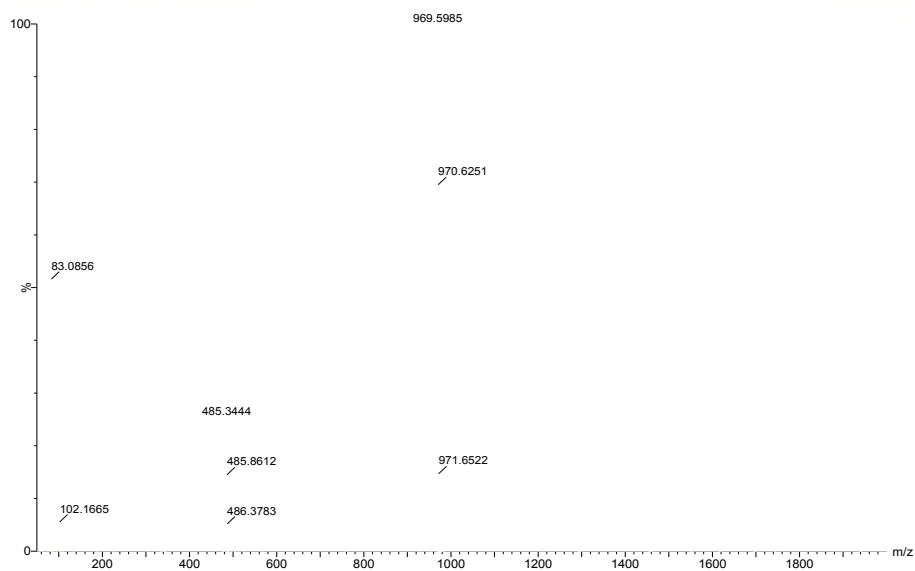
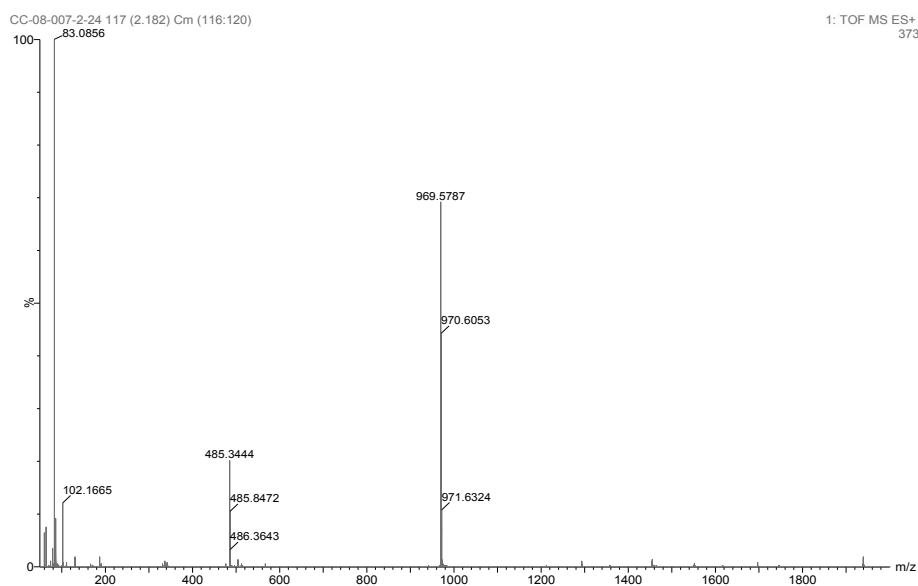
ESI<sup>+</sup> Mass Spectrum for 3.3fESI<sup>+</sup> Mass Spectrum for 3.3g

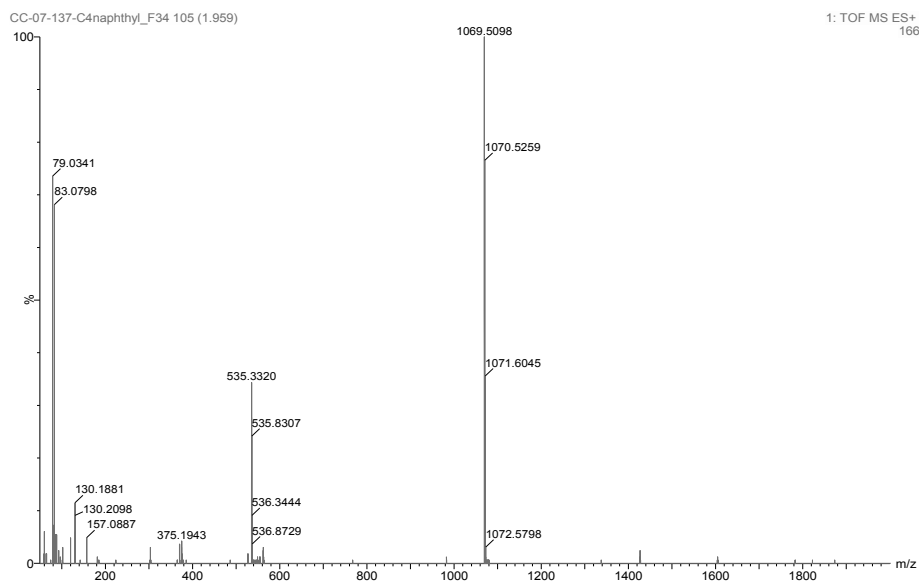
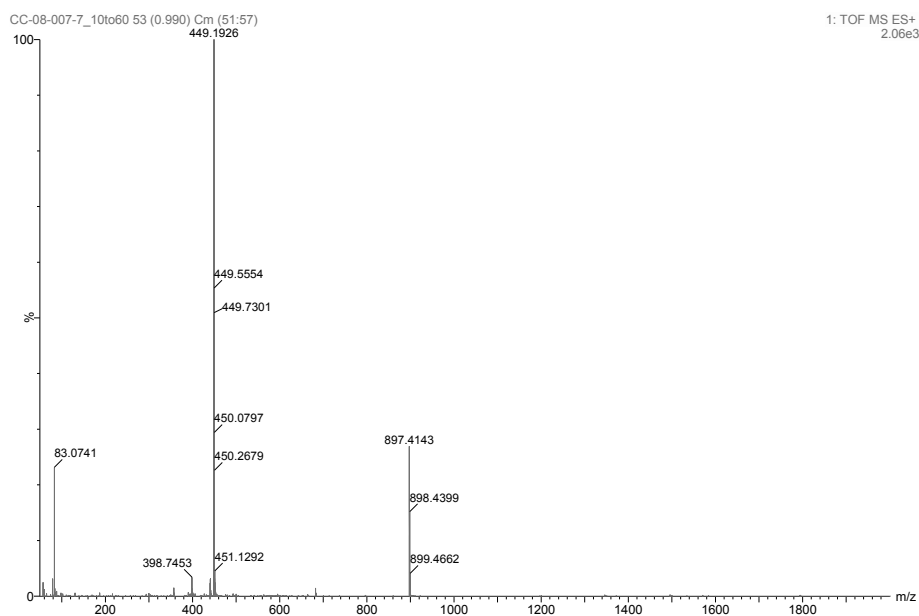


ESI<sup>+</sup> Mass Spectrum for **3.3h**ESI<sup>+</sup> Mass Spectrum for **3.3i**

ESI<sup>+</sup> Mass Spectrum for 3.3jESI<sup>+</sup> Mass Spectrum for 3.4c

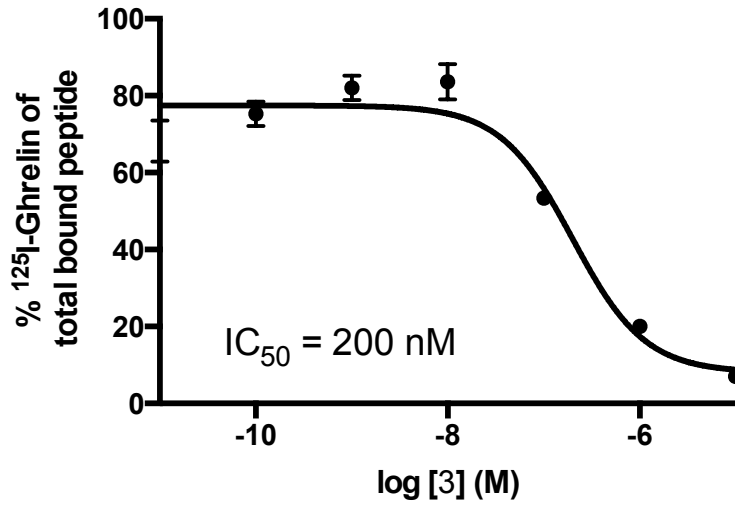
ESI<sup>+</sup> Mass Spectrum for **3.5a**ESI<sup>+</sup> Mass Spectrum for **3.5c**

ESI<sup>+</sup> Mass Spectrum for **3.6a**ESI<sup>+</sup> Mass Spectrum for **3.6b**

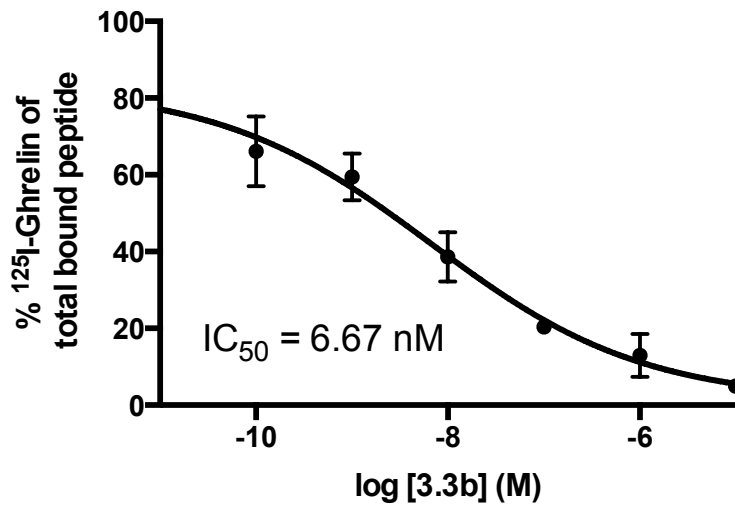
ESI<sup>+</sup> Mass Spectrum for 3.7ESI<sup>+</sup> Mass Spectrum for 3.17

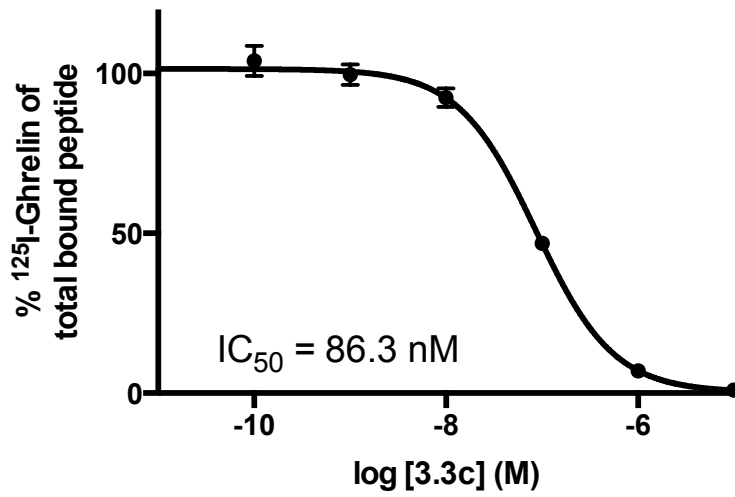
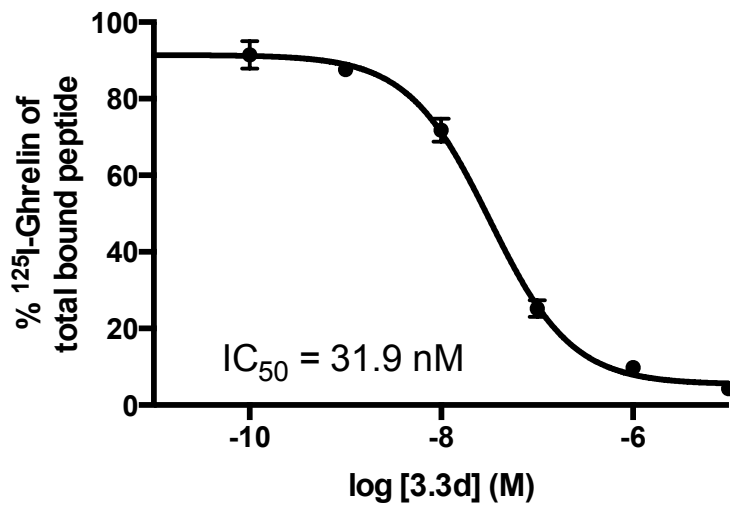
## 6.4 Chapter 3 IC<sub>50</sub> Curves

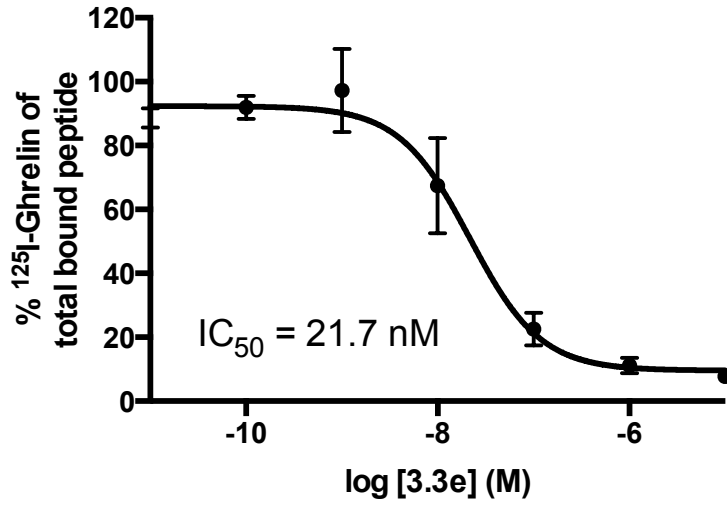
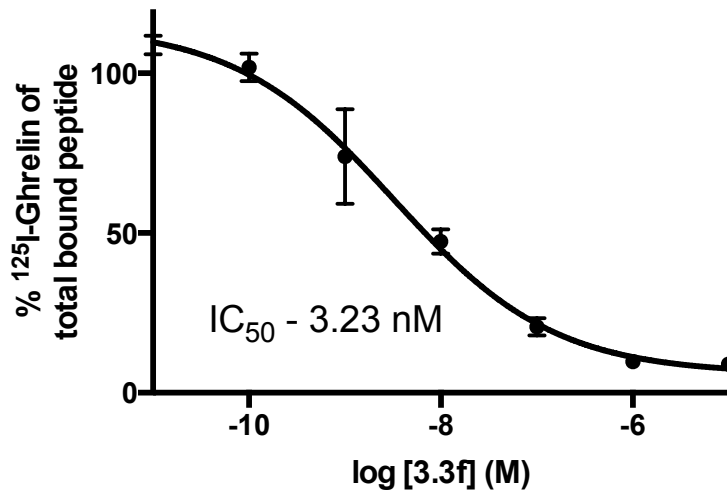
IC<sub>50</sub> curve for 3.3



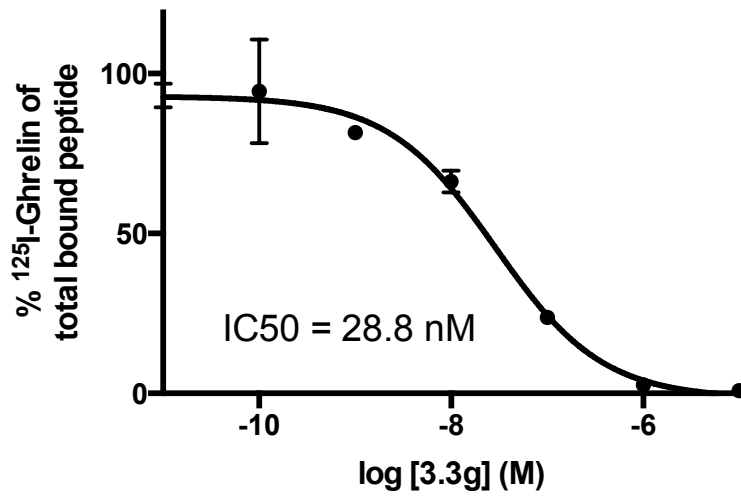
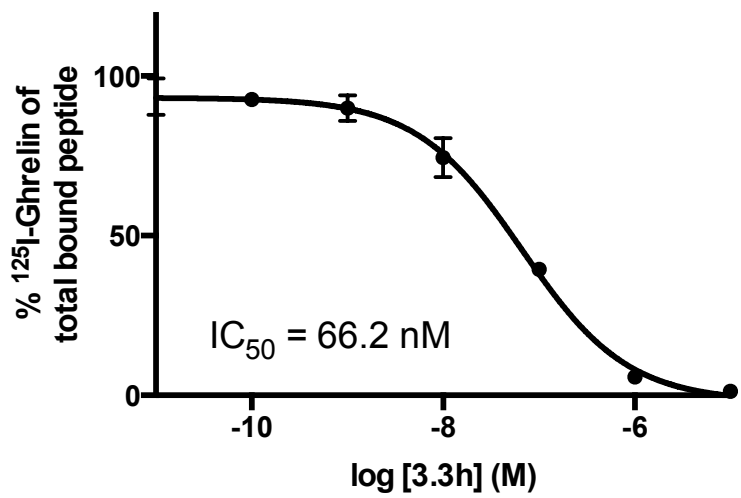
IC<sub>50</sub> curve for 3.3b

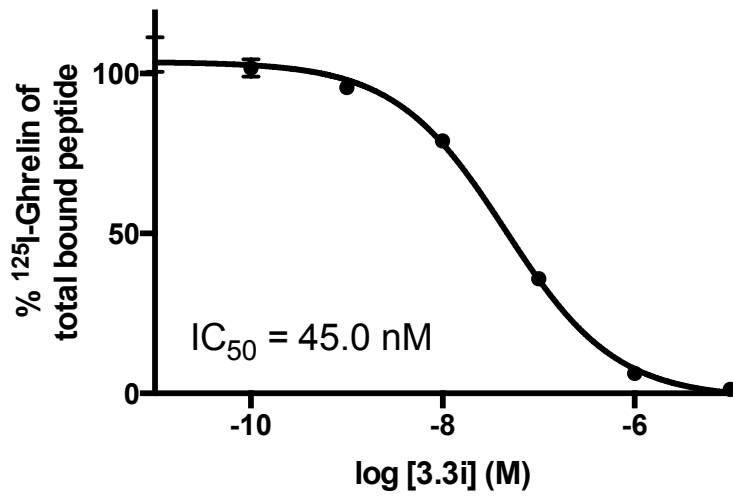
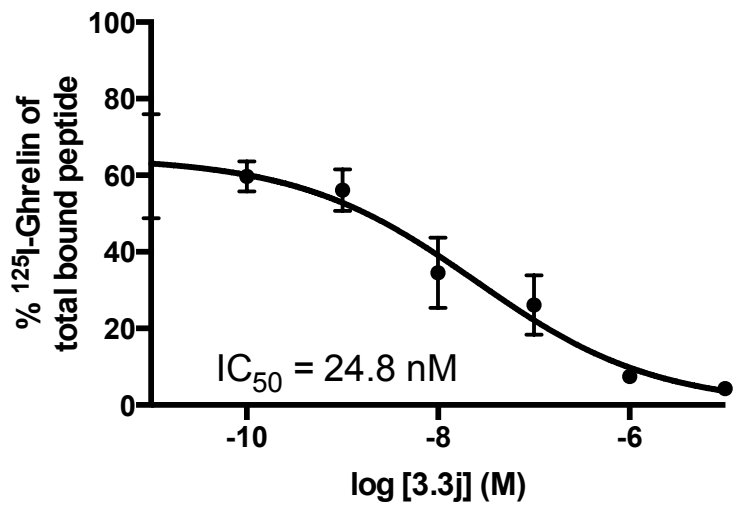


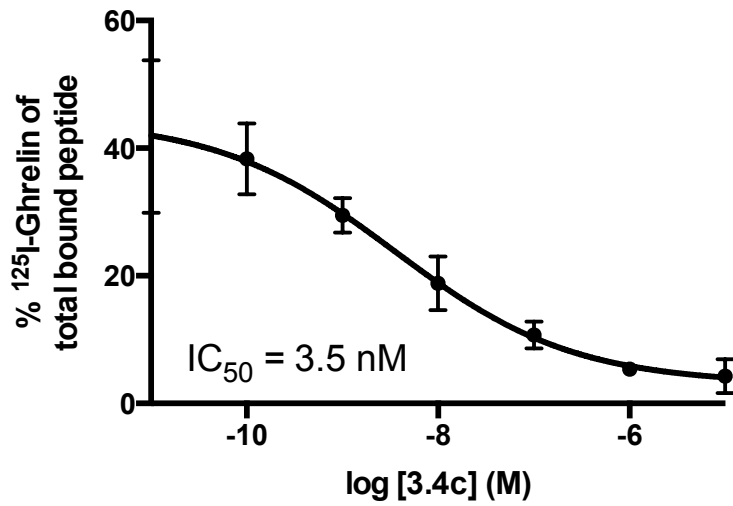
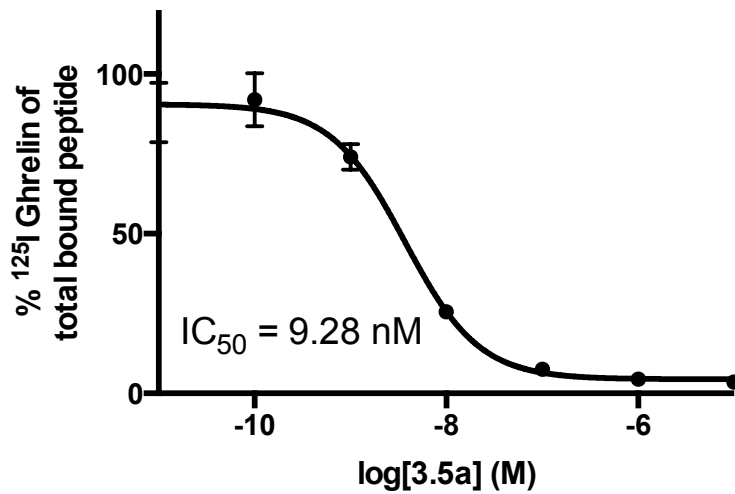
IC<sub>50</sub> curve for 3.3cIC<sub>50</sub> curve for 3.3d

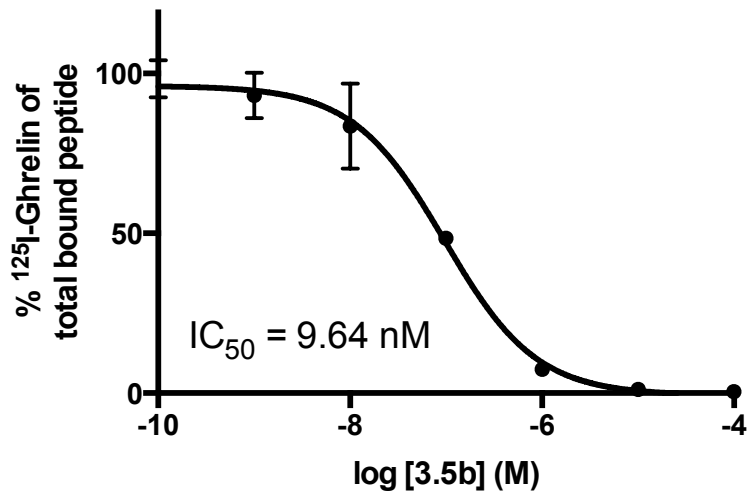
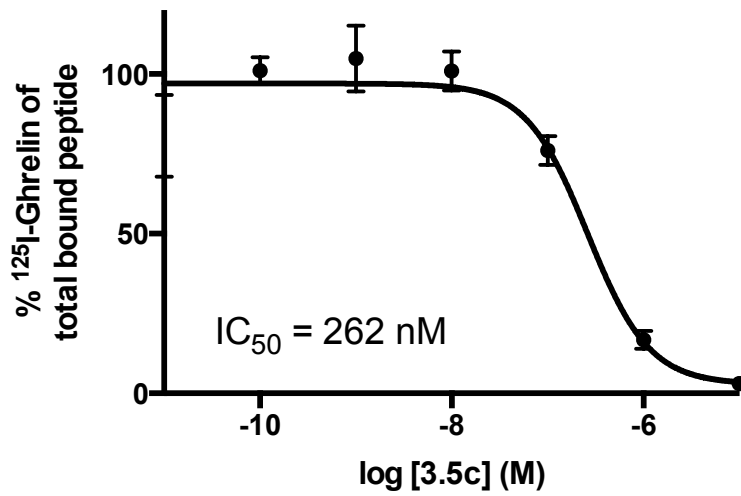
IC<sub>50</sub> curve for 3.3eIC<sub>50</sub> curve for 3.3f

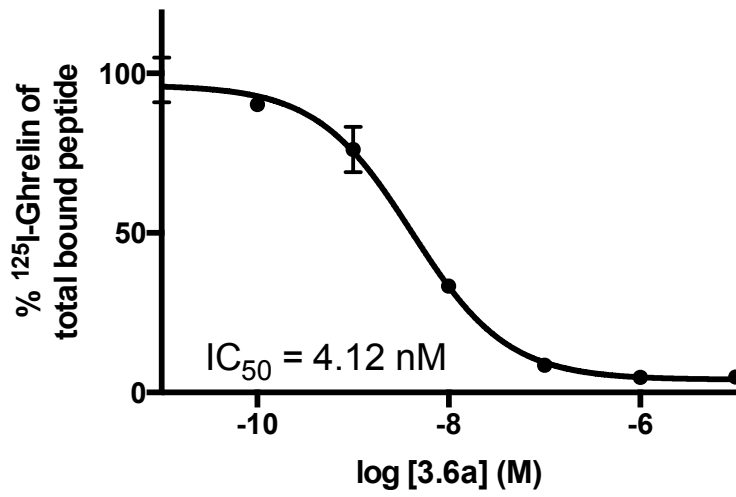
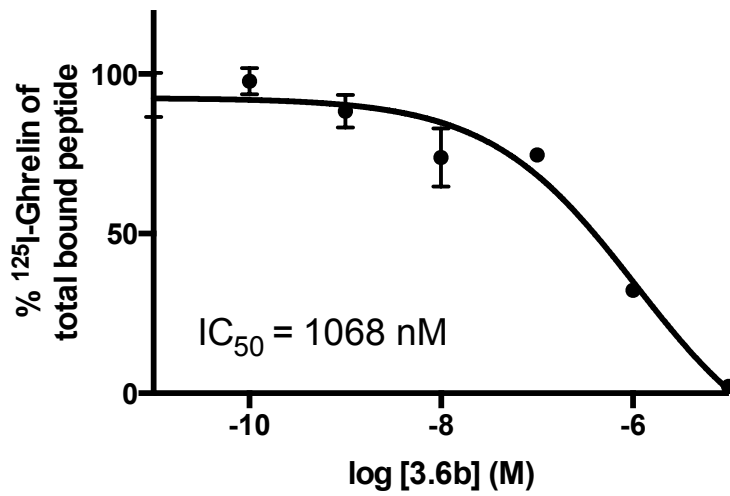


IC<sub>50</sub> curve for 3.3gIC<sub>50</sub> curve for 3.3h

IC<sub>50</sub> curve for 3.3iIC<sub>50</sub> curve for 3.3j

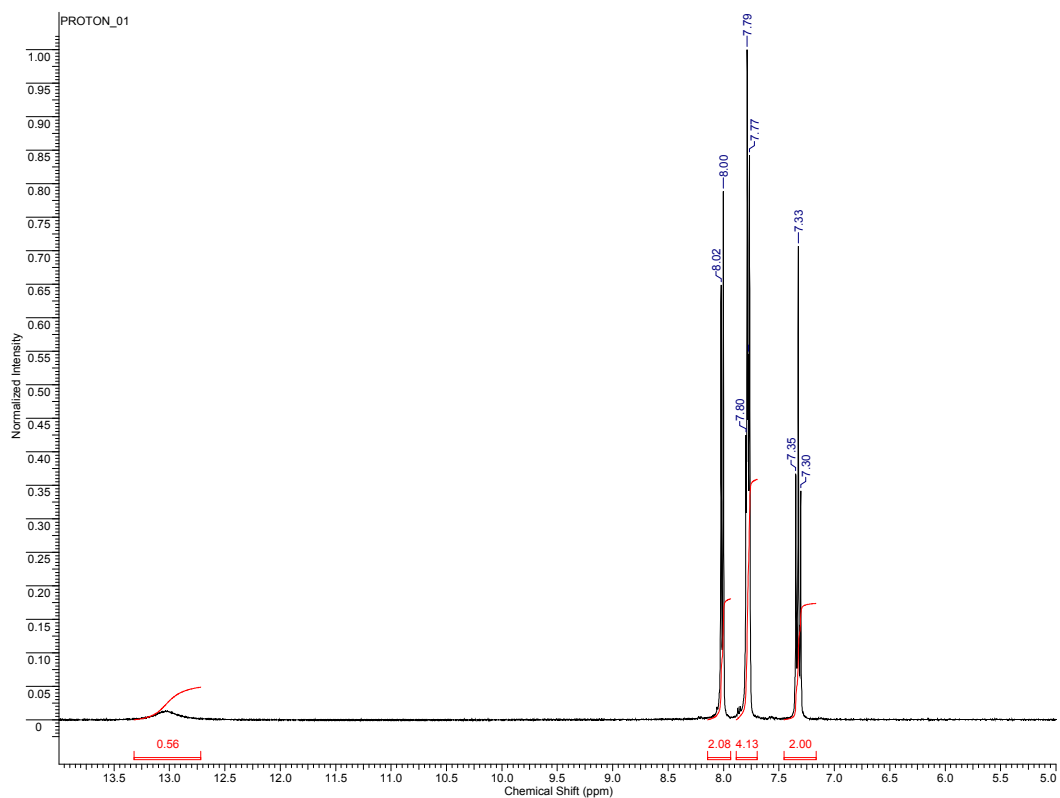
IC<sub>50</sub> curve for 3.4cIC<sub>50</sub> curve for 3.5a

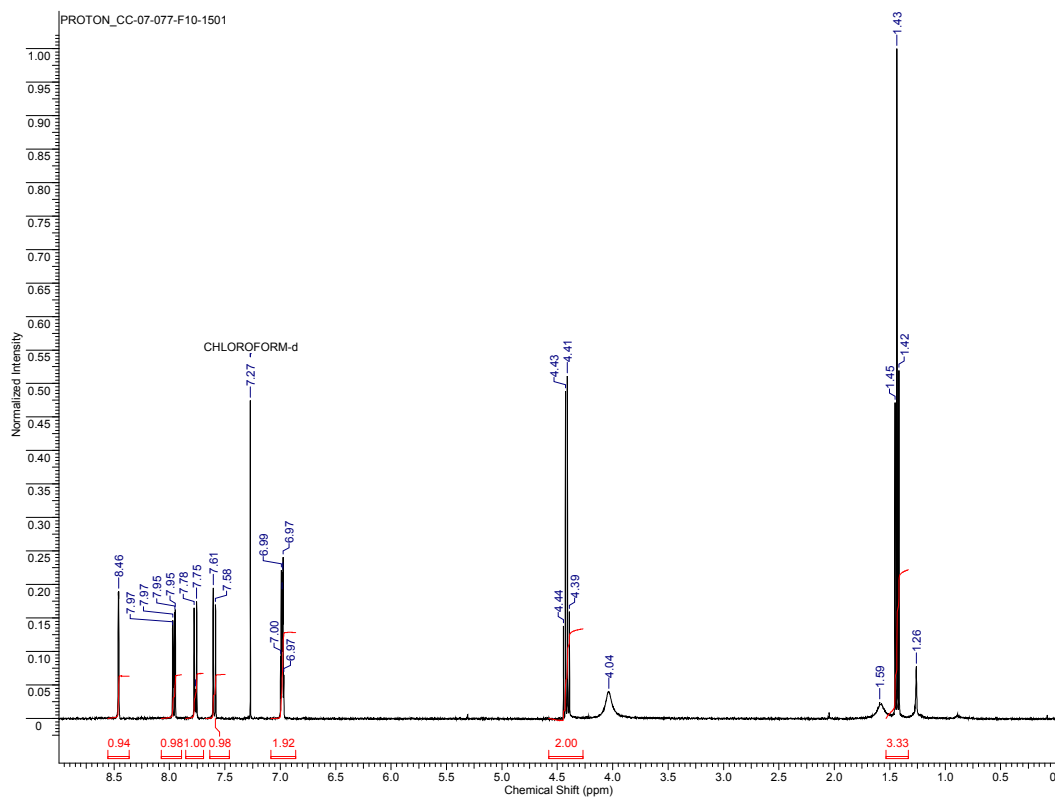
IC<sub>50</sub> curve for 3.5bIC<sub>50</sub> curve for 3.5c

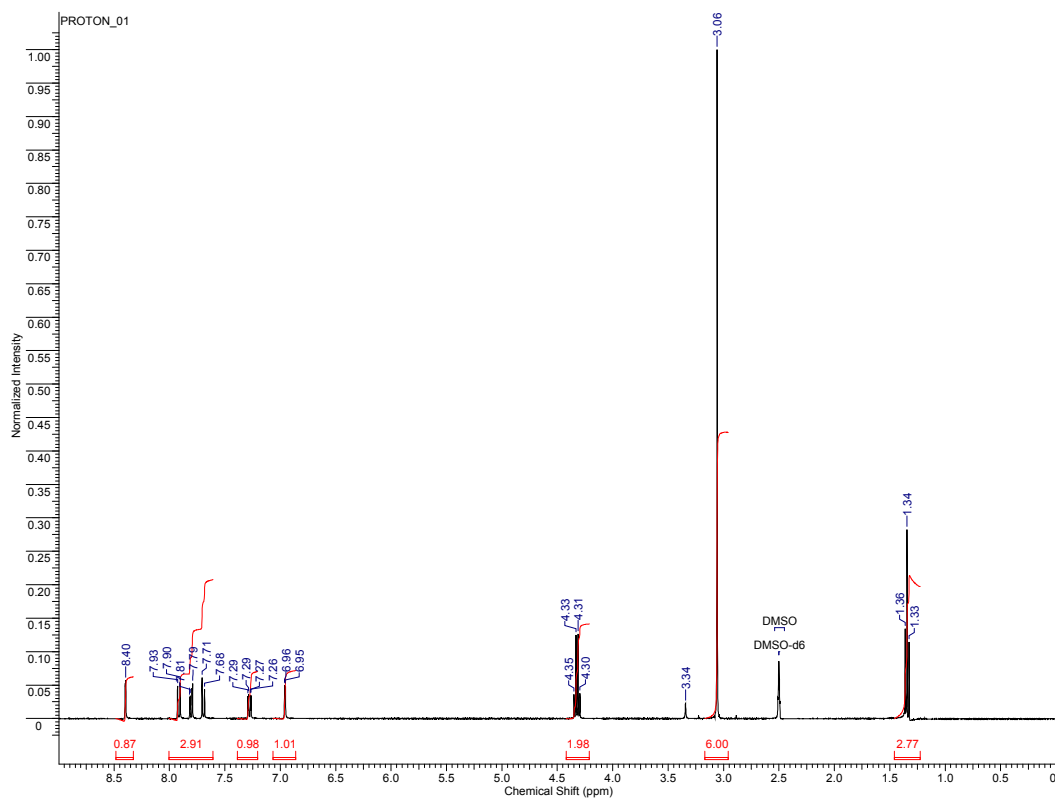
IC<sub>50</sub> curve for 3.6aIC<sub>50</sub> curve for 3.6b

## 6.5 Chapter 3 $^1\text{H}$ NMR

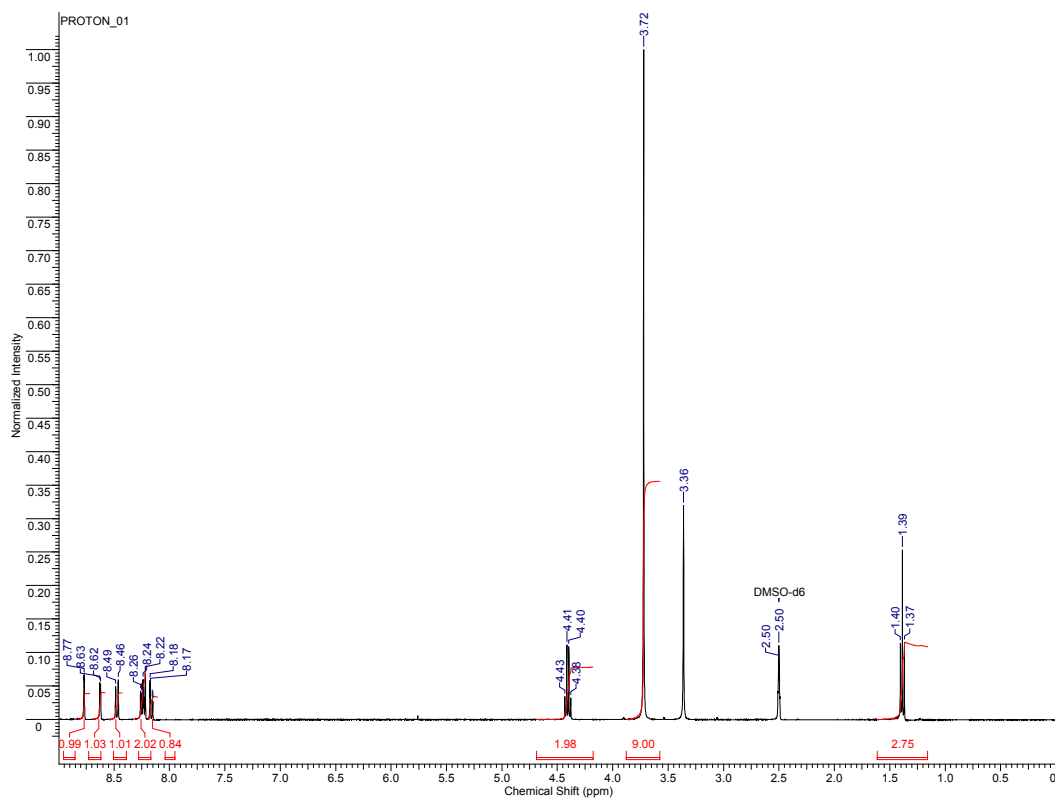
$^1\text{H}$ -NMR of **3.4c** (4'-FBC) in DMSO

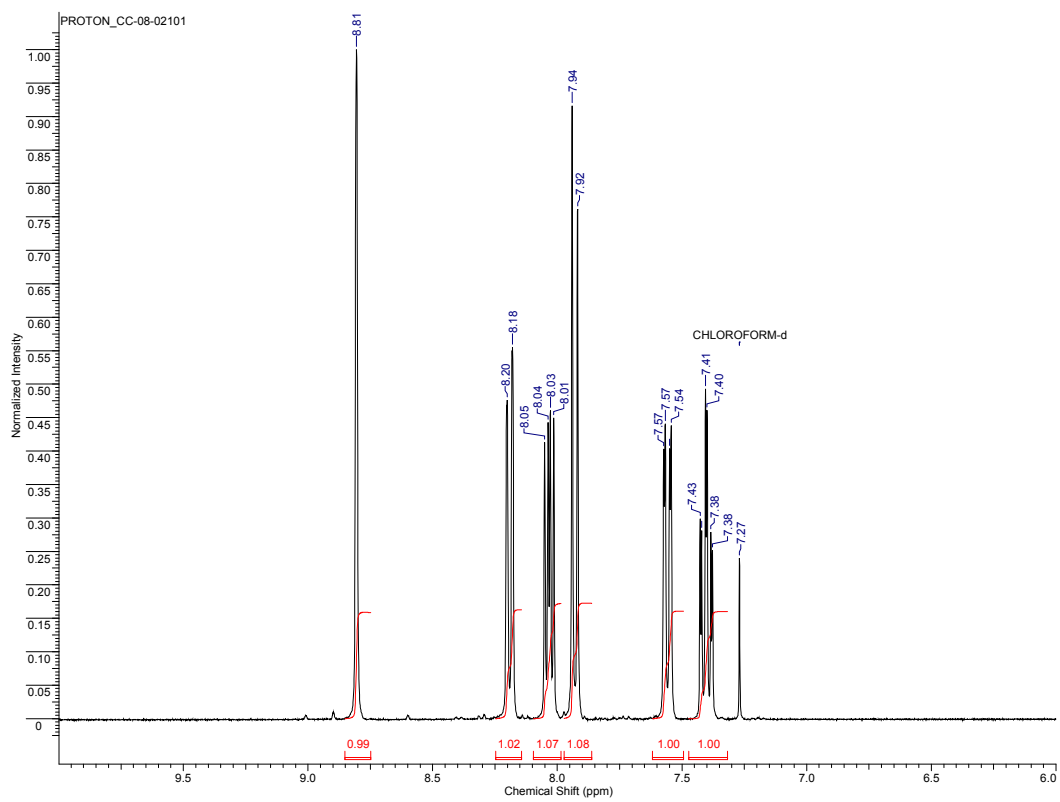


$^1\text{H-NMR}$  of **3.9** in  $\text{CDCl}_3$ 

$^1\text{H-NMR}$  of **3.10** in DMSO

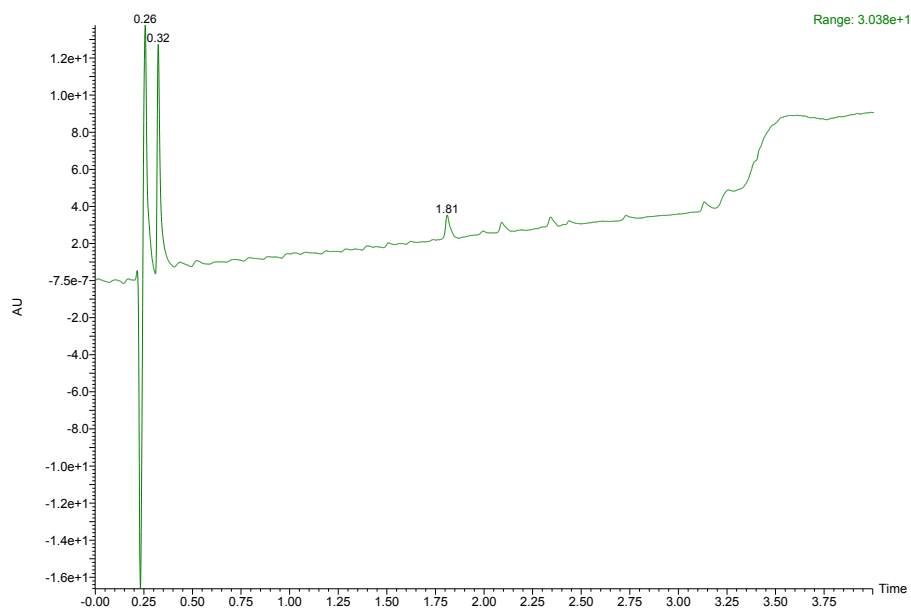


$^1\text{H-NMR}$  of **3.11** in DMSO

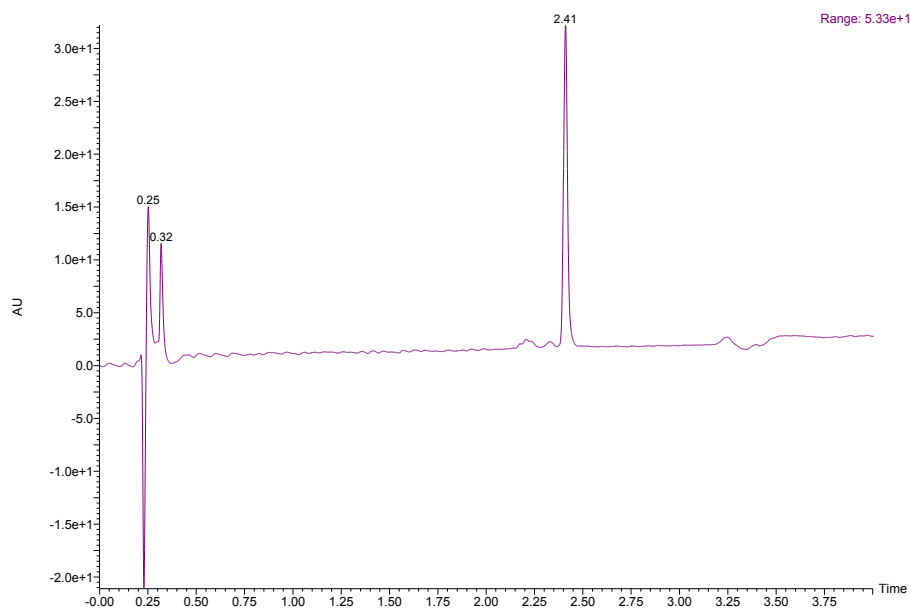
H-NMR of **3.13** in CDCl<sub>3</sub>

## 6.6 Chapter 4 UHPLC Traces

UHPLC for **4.4**: Analytical 10 – 60 % acetonitrile in water – 4 minutes

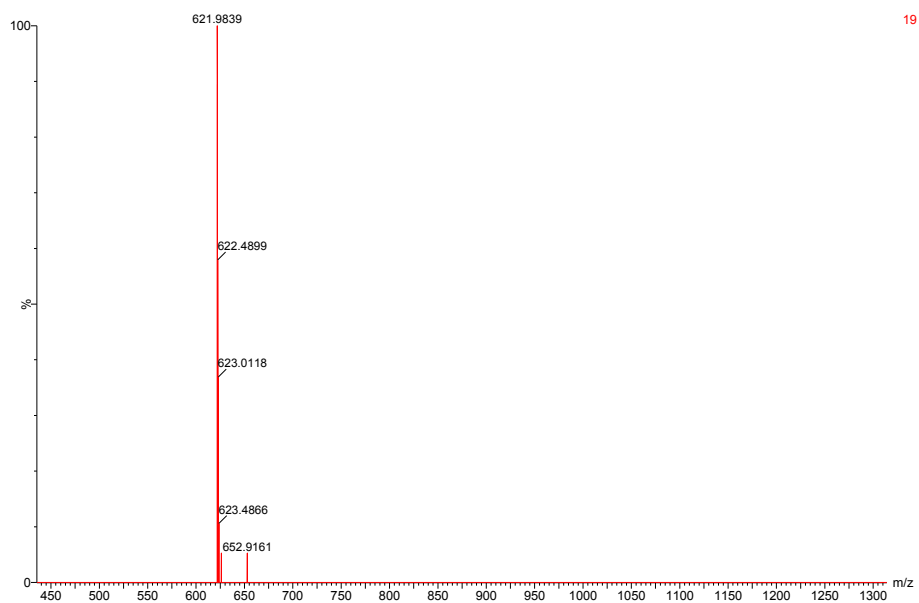


UHPLC for **4.10**: Analytical 10 – 60 % acetonitrile in water – 4 minutes

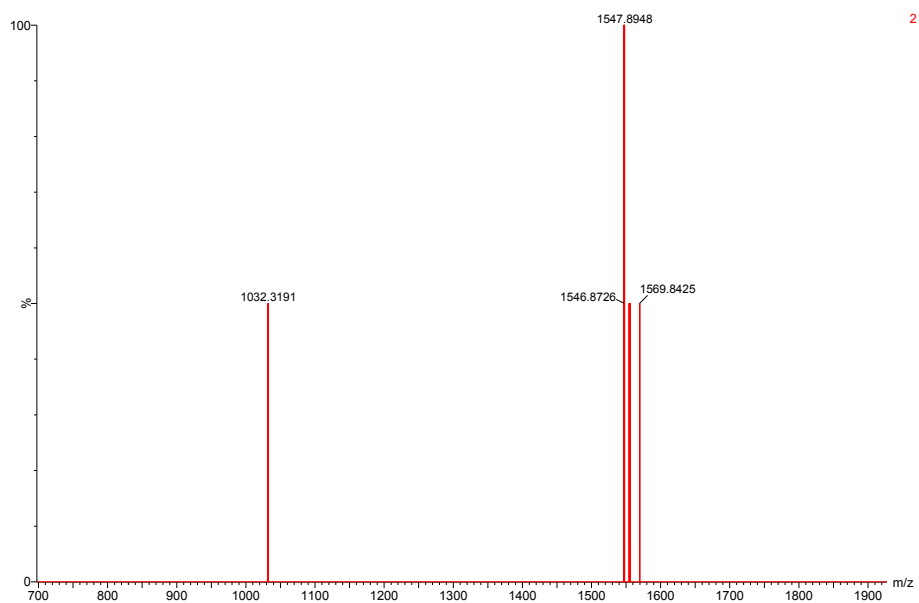


## 6.7 Chapter 4 ESI<sup>+</sup> Mass Spectrums

ESI<sup>+</sup> Mass Spectrum for 4.4



ESI<sup>+</sup> Mass Spectrum for 4.10



## Curriculum Vitae

### ACADEMIC EXPERIENCE

- Sept. 2011 – Feb 2016: PhD Student at The University of Western Ontario  
 Supervisor: Dr. Leonard Luyt  
 Ph.D. Thesis: Design and Synthesis of Ghrelin Analogues as Non-Invasive GHS-R1a Imaging Probes
- Apr. 2010 – Aug. 2010 CaRTT Summer Studentship at The London Regional Cancer Center  
 Supervisor: Dr. Leonard Luyt  
 Project Title: Peptide Mimics of Hyaluronan as Molecular Imaging Probes for Rhamm-Expressing Carcinomas
- Sept. 2010 – Apr. 2011 Fourth year Honours Project at Dalhousie University  
 Supervisor: Dr. Norman Schepp  
 Honours Thesis: Effect of Media Polarity on Two-Photon Photochemistry of BODIPY and Stilbene Derivatives

### TEACHING EXPERIENCE

- 2015 Resource Room Instructor for Organic Chemistry of Biological Molecules, The University of Western Ontario
- 2011 – 2014 Teaching Assistant for Organic Chemistry of Life Sciences, The University of Western Ontario
- 2011 – 2014 Teaching Assistant for Organic Chemistry of Biological Molecules, The University of Western Ontario

### HONOURS AND AWARDS

- 2015 Travel Award, Society of Radiopharmaceutical Sciences, Columbia, MO, USA.
- 2014 Poster Award, Imaging Applications in Prostate Cancer, London, ON, CA.
- 2013 Travel Award, Society of Radiopharmaceutical Sciences, Jeju, South Korea.

2012	Poster Award, CIHR Oncology Research and Education Day, London, ON, CA.
2011 – 2014	Western Graduate Research Scholarship
2011	Dean's List, Dalhousie University
2010	CaRTT Summer Studentship, London Regional Cancer Centre, London, ON, CA.
2009	In-Course Scholarship, Dalhousie University
2008	Dean's List, Dalhousie University
2008	Entrance Scholarship, Dalhousie University

### PUBLICATIONS

- **Charron, C. L.**; Hickey, J.; Cruickshank, D. Nsiama, T.; Luyt, L.G., Molecular Imaging Probes Derived from Natural Peptides, *Nat. Prod. Rep.*, **2016**.
- Douglas, G. A. F.; McGirr, R.; **Charlton, C. L.**; Kagan, D. B.; Hoffman, L. M.; Luyt, L. G.; Dhanvantari, S. Characterization of a far-red analog of ghrelin for imaging GHS-R in P19-derived cardiomyocytes. *Peptides*, **2014**, 54, 81-88.

### PUBLISHED ABSTRACTS

- **Charlton, C.L.**; McGirr, B; Dhanvantari, S; Kovacs, M; Luyt, L. [68Ga] Labeled Ghrelin (1-19) Analogue for Targeting Growth Hormone Secretagogue Receptor. 20<sup>th</sup> International Symposium for Radiopharmaceutical Sciences, **2013**, *J. Labelled Cpmds. Radiopharm.* 56, S192.
- **Charlton, C.L.**; Hou, J.Q; McGirr, R; Dhanvantari, S; Lee, T-Y; Kovacs, M; Luyt, L. Development of High Affinity Ghrelin(1-8) Analogues for Imaging GHSR-1a with Fluorine-18, 21<sup>st</sup> International Symposium for Radiopharmaceutical Sciences, **2015**, *J. Labelled Cpmds. Radiopharm.* 58, S177

### CONFERENCE ABSTRACTS

- **Charlton, C.L.**; Hou, J.Q; McGirr, R; Dhanvantari, S; Lee, T-Y; Kovacs, M; Luyt, L. Development of High Affinity Ghrelin(1-8) Analogues for Imaging GHSR-1a with Fluorine-18, CIHR-STP in Cancer Research & Technology Transfer Research and Education Day, June 23, 2015, London, ON, CA.
- **Charlton, C.L.**; McGirr, B; Dhanvantari, S; Kovacs, M; Luyt, L. Preliminary In Vitro and In Vivo Evaluation of [68Ga] Labeled Ghrelin(1-19) Analogue for Targeting the Growth Hormone Secretagogue Receptor, Imaging Applications in Prostate Cancer, November 15, 2013, London, ON, CA.
- Siddiqui, K; Biggs, C; Billia, M; **Charlton, C.L.**; Mazzola, C; Power, N; Chambers, A; Yang, J; Luyt, L; Chin, J; Leong, H. Prostate cancer microparticles as a next generation screening tool for prostate cancer. Society of Urologic Oncology Annual Meeting, 2013, Bethesda, MD.
- **Charlton, C.L.**; McFarland, M.; Dhanvantari, S.; Kovacs, M.; Luyt, L. Ghrelin Analogues as Non-Invasive Prostate Cancer Imaging Proves. Imaging Applications in Prostate Cancer, November 2013, London, ON, CA
- **Charlton, C.L.**; McFarland, M.; Dhanvantari, S.; Kovacs, M.; Luyt, L. Ghrelin Analogues as Non-Invasive Prostate Cancer Imaging Proves. CIHR-STP in Cancer Research & Technology Transfer Research and Education Day. June 2012, London, ON, CA.

## MANUSCRIPTS IN PREPARATION

- **Charron, C. L.**; Hou, J.Q.; Kovacs, M.; Luyt, L.G., Design, Synthesis and Radiolabelling of a High Affinity Ghrelin (1-8) Analogue Bearing a New 6-[<sup>18</sup>F]fluoronaphthoate Prosthetic Group, Manuscript in preparation.
- Hou, J. Q.; **Charron, C. L.**; Fowkes, M. M.; Luyt, L. G., Bridging Computational Modeling to Amino Acid Replacements to Investigate GHSR-1a-Peptidomimetic Recognition, Manuscript in preparation.
- **Charron, C. L.**; Hou, J.Q.; Groom, H.; McFarland, M.; Luyt, L.G., Development and Evaluation of [(Dpr<sup>3</sup>(octanoyl), Lys<sup>19</sup>(<sup>68</sup>Ga-DOTA)]-Ghrelin(1-19) for the Detection of GHS-R1a *In Vivo*, Manuscript in preparation.

## SEMINARS AND ORAL PRESENTATIONS

- “Evaluation of <sup>68</sup>Ga-DOTA Ghrelin(1-19) in LNCaP Prostate Carcinoma” presented at the 2<sup>nd</sup> International Symposium on Technetium and Other Radiometals in Chemistry and Medicine, on September 10-13, 2014, Bressanone, Italy.
- “The Design of Ghrelin Analogues as PET Imaging Probes for Prostate Cancer” presented at the Cancer Research Laboratory Program Seminar Series, London Regional Cancer Program, on November 22, 2012, London, ON, CA.

## WORKSHOPS

- Advanced Molecular Imaging and it’s Clinical Translation on October 27 - 30, 2013, Boston, MA., USA.